

NASA Contractor Report 179614  
SPI-25-1

# Megawatt Class Nuclear Space Power Systems (MCNSPS) Conceptual Design and Evaluation Report

Volume II—Technologies I: Reactors, Heat Transport,  
Integration Issues

J.R. Wetch, et al.  
*Space Power, Inc.*  
*San Jose, California*

September 1988

Prepared for  
Lewis Research Center  
Under Contract NAS3-23867



National Aeronautics and  
Space Administration

(NASA-CR-179614-Vol-2) MEGAWATT CLASS  
NUCLEAR SPACE POWER SYSTEMS (MCNSPS)  
CONCEPTUAL DESIGN AND EVALUATION REPORT.  
VOLUME 2, TECHNOLOGIES I: REACTORS, HEAT  
TRANSPORT, INTEGRATION ISSUES Final Report

N89-22981

Unclas  
G3/44 0190055

SPI-25-1  
TABLE OF CONTENTS

		VOLUME-PAGE
1.0	Abstract . . . . .	I-1
	1.1 Objectives . . . . .	I-2
	1.2 Performance Requirements . . . . .	I-3
	1.3 Study Goals . . . . .	I-3
	1.4 Systems Considered for MCNSPS . . . . .	I-3
	1.5 Study Results . . . . .	I-5
2.0	Conclusions . . . . .	I-10
	2.1 Study Concept . . . . .	I-10
	2.2 Application . . . . .	I-13
	2.3 Technology Status . . . . .	I-14
	2.4 Candidate Technologies . . . . .	I-15
	2.5 Study Results . . . . .	I-16
	2.6 Critical Technology Development Requirements . . . . .	I-22
3.0	Introduction and Background . . . . .	I-28
4.0	Technologies Considered . . . . .	II-1
	4.1 MCNSPS Objectives . . . . .	II-1
	4.2 Candidate Systems . . . . .	II-2
	4.3 Heat Rejection . . . . .	II-15
	4.4 Space Power Reactors and Fuel . . . . .	II-75
	4.5 Power Conversion Systems . . . . .	III-1
5.0	Concepts Selection . . . . .	IV-1
	5.1 Selection Criteria and Screening for Preferred Systems . . . . .	IV-1
	5.2 Evaluation and Selection . . . . .	IV-3
	5.3 System Configuration . . . . .	IV-17
	5.4 Survivability . . . . .	IV-22
	5.5 Orbital Assembly/Start Up/Shutdown/Dormancy/ Restart/Reliability . . . . .	IV-31
6.0	Conceptual Designs . . . . .	IV-36
	6.1 Rankine Turbo Electric Systems . . . . .	IV-36
	6.2 Thermionic System . . . . .	IV-60
7.0	Summary of Development Requirements and a Preliminary Development Plan . . . . .	IV-97
	7.1 Power System Development . . . . .	IV-97
	7.2 Adjunct Activities . . . . .	IV-107
REFERENCES		
	References to Volume I . . . . .	I-36
	References to Volume II . . . . .	II-130
	References to Volume III . . . . .	III-106
	References to Volume IV, Section 5 . . . . .	IV-35
	References to Volume IV, Section 6 . . . . .	IV-96
APPENDIX A (VOLUME III)		
	References to Appendix . . . . .	A-1
	References to Appendix . . . . .	A-33

## 4.0 TECHNOLOGIES CONSIDERED

### 4.1 MCNSPS OBJECTIVES

The objectives of the Megawatt Class Nuclear Space Power System study were given in Section 1.1. Briefly restated, they are to:

- o Identify and assess past, current, and future space nuclear power plant concepts that could potentially meet MCNSPS objectives of 1 to 10 MWe for 5-years (or longer) full power life in orbit or on deep space probes.
- o Recommend concepts that should be considered for more detailed conceptual design definition.
- o Report to the NASA MCNSPS project office and brief them on the assessment results. Assist in selecting the preferred concepts for conceptual design.

A complete MCNSPS would consist of an optimum integration of the following subsystems.

- o Reactor heat source and shield
- o Power conversion
- o Heat rejection
- o Power processing - transmission and control
- o Potential electric orbital transfer and/or station keeping engine
- o MCNSPS payload separation and cooling boom
- o Payload and mission hardware
- o Integrating structure, deployment, stability, and vehicle control

This study concentrated upon:

- o The reactor-shield subsystem
- o The power conversion subsystem
- o The radiator subsystem
- o The power processing subsystem

Future studies will more extensively consider the entire launch vehicle system.

#### 4.2 CANDIDATE SYSTEMS

The conversion of reactor heat to electric power impacts the reactor size, mass and technology, the radiator size, mass and technology, and the vehicle size, mass and configuration.

The high cost of placing mass or volume into LEO, ~\$5000 to 10,000 kilogram and ~\$500,000 to 1,000,000 cubic meter respectively, with the Space Transportation System (STS) shuttle places unprecedented emphasis upon the reactor power system to be capable of achieving high power density and endurance with low failure rate. The necessity to radiate all waste heat away from the spacecraft requires very large radiating areas. For example, a payload use of 10,000 kWe at an ambient temperature of 300 K (80°F) would require a waste heat radiator of 40,000 m<sup>2</sup> (10 acres). Since the payload electrical energy is eventually converted to heat energy only a fraction is beamed overboard (e.g., in the form of an electric propulsion jet, a weapon (or an energy beam), the payload, as well as, the power system must have a waste heat rejection radiator.

Heat dissipation in space is radiated in accordance with the radiation law

$$P_R = \sigma \epsilon A (T_R^4 - T_B^4)$$

where  $\sigma$  - Stephen-Boltzman Const. ( $5.7 \times 10^{-11}$  kW/m<sup>2</sup>-K)

and  $\epsilon$  - The radiator emissivity (0.85 to 0.9)

$T_R$  - Radiator Temperature

$T_B$  - Background Temperature

Near earth  $T_B \approx 255$  K. In nuclear operating orbits (>900Km)  $T_B$  will usually be 210 K or less. Clearly  $T_R$  must be increased to as high a value as possible in order to reduce radiator area and consequently the associated mass and launch volume.

For each payload electrical kilowatt generated that must ultimately be dissipated, 2 to 9 thermal kilowatts of power system waste heat must also be rejected by radiation to space, assuming system generation efficiencies ranging from 30% to 10%, respectively. Fig. 4.2.1 shows the radiator areas required for a 10,000 kWe payload and conversion system versus the payload and the power conversion system radiator temperatures. Curve 1 assumes all of the 10,000 kWe are utilized on board, as for example would be the case for a space station factory or a lunar base. Curve 2 assumes 50% of the generated electricity leaves the space craft via an electric propulsion jet, an RF beam, kinetic energy projectiles, or via a weapon energy beam. The remaining curves show the radiator size for the power plant system as a function of the power conversion system efficiency.

To put the total surface area of a radiating cylinder the size of the areas indicated into perspective, the STS shuttle (4.3 meter diameter x 17.5 meter length) is about 230 square meters and about 800 square meters are available on the cylindrical surface of the shuttle derived cargo vehicle (9m outer diameter by 30m long).

It is clear from Fig. 4.2.1 that much larger areas (2 to 10 fold) will be required for the 10 MWe payloads than for the heat dissipation from the power conversion system. Payload temperatures well above 400 K are required to keep payload radiators below 5000 m<sup>2</sup>. Similarly, power system radiators must be at temperatures of at least 800K to 1100 K, depending upon the cycle efficiency, in order to remain in a practical size range of 1000 to 2000 M<sup>2</sup>.

All systems will use or dissipate about 15% of the gross power output in the form of system thermal losses, coolant pumping, power regulation and control, power transmission and power conditioning ( $f_s$ ). An allowance of at least 10% of beginning of life capability will be made for system degradation over 7 years of operation ( $f_d$ ). Different heat engine systems will be capable of conversion efficiencies ( $f_e$ ) of 30% to 70% of the Carnot efficiency ( $\eta_c$ ). Consequently, the reactor power system efficiency ( $\eta_s$ ) is:

$$\eta_s = (1-f_s)(1-f_d)f_e \eta_c$$

RADIATOR AREA REQUIRED FOR CLOSED CYCLE  
 10MWE SPACE POWER GENERATING SYSTEMS  
 (4000 m<sup>2</sup>/acre)

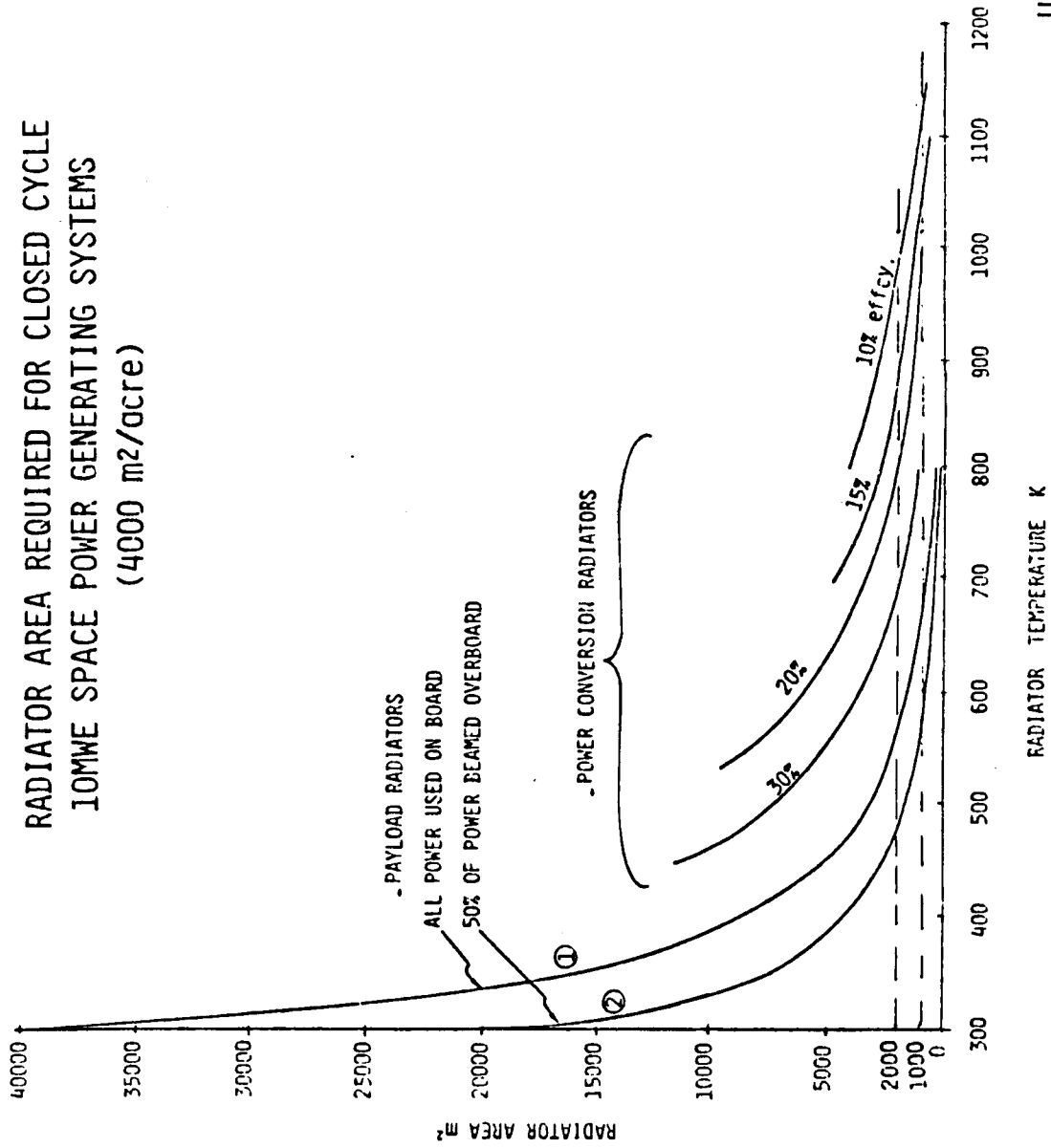


Fig. 4.2.1

Unclassified

For example, a representative engine-alternator might have a conversion efficiency of 45% of Carnot output. With the above representative values for  $f_s$  and  $f_d$ ,

$$\eta_s = (.85)(.9)(.45) \eta_c = 34.4\% \eta_c,$$

Where  $\eta_c = 1 - T_C/T_H$

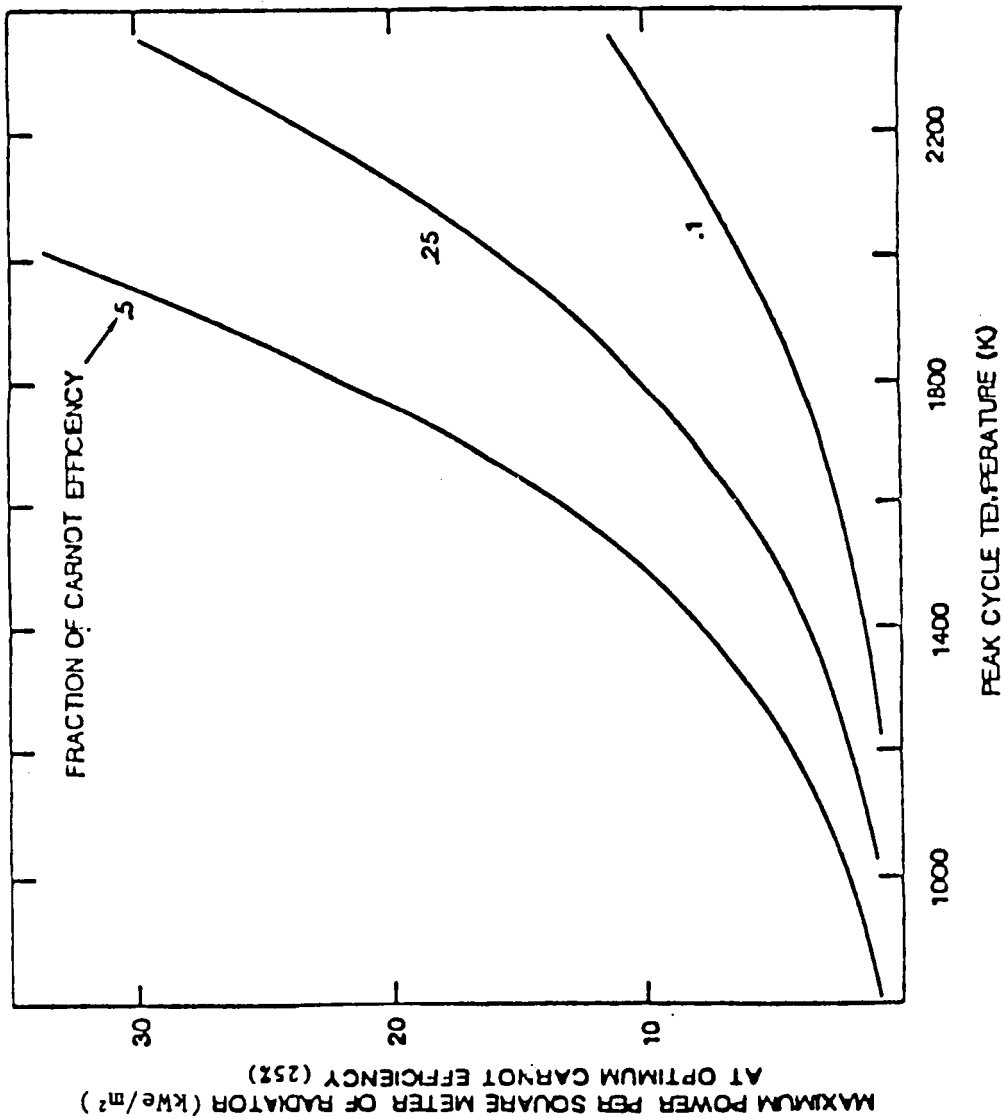
If  $T_C/T_H = 0.5$

Then  $\eta_s = 17.2\%$

From Fig. 4.2.1 for this system conversion efficiency and a radiator area constrained to 2000 m<sup>2</sup> (1/2 acre), an average radiator surface temperature of about 850 K will be required. Assuming that the cycle cold leg temperature is 50 K above the average radiator temperature and  $T_H = T_C/0.5$  as above, the cycle heat source temperature must be  $T_H = 900/0.5 = 1800$  K. Different cycles will produce higher or lower  $f_e$  and will optimize at different  $T_C/T_H$  ratios and radiator temperatures.

The  $T_H$  required for power system concepts with radiator areas less than 2000m<sup>2</sup> will vary from 1600 K to 2000 K. Fig. 3.2 of Vol I, reproduced here for convenience, showed the electric power producible per square meter of radiator area versus the peak cycle temperature with the system fraction of Carnot, i.e.  $\eta_s/\eta_c$ , as parameter. In all cases except for incore thermionics, the reactor coolants must operate at temperatures above  $T_H$ . In the thermionic system only the fuel element surface experiences  $T_H$ . The thermionic fuel element outer sheath, the reactor coolant and the reactor and coolant loop structures all operate below  $T_C$  of the thermionic heat engine.

The real extent of the peak cycle temperature problem is dramatized by examination of Fig. 3.3 of Vol I, also reproduced here for convenience, which shows reactor coolant outlet temperatures for actual U.S. systems vs. hours of successful operation. For 5 to 7 years of operation (44,000 to



Maximum electric power output per unit radiator area vs. peak power conversion cycle temperature - as function of fraction of optimum Carnot efficiency capability of P.C.S.

FIG. 3.2

# REACTOR COOLANT SYSTEM TEMPERATURES VS. OPERATING LIFETIME

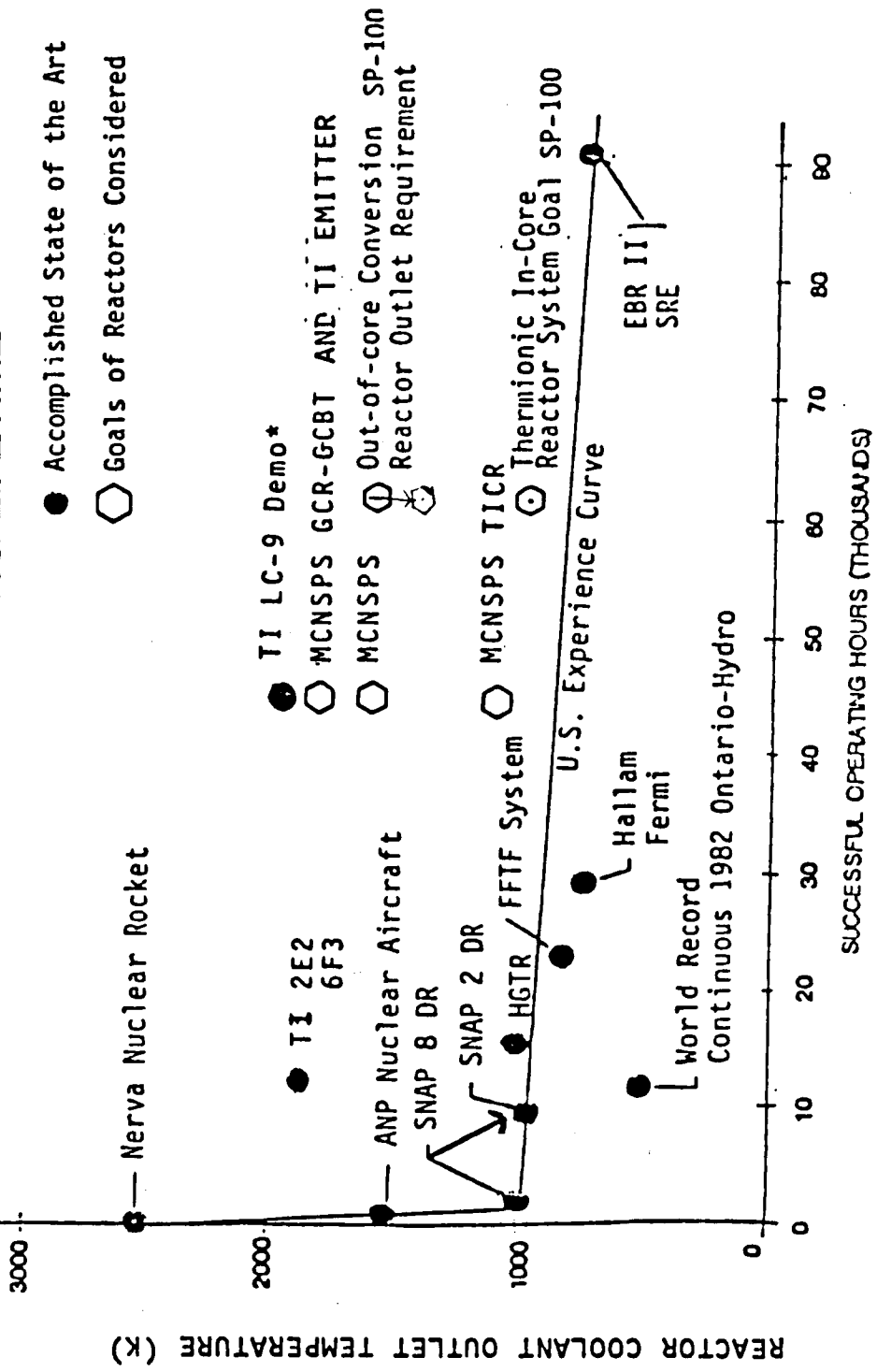


FIG. 3.3

\* OUT-OF-PILE THERMIONIC CONVERTER DEMO.

62,000 hours), reactor outlet temperatures of less than 1000 K have been achieved, (after 35 years of U.S. investment in power reactor technology).

Fig. 3.3 is presented in terms of reactor coolant outlet temperatures while Fig. 3.2 is presented in terms of the power conversion peak cycle temperature. The relationship between these two temperatures is generically illustrated in Fig. 4.2.2 and Table 4.2.1 for several typical out-of-core power conversion systems and for the in-core thermionic system.

The preliminary system and subsystem candidates are designated in Fig. 4.2.3. The magnitude of the evaluation effort for so many systems requires that some prejudgement be made. The systems designated in Fig. 4.2.3 have all received past attention and have proven to be of some interest. They may all be feasible and might be developed for low power levels by the mid-to late 1990's. The task is to select the more promising candidates and evaluate their potential for success and growth in the multimegawatt power regime.

Although other systems can be conceived, such as plasma reactors with internal direct plasma-electron emission power conversion, gaseous fueled photo-emission gas-cooled systems, or gas-cooled reactors with external MHD, thermoelectric, thermionic or Rankine conversion, they are judged not to add sufficient potential for long life system performance improvement to be considered at this time. As a result, preliminary evaluation yielded four promising power conversion systems warranting further study: alkaline-metal Rankine cycle; Stirling cycle; in-core thermionics; and the closed-loop Brayton cycle. The major components of each of these cycles are shown schematically in Figs. 4.2.4 and 4.2.5.

Some reactor types and power conversion systems (PCS) are uniquely paired. The liquid metal loop-cooled in-core thermionic system, the direct gas-cooled Brayton cycle system, and the direct boiling potassium or sodium Rankine systems are each studied with one unique appropriate PCS. The liquid lithium-cooled, uranium nitride reactor, LUNR, may be considered in conjunction with several principle PCS candidates.

TYPICAL SYSTEM TEMPERATURE PROFILES FOR:

- TICR - Thermionic In-Core Reactor
- GCR - Gas Cooled Reactor
- LMCR - Liquid Metal Cooled Reactor
- FHPR - Finned Heat Pipe Reactor

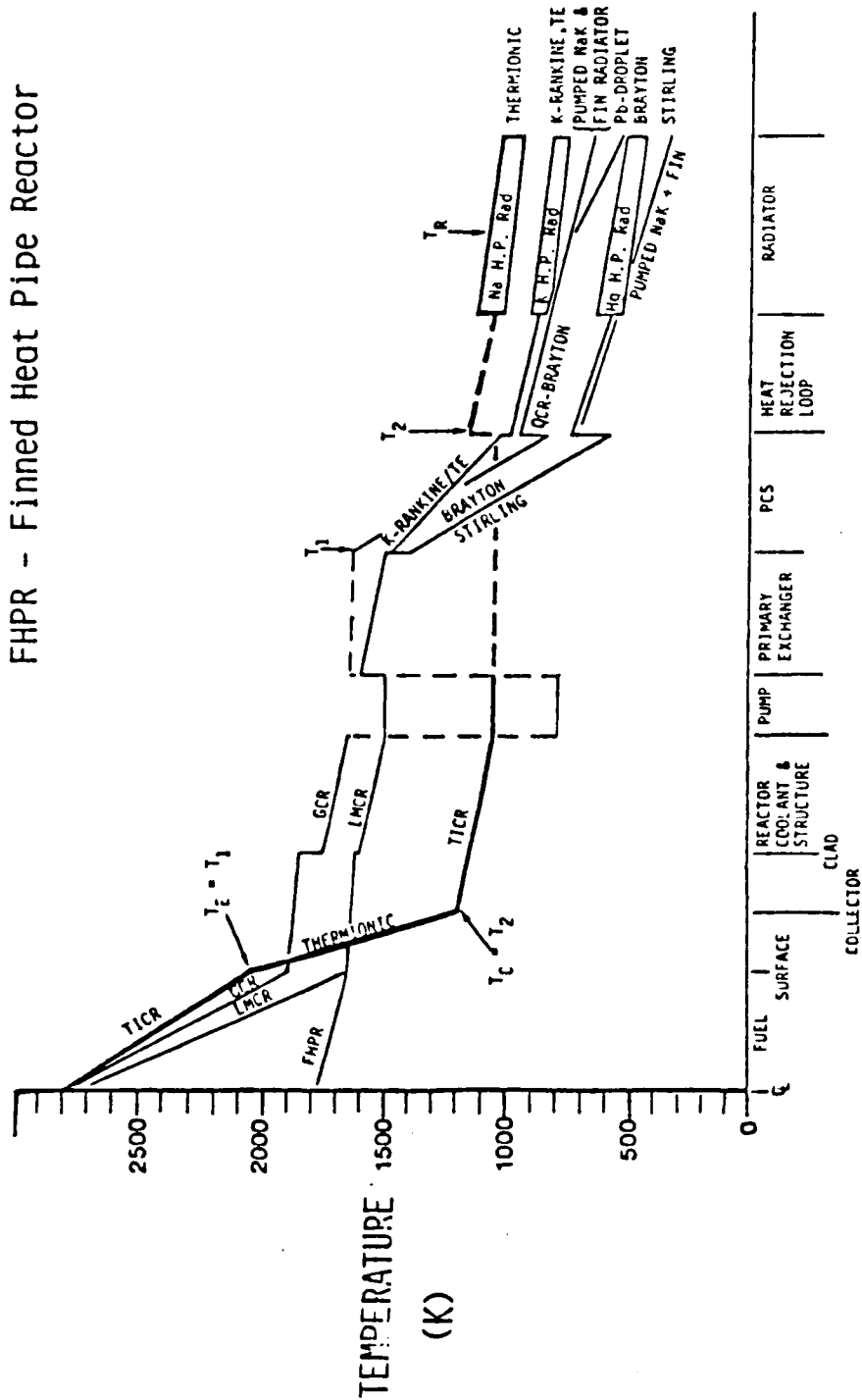


FIG. 4.2.2

# TYPICAL APPROXIMATE TEMPERATURES IN SPACE POWER SYSTEMS

	OUT-OF-CORE		IN-CORE
	INDIRECT LMCR OR HEAT PIPE	DIRECT GAS-COOLED OR BOILING POTASSIUM	THERMIONIC
PEAK PERMISSIBLE FUEL TEMPERATURE:	2700 K	2700 K	2700 K
TYPICAL FUEL SURFACE:	1600	2000 GAS 1500 POTASSIUM	1900
TYPICAL REACTOR COOLANT TEMPERATURE:	<1600	1800 GAS 1500 POTASSIUM	1050
PEAK CYCLE TEMPERATURE:	~1500	~1800 GAS ~1500 POTASSIUM	1900 EMITTER
TYPICAL CYCLE REJECT TEMPERATURE:	~1000	600 GAS 1000 POTASSIUM	1100
TYPICAL AVERAGE RADIATOR TEMPERATURE:	900	700 GAS 900   POTASSIUM	950

TABLE 4.2.1

# PRELIMINARY MCNSPS CANDIDATE SYSTEMS TO BE EVALUATED

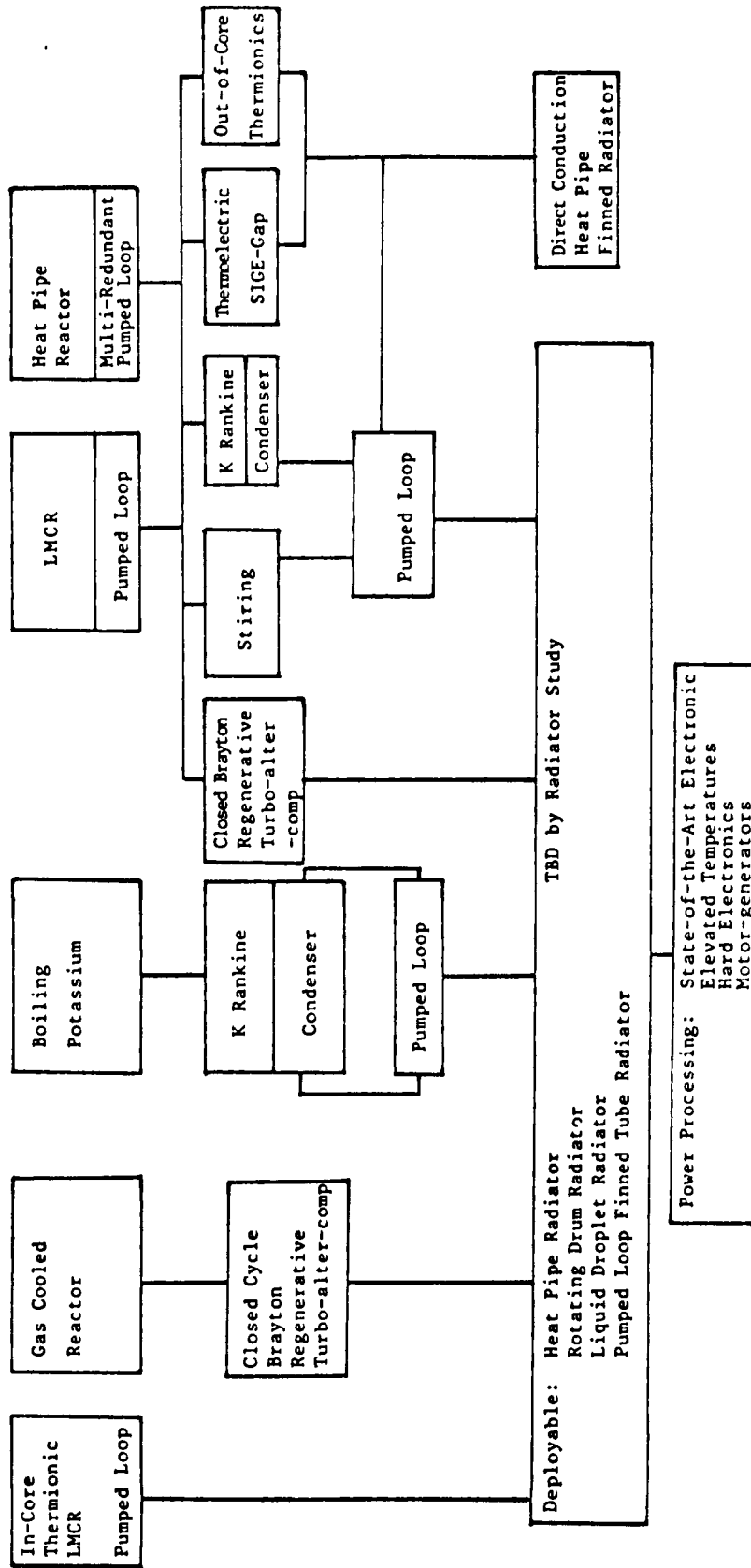


Fig. 4.2.3

Unclassified

# POWER CONVERSION SYSTEMS

## SCHEMATIC OF MAJOR COMPONENTS

### LIQUID METAL COOLED REACTORS

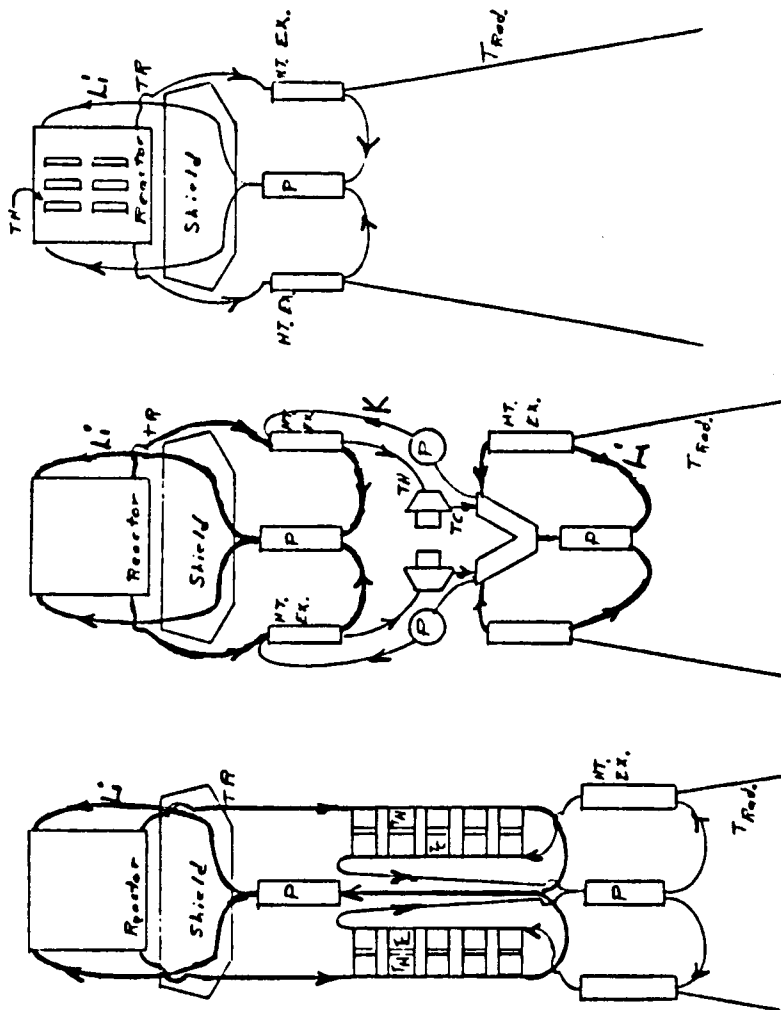


FIG. 4.2.4

STIRLING ENGINE

RANKINE TURBINE

IN-CORE THERMIONICS

Unclassified

# BRAYTON POWER CONVERSION

## SCHEMATIC OF MAJOR COMPONENTS

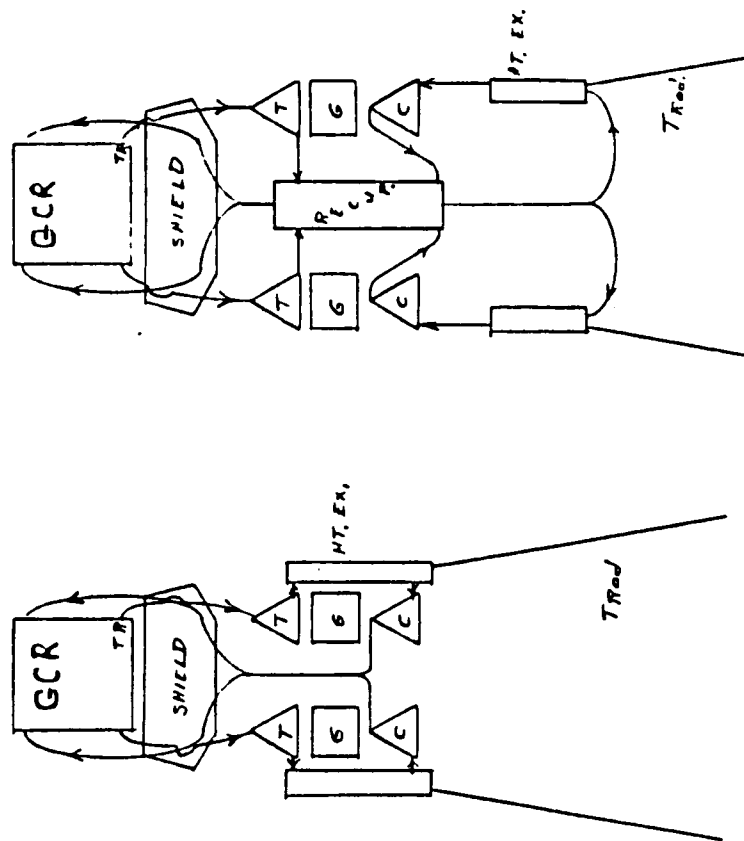


FIG. 4.2.5

NON-REGENERATIVE GAS BRAYTON

REGENERATIVE GAS BRAYTON

Unclassified

11/10/84

In order to limit the number of cases studied, the heat rejection systems were evaluated separately on the basis of weight per square meter of radiator and as a function of operating temperature, total size, deployability, launchability, energy consumption and survivability in the space and strategic defense environment. One preferred radiator was matched to each reactor power conversion system combination based upon appropriate operating temperature range.

The composite power conversion systems have been simulated for computer evaluation of component weights and sizes as a function of power output, endurance and temperature levels.

## 4.3 HEAT REJECTION

### 4.3.1 Required Surface Area

Waste heat will be produced from a variety of sources in both the PCS and the payload. For all closed cycle concepts (as opposed to open-cycle power generation systems) waste heat rejection will be the largest subsystem. Other significant sources of waste heat may arise from power conditioning, transmission, and the payload. The temperature at which these waste heats are produced is of primary importance, since low temperature waste heat rejection requires a large radiator. As shown in Fig 4.3.1, electric losses in power conditioning and payload electronics will usually require a larger area radiator than the power generation system. The scope of this study is limited primarily to power system heat rejection.

Rejection of large quantities of heat requires that the heat be spread over a large area with minimum temperature loss in transit from the source to the radiating surfaces. The radiator systems selected must not only be capable of high temperatures, but must also survive laser, and nuclear radiation, meteoroids, debris and pellets and vacuum and plasma space environment. Due to the large area requirement of the radiator, it will be the most vulnerable subsystem to meteoroid and debris damage, space radiation, launch load damage, or overt attack. Failure of a portion of the radiator should not lead to any failure of the PCS or reactor system. That is, if possible, partial radiator failure should only degrade system performance and not constitute a component which could give rise to total power system failure.

Fig. 4.3.1 shows the radiator area required per electrical kilowatt for the power generating system and for the payload power using system, versus their radiator temperatures and their respective generating and utilization efficiencies. It is clear that payload radiator size can easily exceed power system radiator size in some designs, especially as solar incidence is considered on low temperature payload radiators.

The thermal energy conversion systems most attractive for baseload power typically have conversion efficiencies between 5% and 25%. This means that

LIQUID DROPLET RADIATOR  
DEPLOYMENT SEQUENCE

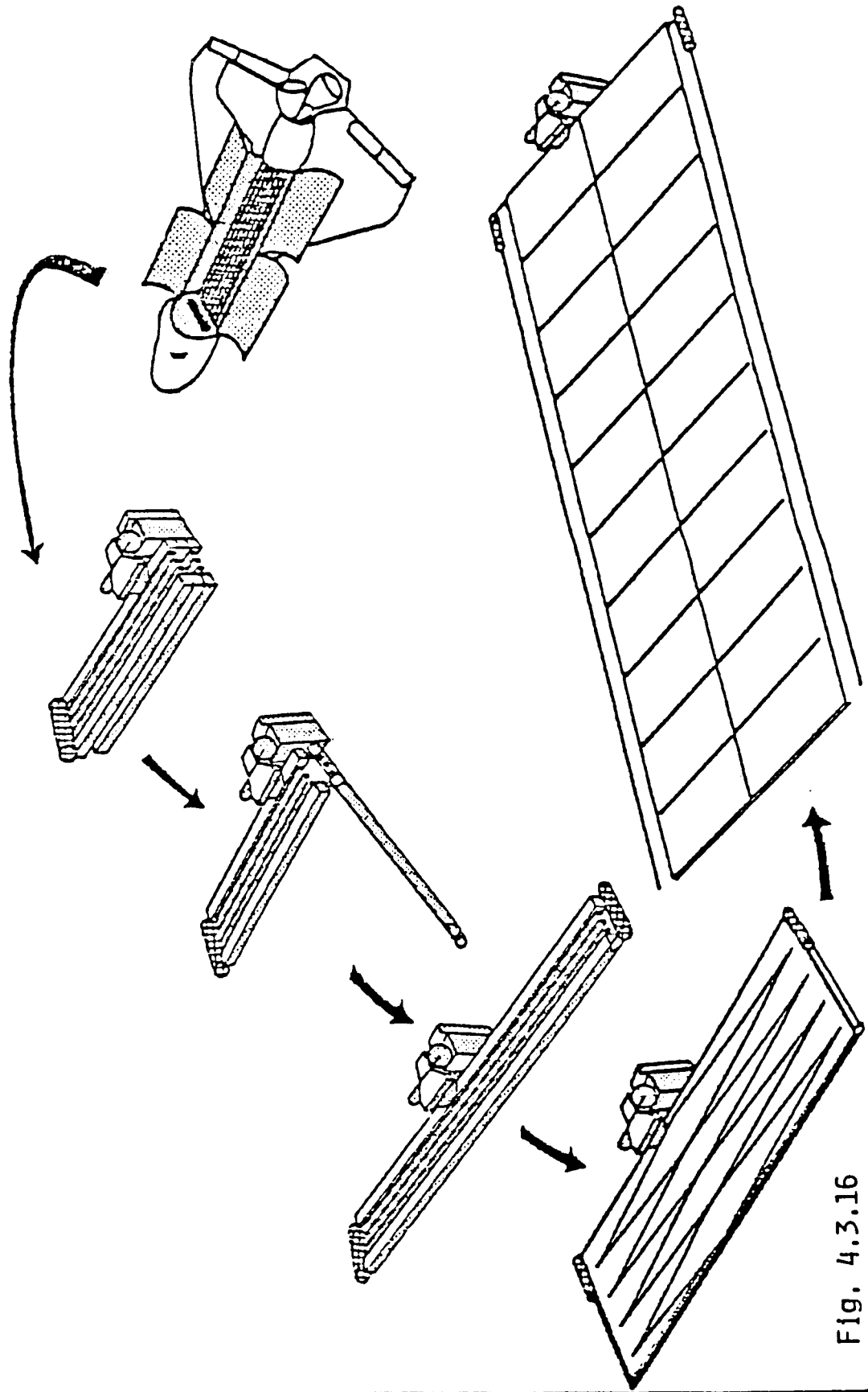


Fig. 4.3.16

functionality are not compatible with welding fabrication. Structural deformation exceeding aiming requirements is probably unavoidable due to sink temperature variations and local solar irradiation. Such large areas are not compatible with placing them behind a shadow shield. Thus they are not readily amenable to application with nuclear power.

From a survivability standpoint, one of many possible defenses is maneuverability. Moving out of the path of an oncoming kinetic energy projectile is a feasible defense. Fig. 4.3.17 shows the thrust required to perform various evasive maneuvers in response to a threat. A thrust of approximately 10,000 lbs. is required to move a 30,000 kg spacecraft a distance of 100 m in 10 seconds. That thrust produces an acceleration of 0.15g. If droplet transit time from generator to collector is only 3 seconds, the droplet will miss the collector by 6.7 m. Regardless of the motion, be it translation or rotation, the liquid droplet radiator is particularly sensitive to accelerations and cannot maneuver and operate simultaneously.

The liquid droplet technology does not appear to hold significant promise for military applications, high power levels or high temperature service. The liquid droplet radiator was therefore not considered as a feasible power conversion heat rejection concept.

Moving Belt. The moving belt concept is depicted in Fig. 4.3.18. In this scheme [20], a hot rotating drum passes heat into a belt which is passing over the drum. During the belt travel, out from and back to the heated drum, the belt radiates the heat gained from the drum. The heat capacity, mass, speed, and  $\Delta T$  determine the rate of heat transport. The projected area of the belt, its emissivity and its absolute temperature determines the heat rejection rate.

Low temperature experiments [20] have been performed using a Kapton belt on an aluminum drum. The experiment reported an improved heat transfer coefficient between the drum and belt approaching 200 W/m<sup>2</sup> K. This low value was achieved by applying a thin film of low vapor pressure vacuum grease to the contact surface of the drum. The grease greatly aids thermal

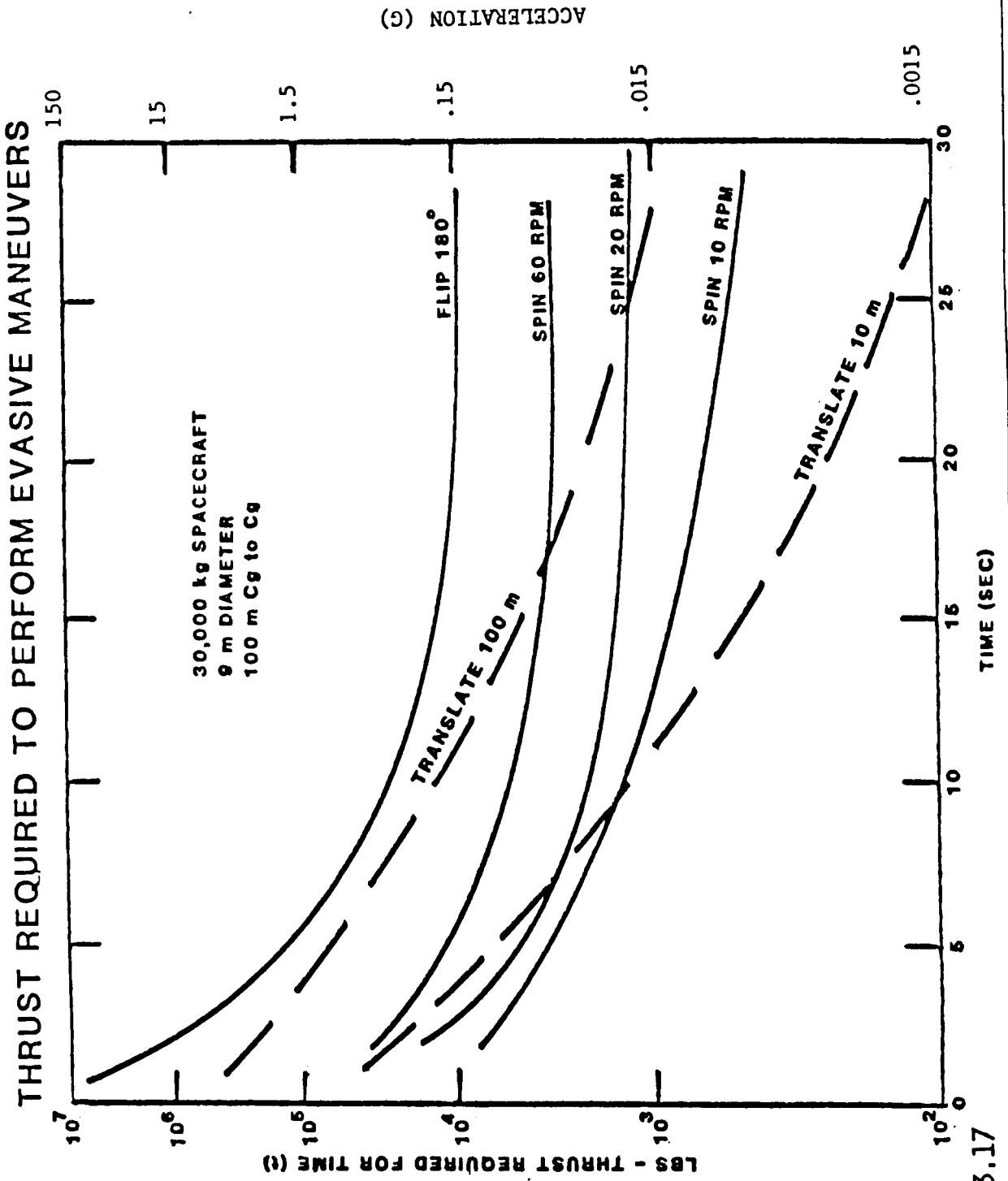
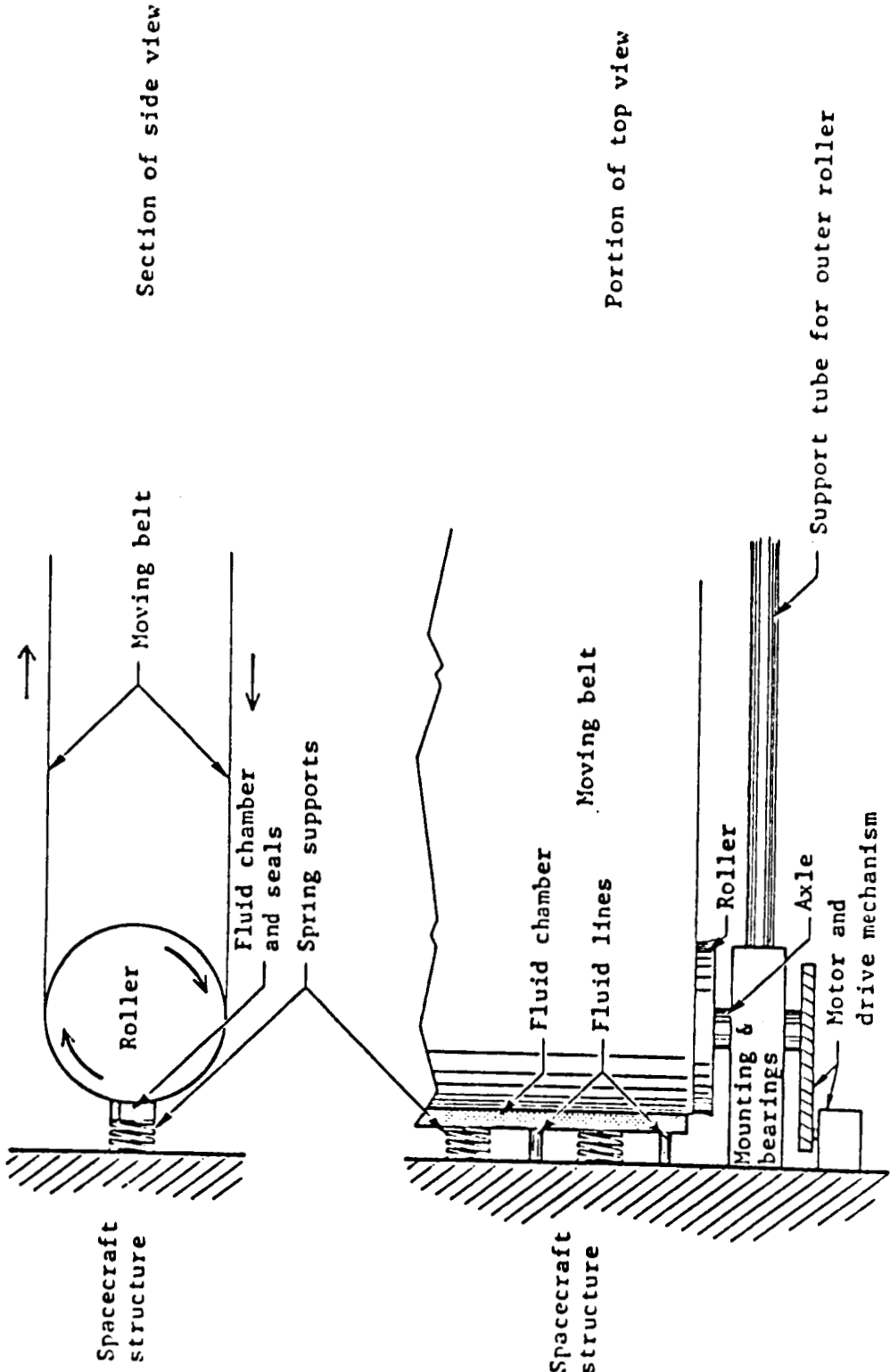


Fig. 4.3.17

# MOVING BELT RADIATOR



# CONVECTION HEATED BELT RADIATOR

conduction across the belt/drum interface. Even with an improved heat transfer coefficient, the temperature drop across the belt/drum interface is prohibitive when thermal loads approach the multimegawatt range. For example, passing 10 MWt of reject heat across a 100 m<sup>2</sup> belt/drum interface area would produce a 500 K temperature drop.

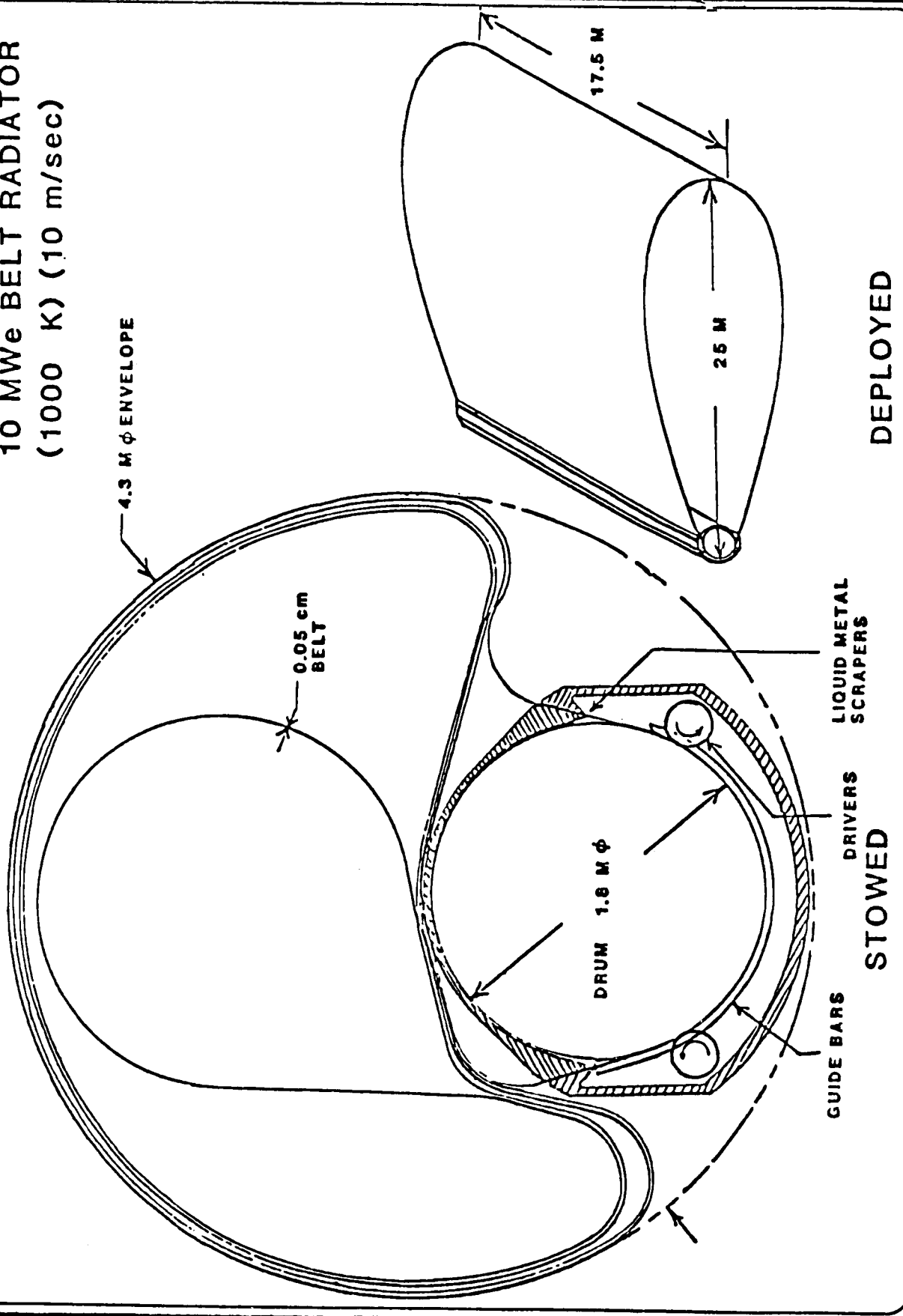
A practical rotating drum-belt system would require heat fluxes of the order of hundreds of watts/cm<sup>2</sup> and belt speeds of 10 meters/sec. at 1000K. In order to achieve this, a concept has been advanced [20] which allows the belt to come into direct contact with the working fluid. This concept is shown in Figs. 4.3.19 and 4.3.20. However, it necessitates a large working fluid dynamic seal. As the working fluid temperature increases, the belt would have to be a metallic belt with a ceramic emissivity coating in order to enhance the low emissivity surface characteristic of metals. A low emissivity coating that is not attacked, by liquid metal or molten salt heat transport fluids must be found. Because the emissivity coating would tend to spall off if the belt had to follow short radii corners, the conceptual design in Fig. 4.2.20 uses one large diameter drum. A belt of the dimensions shown would reject 40 MWt, 20 MWt, and 5 MWt at average belt temperatures of 1000 K, 800 K and 600 K, respectively.

Since the direct contact concept requires a seal, a hole or crack in the belt could provide a path for fluid leakage when the hole or crack is entering or leaving the seal. If seal leakage, either steady state or due to belt puncture, can not be resolved for long life applications, the moving belt might be a suitable burst-power heat rejection system. Since the time span is short in this type of application, some fluid loss through the seal may be acceptable. Because so many aspects of the technology of this concept have not yet been resolved, it can not be considered as a candidate heat rejection concept for long lived systems. If developed, the concept might benefit short life reactor-power conversion concepts.

Single Phase Pumped Loop. A schematic of a single phase pumped loop heat rejection system is shown in Fig. 4.3.21. The major components in the system include a heat exchanger, the tube-fin radiator, the heat transport fluid, a pump and the volume expansion compensator.



10 MWe BELT RADIATOR  
(1000 K) (10 m/sec)



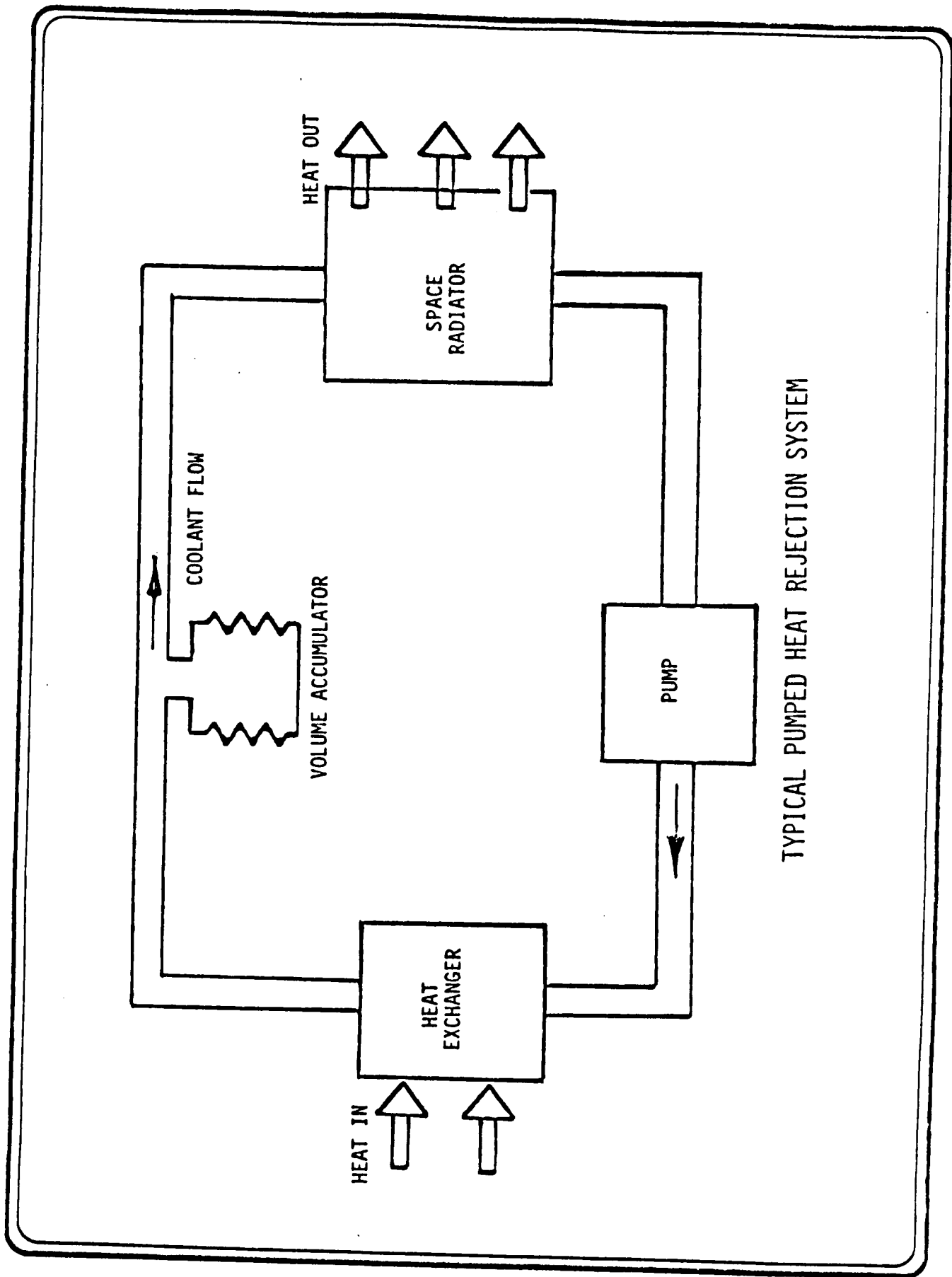


Fig. 4.3.21

11/13/84

The heat exchanger removes the heat from the power conversion system working fluid. When organic heat transport or molten salt fluids are used, the pump must be a mechanical type or a capillary type. Electro-magnetic (EM) pumps are commonly used in liquid metal loops. The radiator component radiates heat from the heat transport fluid to the space environment. The expansion compensator accommodates differential liquid volume changes due to thermal expansion and can be used to maintain a constant internal pressure.

The technology associated with this system was developed and demonstrated in the SNAP program, therefore it is one of the most developed. Both electro-magnetic and centrifugal liquid metal pumps have been operated with success. Liquid metal heat exchangers and radiators have been used and no basic technology obstacle prevents their operation in space. Deployable pumped loop radiators which can be stowed in the shuttle and deployed in space to gain increased radiator area are technologically practicle. The pumped loop heat transport depends upon the heat transport fluid heat capacity, flow rate and total  $\Delta T$ .

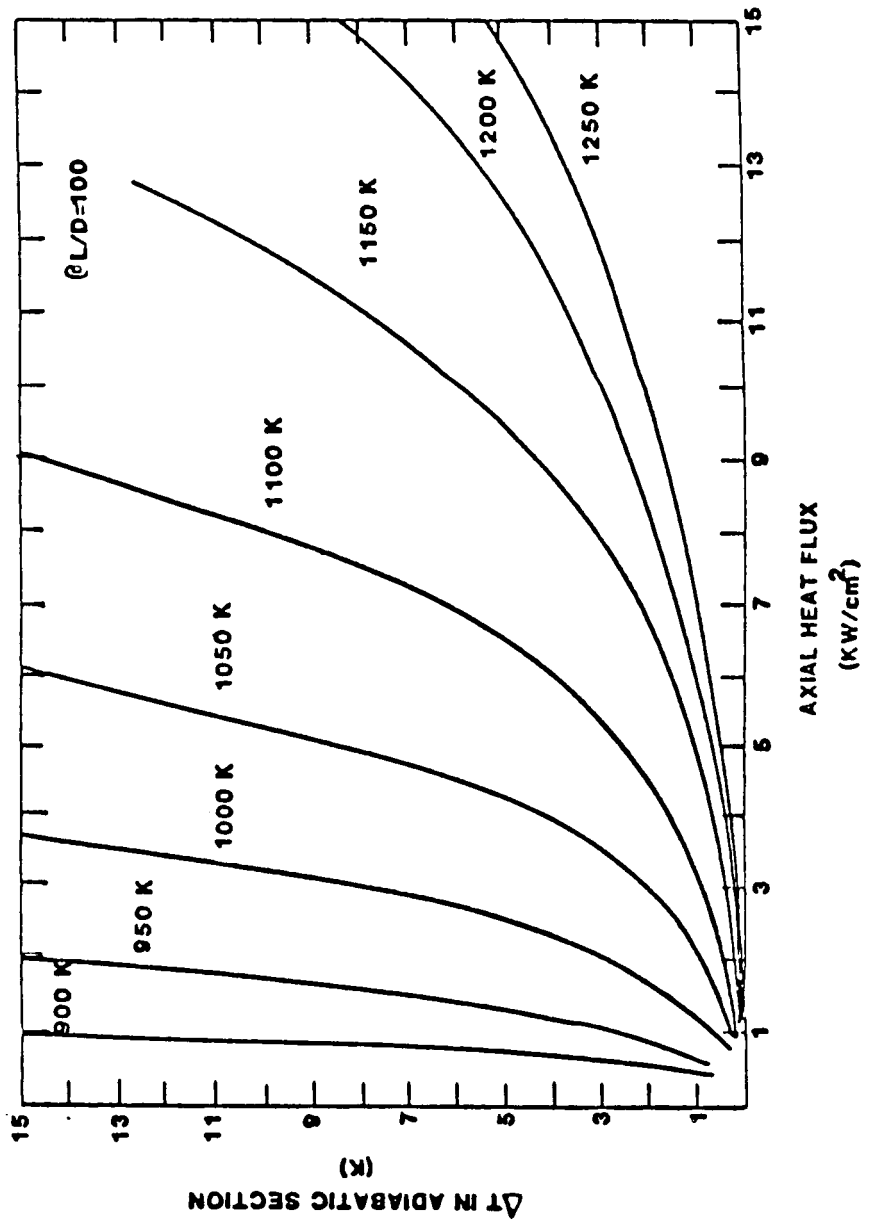
The pumped loop system suffers a performance disadvantage relative to a heat pipe or 2 phase pumped liquid-vapor latent heat of evaporation heat rejection system. In order to avoid fluid freeze up and to accommodate after-dormancy startup, only NaK-78 or CsK-23 are suitable as heat rejection radiator liquids for large high temperature space power systems. The heat capacities of these two liquids are small, and therefore the pumping power is large at small temperature differentials. At large temperature differentials, the radiator becomes large due to the  $T^4$  radiator law. Because very small pumps are generally low efficiency and high specific weight, less redundancy is possible, the micrometeoroid armor requirement to attain equal probability of lifetime is generally greater for a pumped loop system than for more compartmentalized radiators (e.g. heat pipe based concepts). Fins can protect the pumped loop tubes from micrometeorites but are heavy at high temperatures. The sub-divided multi-loop pumped NaK systems are preferred for temperatures below  $\sim 700$  K (where, for example, high L/D, Cs-K heat pipes cease to function), as in the case of payload and auxiliaries cooling. Alternatively, heat pipes are not considered because their useful temperatures are low, they are heavy in long large tubes and

could excessively contaminate the spacecraft after each micrometeorite puncture.

Heat Pipe Systems. Each different power conversion system generally optimizes at a different heat rejection temperature. The temperature range over which an individual heat pipe must operate will determine the selection of the pipe working fluid. From a micrometeorite and pressure boundary point of view, small diameter heat pipes result in a lower specific weight ( $\text{kg/m}^2$ ), because less wall thickness is required to protect the pipe or restrain the pressure load. Keeping pipe diameters small while designing pipes as long as possible (shuttle length = 17.5 meters) results in large L/D ratios.

Heat pipe working fluids are temperature range limited. At low temperatures and low vapor pressures the axial heat carrying capacity of the working fluid can be reduced to such a degree that the heat pipe is virtually inoperative. Using the heat pipe computer code, developed by Thermacore for this study, the thermal/hydraulic performance of heat pipes using the following working fluids was investigated: sodium; potassium; cesium; rubidium; mercury; and Dowtherm A. The results of this work are presented in Figs. 4.3.22 through 4.3.26, at a heat pipe length to diameter (L/D) ratio of 100. An example output from the Thermacore heat pipe program is shown in Fig. 4.3.27. There is a good choice of working fluids among cesium, potassium and sodium in the 840 K to 1250 K operating temperature range. Below 840 K rubidium appears to be the working fluid of choice down to ~700 K. Below 700 K, mercury is used. Mercury has adequate heat carrying capacity below ~720 K, but has a vapor pressure of 4.1 atmospheres at that temperature. Mercury vapor pressure only drops to two atmospheres at ~670 K. Mercury has been shunned as a radiator working fluid due to the concern that leaks from micro meteorite punctures would result in mercury contamination, amalgamation and deterioration of satellite electrical connections. At L/D ratios of 100, Dowtherm A reaches a capillary limit at heat carrying rates well below  $1 \text{ kW/cm}^2$  because of its poor surface tension characteristics. Both mercury nad Dowtherm or other biphenyl based mixtures suffer from excess pressure generation upon laser attack. The organics could also carborize in the wicks and destroy their pumping functions.

# HEAT PIPE TRANSPORT CAPABILITY SODIUM WORKING FLUID



# HEAT PIPE TRANSPORT CAPABILITY POTASSIUM WORKING FLUID

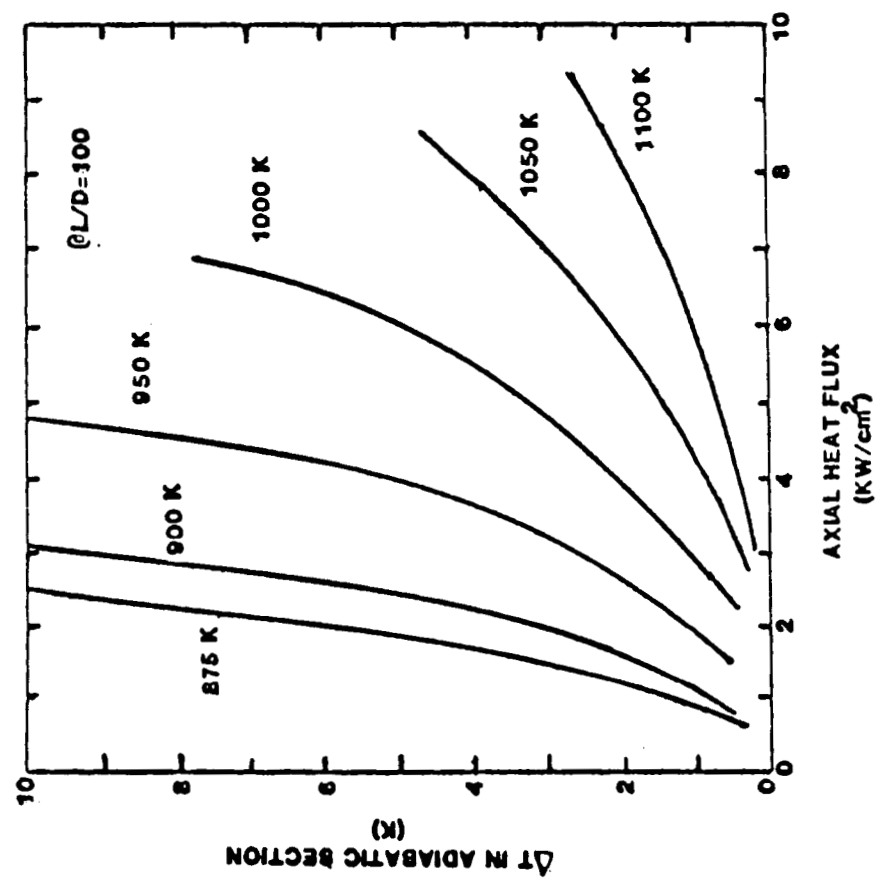
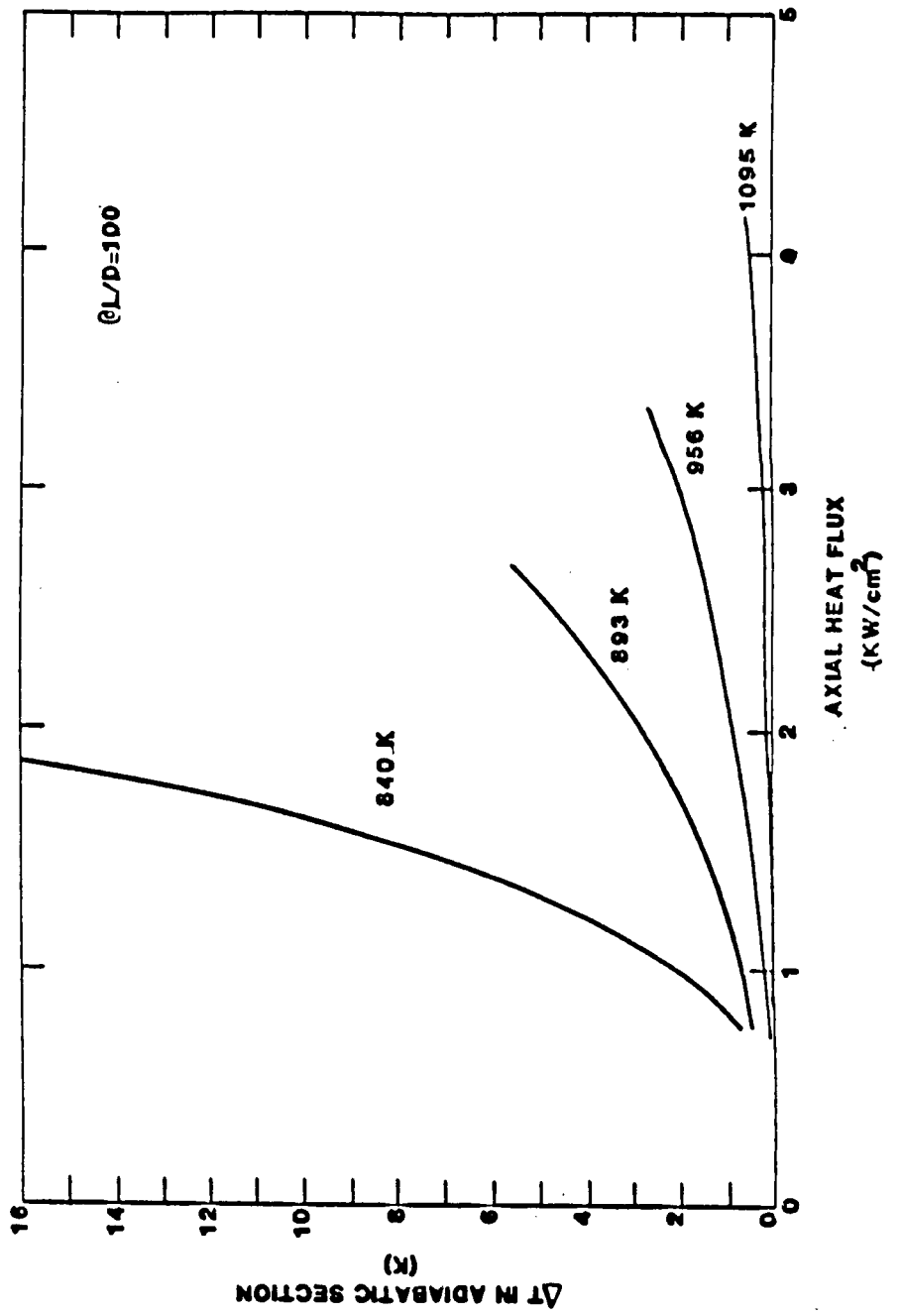


Fig. 4.3.23

11/13/84

# HEAT PIPE TRANSPORT CAPABILITY CESIUM WORKING FLUID



# HEAT PIPE TRANSPORT CAPABILITY BHUBIDIUM WORKING FLUID

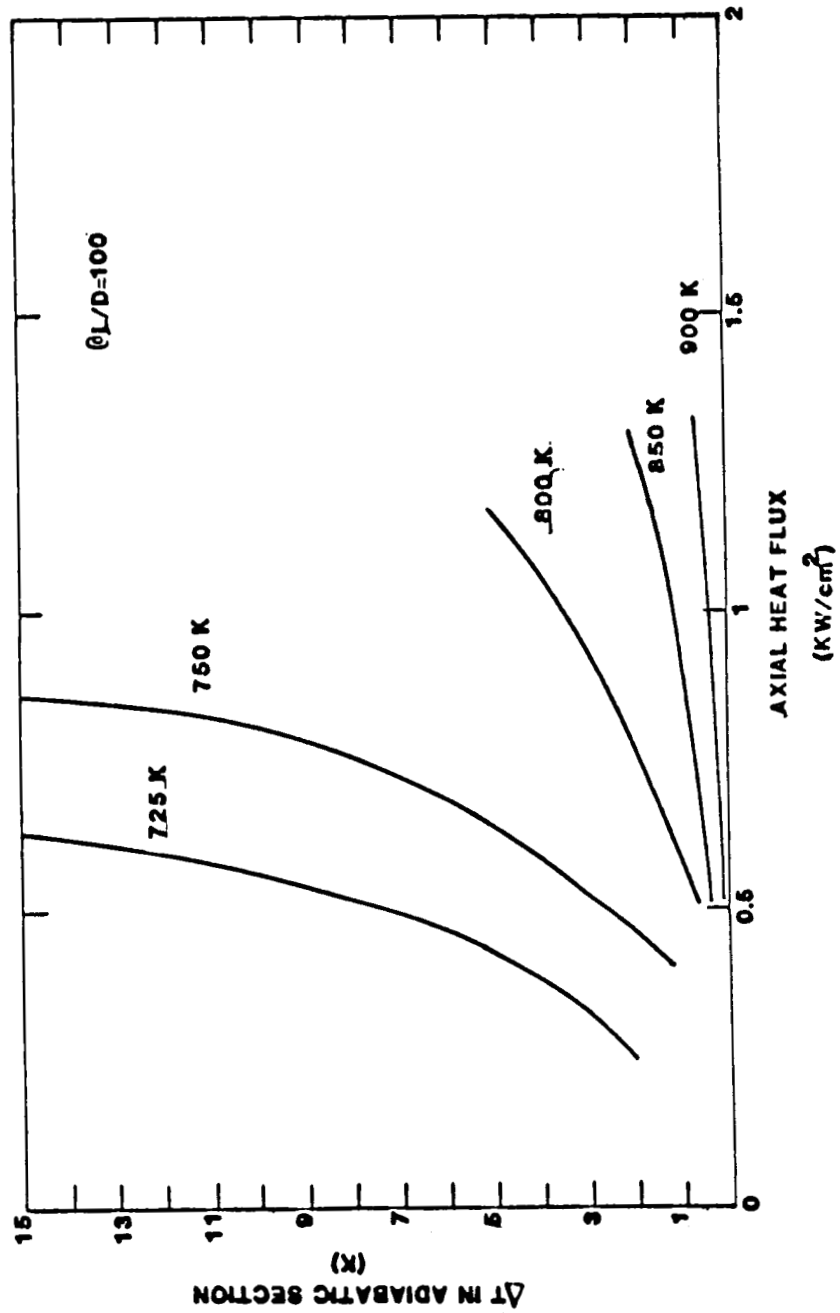
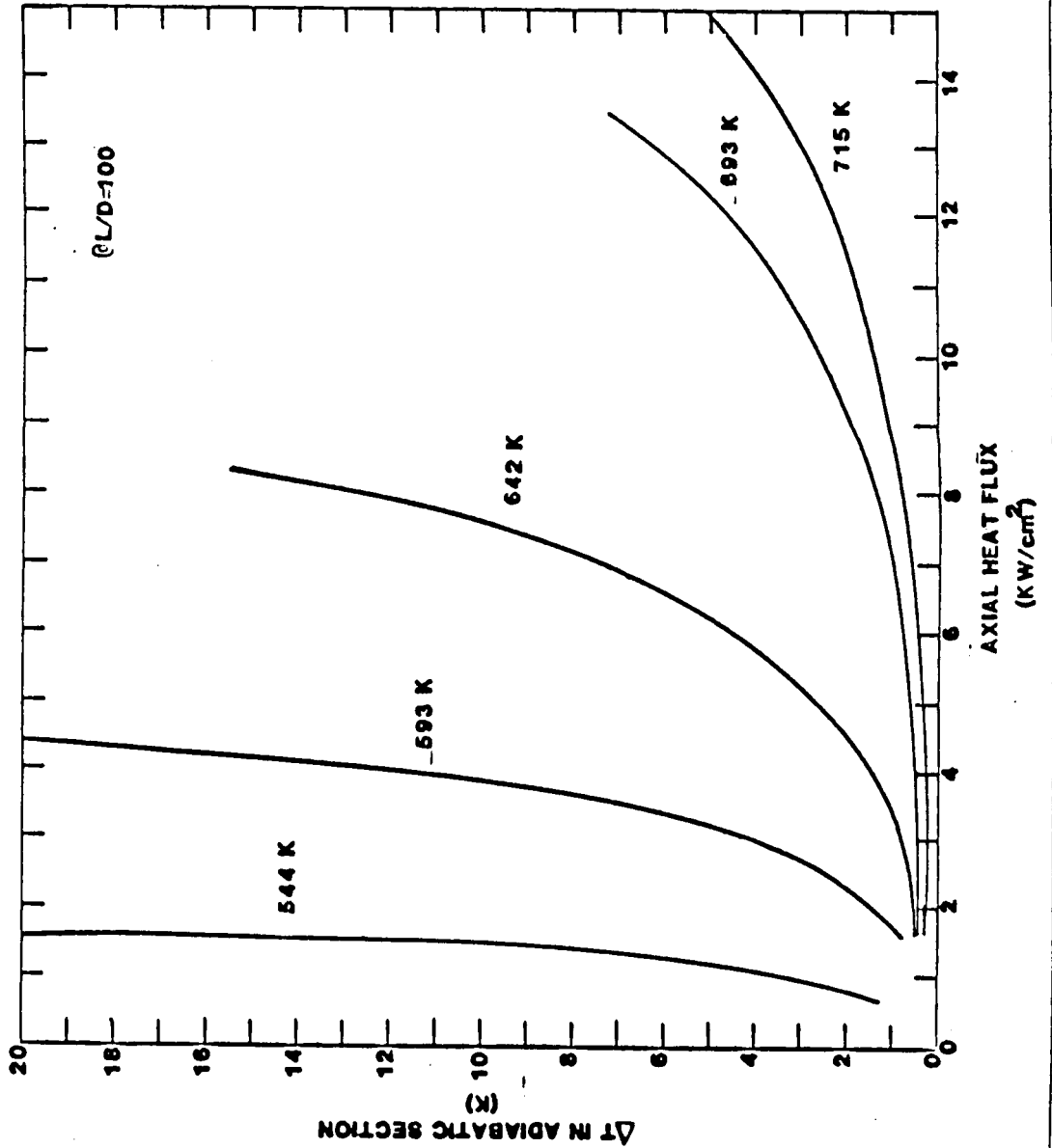


Fig. 4.3.25

11/13/84

# HEAT PIPE TRANSPORT CAPABILITY MERCURY WORKING FLUID



# HEAT PIPE PROGRAM OUTPUT

## HEAT PIPE RESULTS AT 264000 WATTS

EVAPORATOR LENGTH 450 CM WALL MATERIAL MOLYBDENUM  
 ADIABATIC LENGTH 750 CM WICK STRUCTURE 2  
 CONDENSOR LENGTH 450 CM WORKING FLUID POTASSIUM  
 INSIDE DIAMETER 15.00 CM  
 WALL THICKNESS 0.0050 CM EXT EVAP TEMP 820 K OR 547 C  
 WALL EMISSIVITY 0.8500 22 ARTERIES 0.6350 CM I.D.

TEMPERATURES ARE KELVIN, PRESSURES ARE DYNES/SQ CM

547.00 EXTERNAL EVAPORATOR 0.0499 DELTA-T EVAP WALL  
 545.60 BEG EVAP VAPOR TEMP 0.9506 DELTA-T EVAP WICK  
 627.88 EVAP-ADB VAPOR TEMP 0.4000 EVAPORATION DELTA-T  
 514.65 ADB-COND VAPOR TEMP 0.4000 CONDENSATION DELTA-T  
 521.75 FINAL COND VAPOR TEMP 0.9417 DELTA-T COND WICK  
 520.36 EXTERNAL CONDENSER 0.0496 DELTA-T COND WALL

26.64 TOTAL DELTA-T

VAPOR PRESSURES: VAPOR PRESSURE DROPS: LIQUID PRESSURE DROPS:

83442 BEG EVAP 19757 EVAP INERTIAL 714 EVAP ARTERY  
 63511 EVAP-ADB 174 EVAP VISCOUS 473 EVAP WICK  
 51370 ADB-COND 12141 ADB VISCOUS 2417 ADB ARTERY  
 57621 FINAL COND 3169 COND VISCOUS 734 COND ARTERY  
 -9420 COND INERTIAL 486 COND WICK

161909 COND CAPILLARY

4.011 KILOGRAMS PIPE  
 36.749 KILOGRAMS WICK  
 11.626 KILOGRAMS ARTERIES  
 3.106 KILOGRAMS FLUIDCHARGE

55.491 KILOGRAMS TOTAL MASS

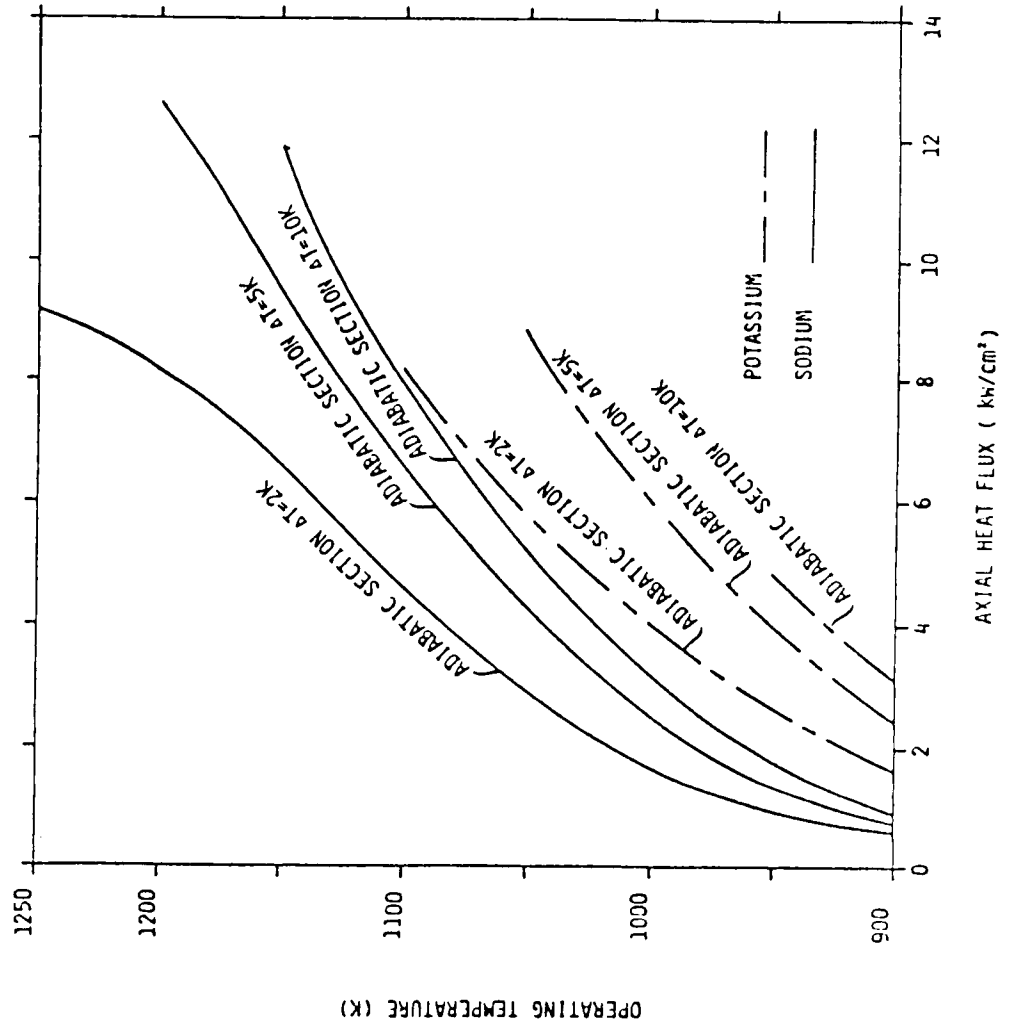
PIPE WILL RADIATE 12896 WATTS ALONG AN AREA OF CONDENSER LENGTH X PIPE O.D.  
 POWER EATING 1493.931 WATTS/SQUARE CM

There doesn't seem to be an adequate inorganic radiation resistant heat pipe working fluid, from a heat carrying areal distribution standpoint, below ~800 K. The effective use of a heat pipe heat rejection (transport) system, whatever the configuration, will be limited to those power conversion cycles with a heat rejection temperature  $\geq 800$  K (minimum cycle heat rejection temperature of about 850-875 K). From a transport performance standpoint, potassium is the working fluid of choice up to  $\approx 1100$  K where its vapor pressure is 2 atmospheres. As seen in Fig. 4.3.28, potassium actually has better axial heat transport properties than sodium up to its limit. But while potassium is limited to  $\approx 1100$  K, sodium has the ability to operate well over 1250 K and has better radial heat flux (power density limits). Sodium is generally more survivable for that reason.

From strictly a performance standpoint, it is beneficial to use potassium over sodium until its capillary limit is reached or its vapor pressure causes an excessive weight penalty due to increases in wall thickness. From a survivability standpoint, sodium would be the high temperature fluid of choice. As shown in Fig. 4.3.29, as temperature increases, the ability of sodium and potassium to carry heat ( $\text{kW}/\text{cm}^2$ ) also increases. Sodium, however, will operate at temperatures and heat fluxes where the capillary limit of potassium has been exceeded. Attempting to force a heat pipe to operate near the capillary limit leads to evaporator burnout due to a dry wick. This logic applies not only to potassium and sodium, but to all working fluids wherever they fall on the temperature scale. Based on system requirements, the choice of working fluid is dependent not only on performance, but on survivability considerations.

Triform Heat Pipe Radiator. Two heat pipe configurations were investigated. The first, the triform configuration [22], is shown in Fig. 4.3.30. In the stowed configuration, shown in Fig. 4.3.31, the heat pipes are bent at bellows locations to fit within the 4.5 m shuttle envelope. Figure 4.3.32 shows the side of one of the three wings of the triform radiator as conceived in this study. Upon deployment, the heat pipes can be extended out to a maximum length of 23.3 m. As shown, staying within a  $30^\circ$  shield cone angle the first shuttle-stowable segment has  $1123 \text{ m}^2$  of radiator area; the second segment has  $1957 \text{ m}^2$  of radiator area.

HEAT PIPE AXIAL HEAT FLUX VS OPERATING TEMPERATURE  
 (PIPE L/D = 100)

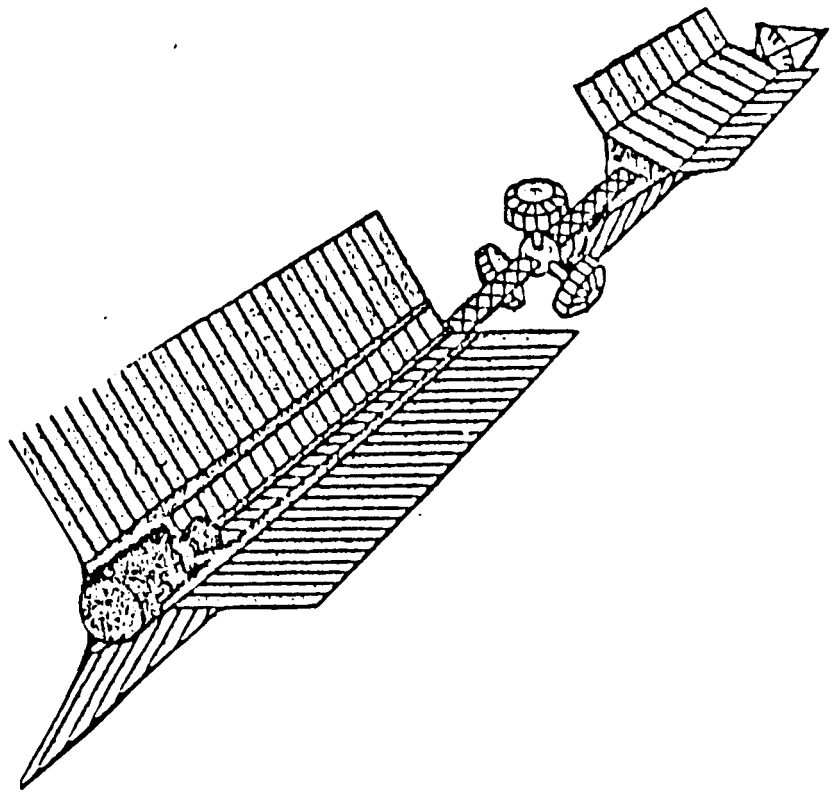


# HEAT PIPE AXIAL CAPABILITY - kW/cm<sup>2</sup>

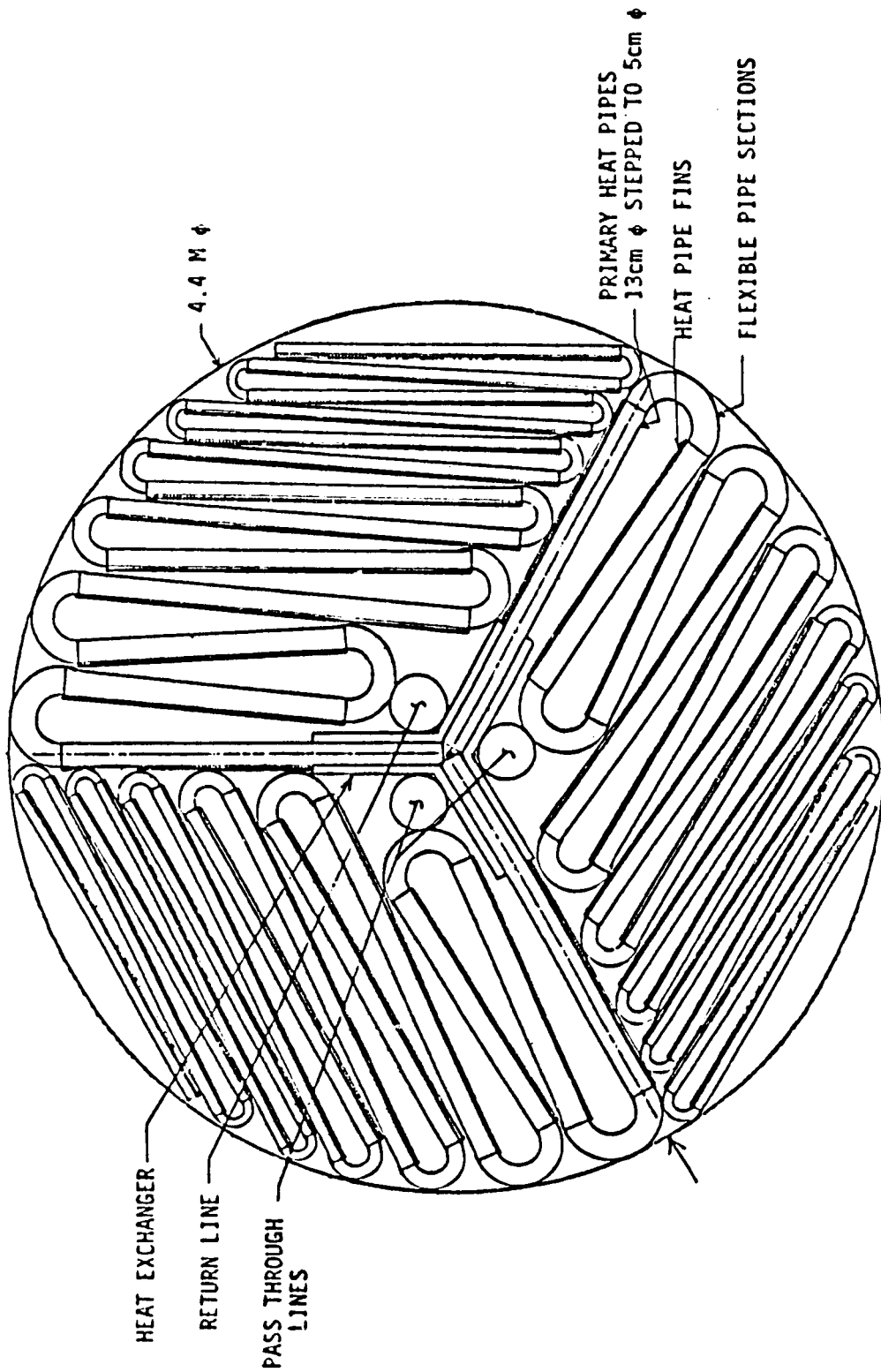
TEMP (K)	WORKING FLUID					
	Na	K	Cs	Rb	Hg	
1250	13.5					
1200	11.5					
1150	8.75					
1100	6.0	11.0				
1050	4.0	6.0				
1000	2.25	4.5				
950	1.25	3.5				
900	.75	2.25	2.5			
850		1.0	1.5	1.0		
800			.5	.5		
750						
700						12.5
650						7.0
600						3.0
550						1.5

Note:  $\Delta T = 4^\circ\text{C}$ ,  $L/D = 100$

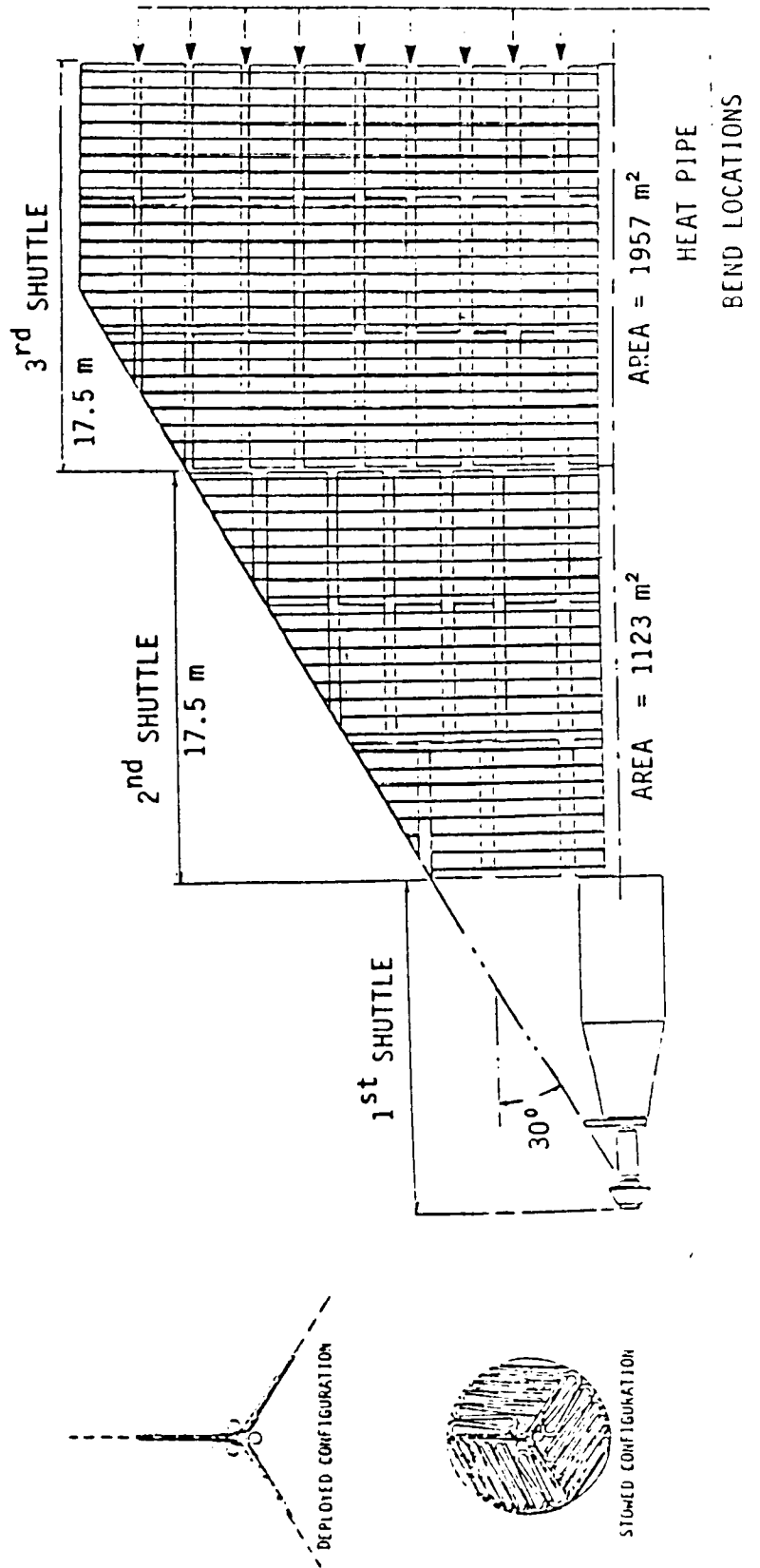
TRIFORM RADIATOR CONCEPT



# TRIFORM RADIATOR STOWED IN SHUTTLE



# TRIFORM RADIATOR CONCEPT



The triform is essentially a large pumped loop that uses long heat pipe fins rather than conduction fins. Different heat pipe working fluids can be used in different temperature regimes as shown in Fig. 4.3.33. This basic concept has been developed and tested by the Soviets, see Figure 4.3.34 [23]. This sensible heat scheme was examined here in an attempt to find a compatible radiator design for the Brayton system.

The preferred arrangement has three "wings" of heat pipes extending outward from a central heat exchanger. Travelling down the central heat exchanger, the individual heat pipe lengths increase, and collectively form a triangular radiator area, yet staying within the radiation scatter shield angle. Since the radial axis of each wing is rotated  $120^\circ$  from each other, each wing "sees" a portion of the adjacent wing. For this reason, the wing areas are multiplied by a view factor of  $\cos 30^\circ$  to obtain the projected radiating area. The triform concept is only slightly heavier than a flat radiator, but more area packs into a launch volume. It radiates more heat from a shielded cone and provides a basis for some structural rigidity.

From a laser survivability standpoint, heat pipes are capable of transferring heat from the side of the pipe being irradiated to the backside virtually instantaneously. Heat is also carried axially away from locations of local heat flux input at vapor sonic velocities. If the heat pipe wick is capable of replacing evaporated fluid in the local area of heat input, the temperature of the entire heat pipe will stabilize when it reaches a level which radiates this incremental quantity of incoming heat. For spot illumination, the temperature rise may be small since the local area of illumination is small in comparison to the total pipe area. For flood illumination, the heat pipe will rise in temperature until it is radiating, from both sides, the quantity of thermal input from one side.

The triform radiator has the inherently good survivability characteristics that can be built into alkali metal heat pipes. Potassium and sodium working fluids and refractory metal heat pipe envelopes have the ability to withstand substantial temperature excursions without forcing system shutdown or damage. However, the poor radial (evaporative) thermal input capacity at

CONCEPTUAL EXAMPLE OF MULTI FLUID HEAT PIPE TRIFORM ARRAY

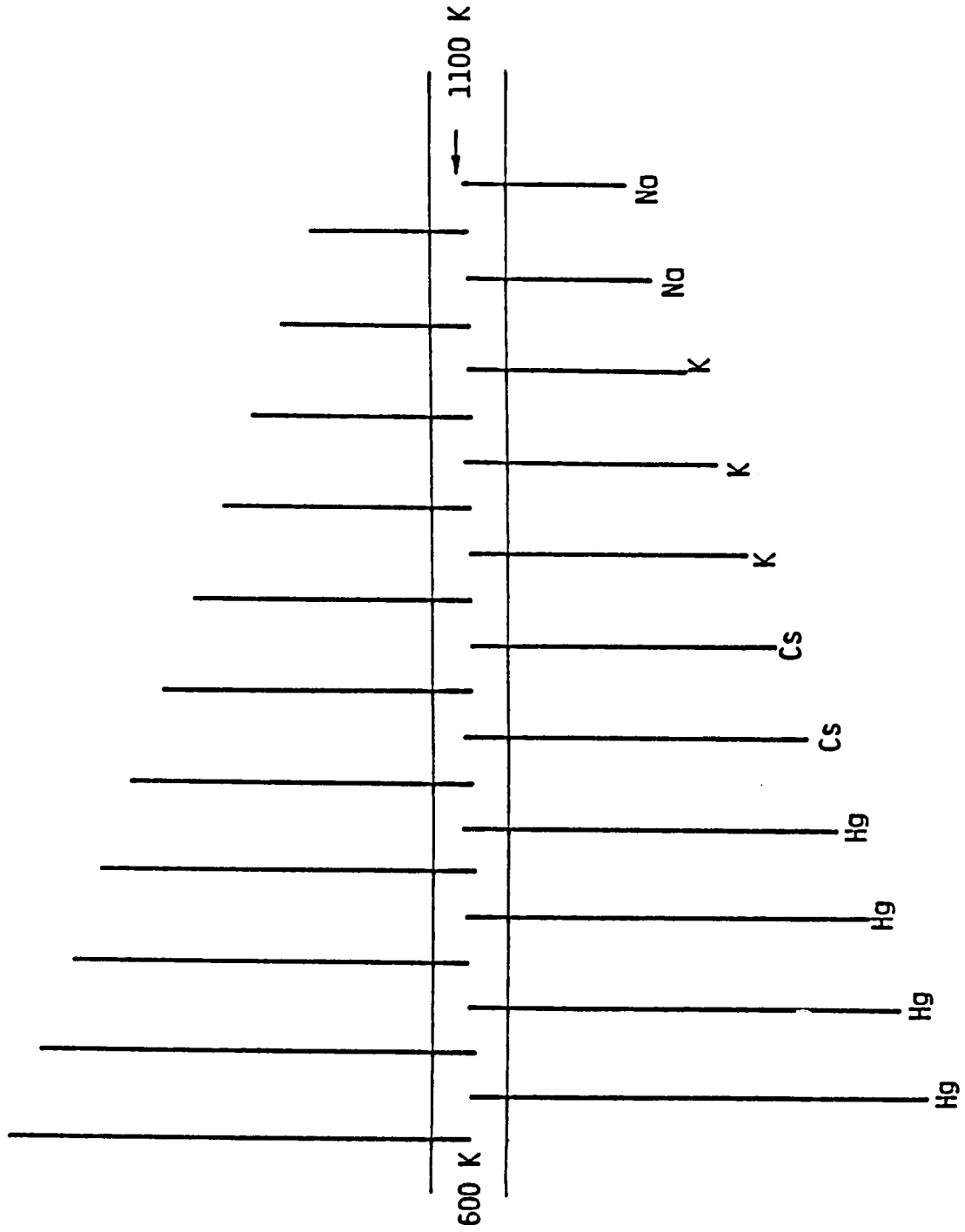
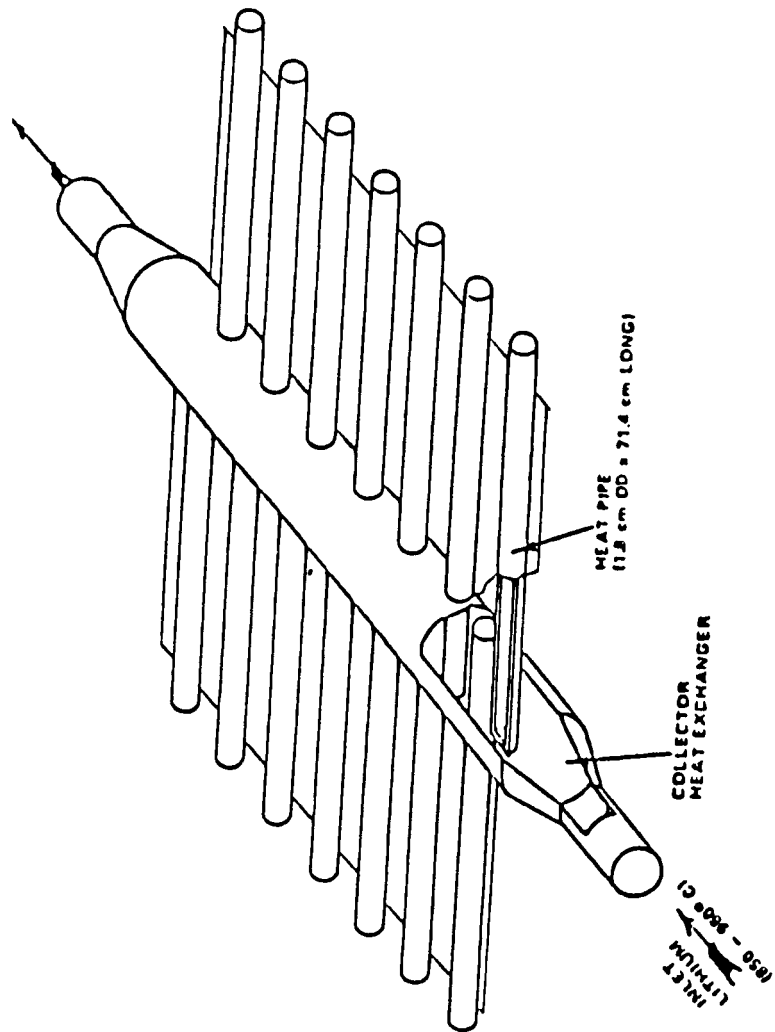


Fig. 4.3.33

SOVIET EXPERIMENTAL SPACE RADIATOR ASSEMBLY



bellows joints could limit survivability tolerance of the flat or triform geometries.

There is a large amount of redundancy built into the concept. Heat passes out of the central heat exchanger, across a pressure boundary joint into individual heat pipes which make up the panels of a wing. Should any one heat pipe be compromised, only the pressure boundary of the individual pipe is breached. Many pipes would have to be lost before a significant loss in heat rejection capacity is realized. The dominant weakness of this concept is the necessity to weld large liquid metal filled piping in space in order to make up radiators large enough for a 10 MWE system. The second inherent disadvantage is the large pumping power and sensible heat loss of the NaK fluid transporting heat from the power conversion system to the extremities of the radiator. The long distribution headers are heavy because their vulnerability to micrometeorite puncture must be reduced to  $\leq 1\%$ . This concept will be used in this study only for power systems that require radiators to operate at minimum temperatures below about 850 K.

Extendable Heat Pipe Radiator. A model of a telescoping heat pipe array concept under development by SPI is shown in Fig. 4.3.35. Cylindrical radiator segments, up to 18 m in length, nest within one another at launch and are then extended in space, similar to a telescope, to form an extended-area radiator. The design leaves a large volume available in the center for the reactor and power conversion subsystems and for additional payload. Heat leaving the condenser of one heat pipe is transported across a mechanical joint to the evaporator of the subsequent heat pipe. The key to this radiator is a reliable, high heat flux, low thermal impedance joint between successive heat pipe radiator segments. This joint, which can be made in space after deployment, will allow very large telescoping boom radiators to be packaged within the space shuttle.

The telescoping heat pipe design, and numerous non-deployable heat pipe designs, use a circular grouping of heat pipes to radiate heat outward. Table 4.3.1 shows the result of a comparable analysis of various circular groupings of heat pipes.

ORIGINAL PAGE IS  
OF POOR QUALITY

3-5 MWe, SHUTTLE-STOWABLE, TELESCOPING RADIATOR

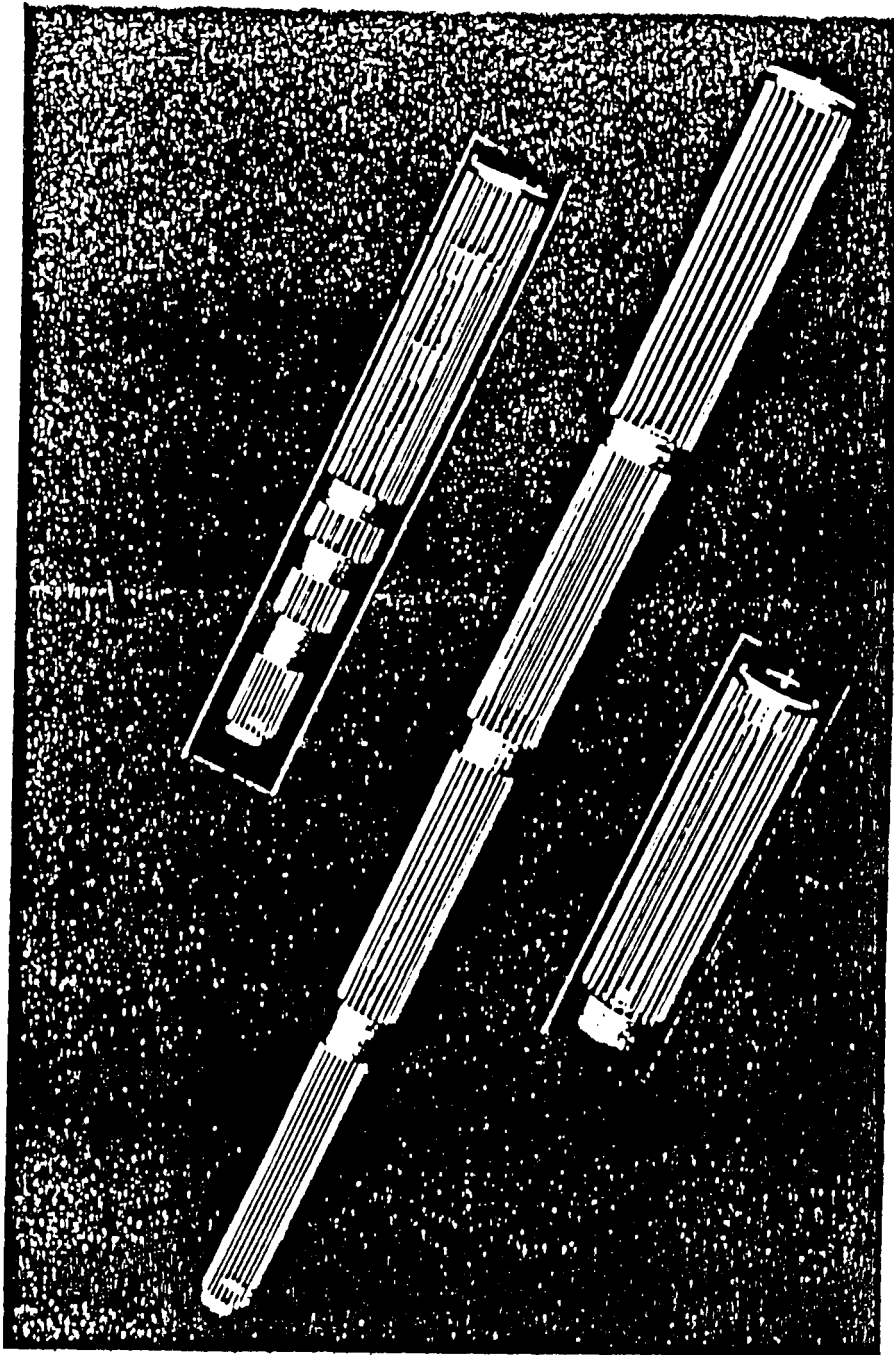


Fig. 4.3.35

# SPECIFIC WEIGHTS OF CIRCULAR ARRAYS OF HEAT PIPES

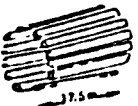
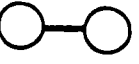
			No ARMOR			Be SHIELD	
TUBES ON 4M Ø CIRCLE, 17.5 M LONG 	RADIATING AREA (M <sup>2</sup> )	EXPOSED AREA PER TUBE (M <sup>2</sup> )	ARMOR THICKNESS (CM)	WEIGHT (KG)	WT/AREA (KG/M <sup>2</sup> )	WT (KG)	WT/AREA (KG/M <sup>2</sup> )
1. 126 TUBES, 10 CM Ø 	225	1.75	.163	10,939	48.6	4,899	21.8
2. 32 TUBES, 20 CM Ø FIN EFF = .8 FIN EFF = .2 	202	3.5	.208	72,736	360	68,390	339
	134	3.5	.208	9,610	71.7	5,272	393
3. 32 TUBES, 20 CM Ø 19 TUBES, 25.7 CM Ø 80 % REFLECTION OF BACK SURFACE 	202	3.5	.208	6,887	38.0	3,612	17.9
	193	4.5	.225	6,440	33.4	2,977	15.4
4. 32 TUBES, 20 CM Ø 14 TUBES, 30 CM Ø 	140	4.38	.225	7,478	53.4	2,858	20.4
	102	7.3	.244	5,262	51.6	1,980	19.4
5. 32 TUBES, 20 CM Ø 	225	0	2 @ .018	4,490	20.0	4,490	20.0

TABLE 4.3.1

The first design considers 10 cm  $\phi$  heat pipes, side by side, each pipe 17.5 m long on a 4 m  $\phi$  circle. A cross section of this circular array of heat pipes is shown in Fig. 4.3.36. Using niobium as the heat pipe material, a heat pipe thickness of .163 cm is required on the exposed circumference for protection against meteoroids and debris. Probability of no critical damage was arbitrarily set to .85 for 10 years. This criteria yields a specific weight of 48.6 kg/m<sup>2</sup> using Nb armor and 21.8 kg/m<sup>2</sup> using Be armor.

The second tube design uses fins of varying effectiveness between heat pipes twice the diameter of Design #1. The mass penalty of high effectiveness fins overwhelms the benefit of increased radiator area. A less effective fin actually works better from a mass to area standpoint, giving a specific weight of 71.7 kg/m<sup>2</sup> using Nb armor and fins and using Be armor and fins.

Design #3, Fig. 4.3.37, is an SPI concept which uses a shaped reflector to reflect 80% of the heat produced on the back side of the tube. This design produces a radiator specific weight of 33.4 kg/m<sup>2</sup> using Nb and 15.4 kg/m<sup>2</sup> using Be.

SPI design #4 uses no fins or reflectors. The back side of the tube (facing the interior of the cylindrical geometry) radiates out between the tubes on the other side of the tube circle. This design, designated as the skip-tube concept, is the most simple in nature but is relatively heavy at 51.6 kg/m<sup>2</sup>, when using the niobium wall thickness as armor and is competitive at 14.4 kg/m<sup>2</sup> using Be armor. The view factor geometry upon which this concept is based is shown in Fig. 4.3.38.

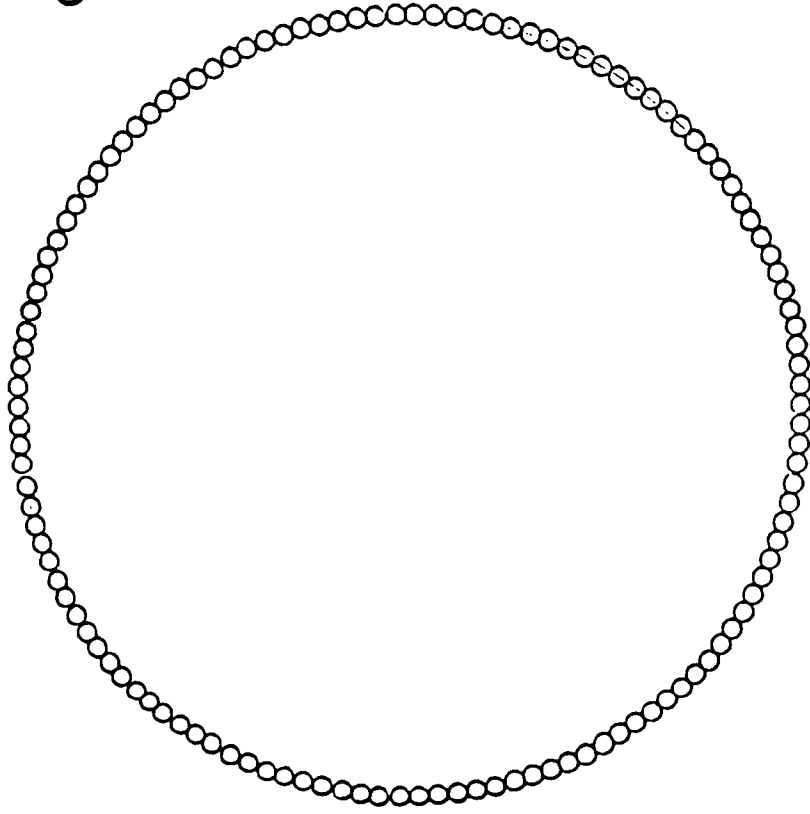
Design #5, another SPI concept, uses large heat pipe headers and small lateral heat pipes which act as light, highly conductive fins and as meteoroid/debris bumpers to the main heat pipe headers. This design, Figure 4.3.39, has a specific weight value of 20.0 kg/m<sup>2</sup> when using all Nb pipes and fins.

Using the beryllium shield concept of meteoroid/debris protection, significant weight savings are achieved. For example, the specific weight of arrangement #3, the shaped reflector, drops to 15.4 kg/m<sup>2</sup>. This concept

**SOLID TUBE ARRANGEMENT**

**CIRCLE DIAMETER = 4m**

**132 TUBES,  $d = 10$  cm**



SPECIFIC RADIATOR REQUIREMENTS  
OF SPACE POWER SYSTEMS AND PAYLOADS  
VS.  
RADIATOR TEMPERATURE (U)

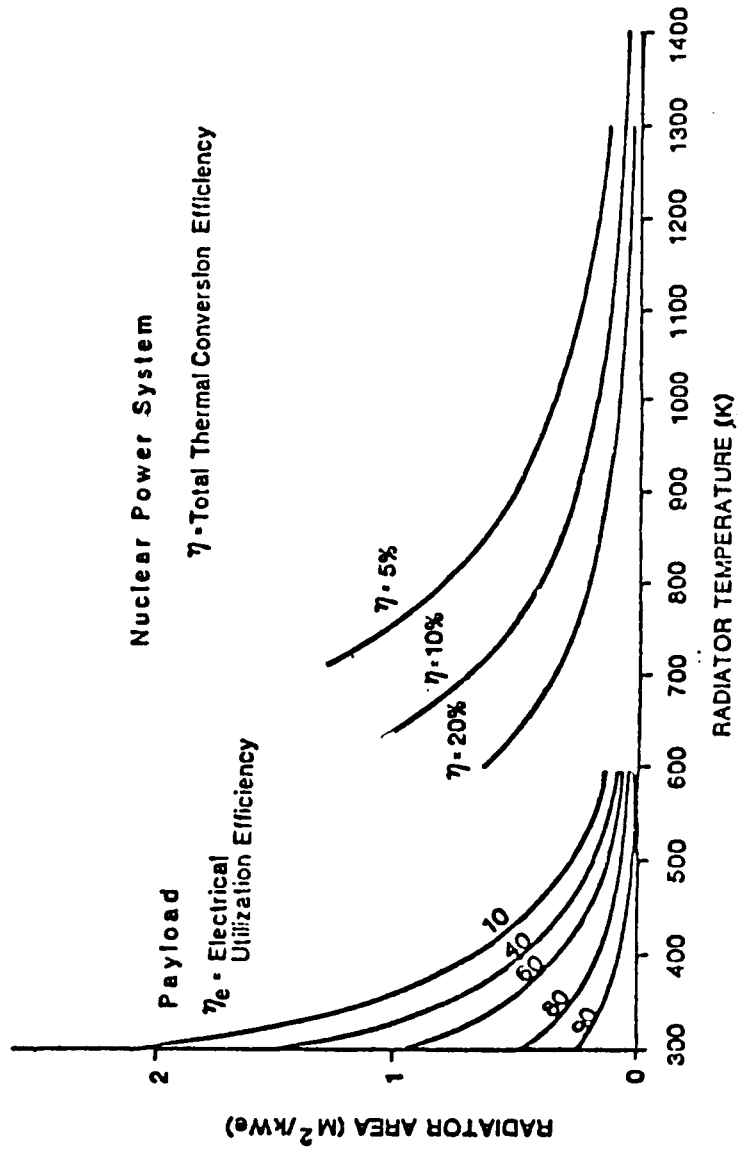


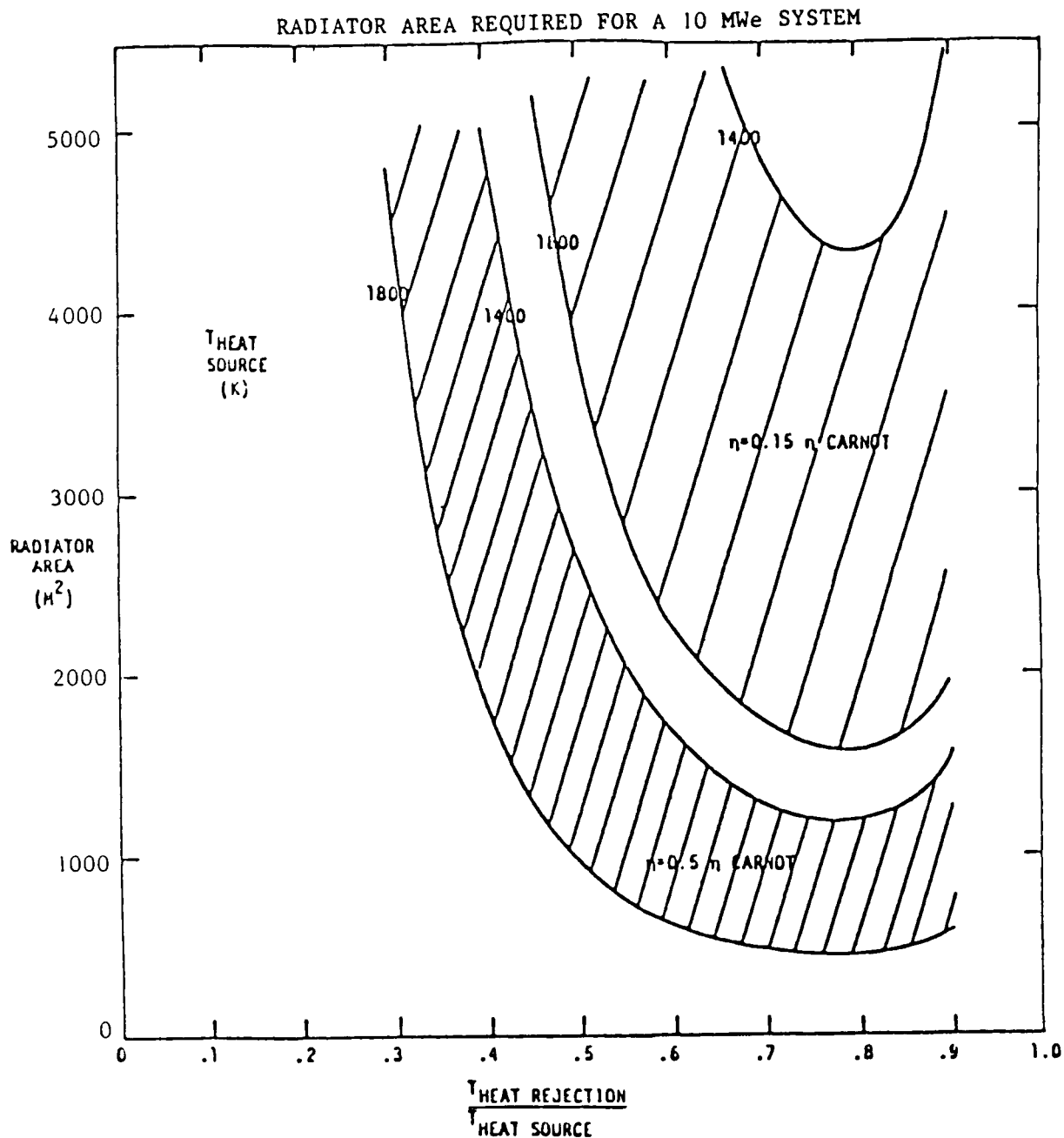
Fig. 4.3.1

they produce about 3 to 19 times as much waste heat as they do electric power.

For high power systems, there is an incentive to go to the highest possible heat rejection temperature to minimize radiator area. However, the energy conversion efficiency is reduced by increasing the heat rejection temperature. Most energy converters perform at a nearly constant fraction of Carnot efficiency, i.e. they perform similarly at various absolute operating temperatures. Thus the system efficiency decreases as the heat rejection temperature is increased. As the efficiency decreases, the waste heat for each kilowatt of electric power produced increases, and the required radiator size and mass increases. But radiator size decreases inversely to the fourth power of temperature. Thus, there is an optimum heat rejection temperature for minimum radiator size.

Figure 3.2, presented previously, showed an idealized power output per unit of radiator area for the optimized rejection temperature. A more realistic evaluation of the optimum is shown in Fig. 4.3.2, where the radiator area required for a 10,000 kWe system is shown as a function of the ratio of heat rejection to heat source temperature. Representative good heat engine (50% of Carnot efficiency) and poor heat engine (15% of Carnot efficiency) cases are shown for heat source temperatures of 1800 K and 1400 K. As can be seen, raising the heat engine effectiveness (the fraction of Carnot efficiency) is very important to realizing decreases in the radiator size and mass. Note that all of the curves show a minimum in the radiator area at  $T_C/T_H = 0.75-0.80$ , i.e.,  $\eta_c = 25-20\%$ . Thus, if the heat rejection temperature is increased in order to make the radiator area acceptable, it is also necessary to simultaneously increase the heat source temperature.

Several types and configurations of heat rejection systems were considered in this study. No single design is optimum for all power conversion systems. Radiator fluid operating temperatures ranged from 530 K for the Brayton Cycle to 1060 K for the Thermionic Cycle. The amount of heat rejected varied from 19 MW for the growth-design Stirling system to 89 MW for the thermionic system. Promising concepts are specified in more detail



For Radiator Dominated Systems, The Optimum Heat Rejection Temperature is  $\sim 80\%$  of the Heat Source Temperature

FIG 4.3.2

11/13/84

in the power conversion portion of this report, where the system-specific heat rejection parameters can be incorporated into the concept design.

A surprising result for a number of the systems is that the quantity of radiator area which can be taken up in a shuttle is constrained by the volume limit of the shuttle bay and not by the weight limit. Efforts have been expended and attractive claims have been made by proponents of individual heat rejection systems about low radiator system specific weights ( $\text{kg/m}^2$ ). There is no need to defend or deny these claims in this report. Because of the relatively large amount of heat to be rejected, large radiator areas are required. Most of the literature published concerning particular radiator concepts are analytical in nature and do not deal with the system hardware engineering problems packaging and deploying a survivable design within practical limits. We have taken system packaging concepts, when they exist (e.g., liquid droplet, tri-form radiators), scaled them to the multimegawatt regime, and tried to determine upper limit shuttle-packagable sizes. When conceptual packaging designs did not exist (e.g., moving belt, rotating disk), we attempted our own design of a shuttle-stowable package and estimated an upper limit on deliverable radiator area.

Unless otherwise noted, surfaces of metallic radiators are assumed coated with an emissivity layer to enhance hemispherical emissivity to .85, corresponding to reported experimental data [1] for iron titanate and calcium titanate. In these tests iron titanate on AISI-310 stainless steel operated for 5300 hours at 1006 K in a vacuum of  $\sim 2 \times 10^{-8}$  torr maintaining an emissivity of .88 or better. Another coating of iron titanate on Nb-1Zr performed for 6250 hrs at 1200 K, yielding an emissivity of .85 or better. Calcium titanate was tested on AISI-300 stainless steel for 6300 hrs at 2005 K with an emissivity of .90 throughout the test. Excellent coating adherence was reinforced by the ability of the coatings to be successfully thermal cycled from operating to room temperature. As still another possibility, Fig. 4.3.3 shows measured emissivity data for  $\text{ZrB}_2$  [2] over a broad temperature range.

# ZIRCONIUM DIBORIDE - SPECTRAL EMISSIVITY

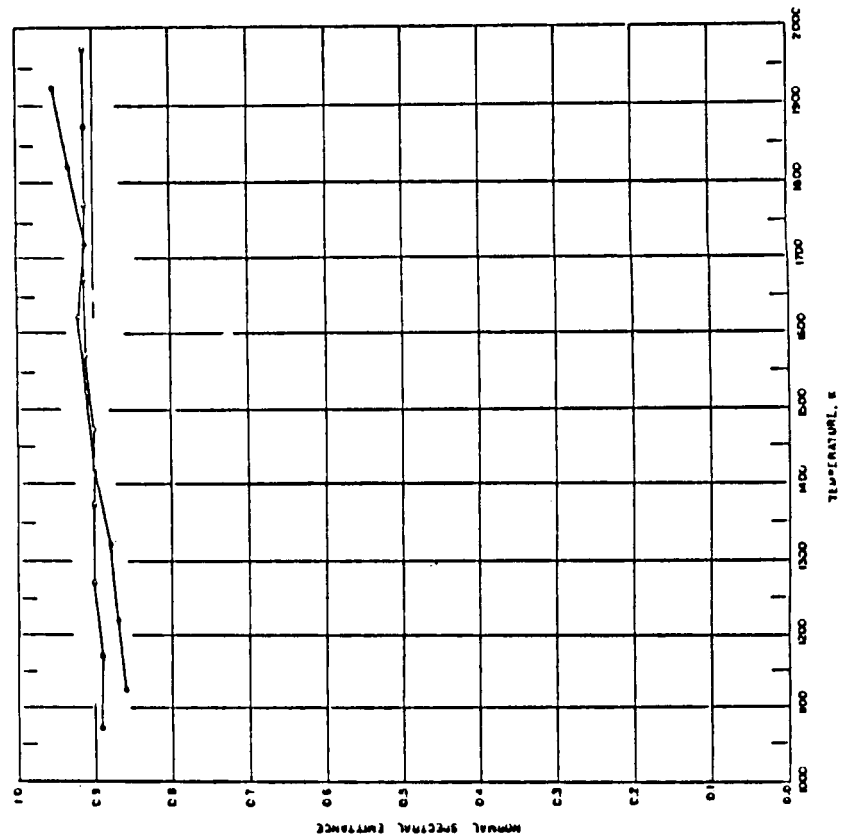


Fig 4.3.3

The available emissivity data support the assumption that an effective, overall emissivity of .85 can be established and maintained on the radiator heat rejection surfaces.

Where weight calculations are made, meteoroid armor requirements were evaluated using the equation below [3]:

$$\delta = \gamma_R^a \left( \frac{\rho_p}{\rho_a} \right)^{1/2} \left( \frac{V_p}{C_a} \right)^{2/3} \left( \frac{6}{\pi \rho_p} \right)^{1/3} \left( \frac{E \alpha A_v t}{-\ln P_0} \right)^{1/3 \beta} \left( \frac{2}{3n\theta\beta + 2} \right)^{1/3 \beta} \left( \frac{T}{T_R} \right)^{1/6}$$

where

- $\delta$  - armor thickness (cm)
- $\gamma_R$  - room temperature cratering coefficient
- $a$  - rear surface damage thickness factor
- $\rho_p$  - meteoroid average density (0.5 g/cm<sup>3</sup>)
- $\rho_a$  - armor density (g/cm<sup>3</sup>)
- $V_p$  - meteoroid average velocity (20 km/s)
- $C_a$  - sonic velocity in armor (km/s)
- $E$  - armor earth shielding factor = 0.7621
- $\alpha$  - meteoroid flux constant (10<sup>-14.37</sup> g <sup>$\beta$</sup> /m<sup>2</sup>·s)
- $A_v$  - vulnerable area (m<sup>2</sup>)
- $t$  - mission time (s)
- $P_0$  - design probability of no critical damage
- $n$  - damage factor for oblique impact = 1.0
- $\theta$  - penetration constant = 0.667
- $\beta$  - meteoroid flux constant = 1.213
- $T$  - armor temperature (K)
- $T_R$  - room temperature (K)

Using the above armor equation, Fig. 4.3.4 through 4.3.9 were generated. For various heat rejection system materials, these curves predict armor requirements for a given probability of no critical damage and exposed area. The curves assume a 7-year lifetime at an orbital altitude of 1000 km.

METEOROID PROTECTION ARMOR REQUIREMENTS - MOLYBDENUM

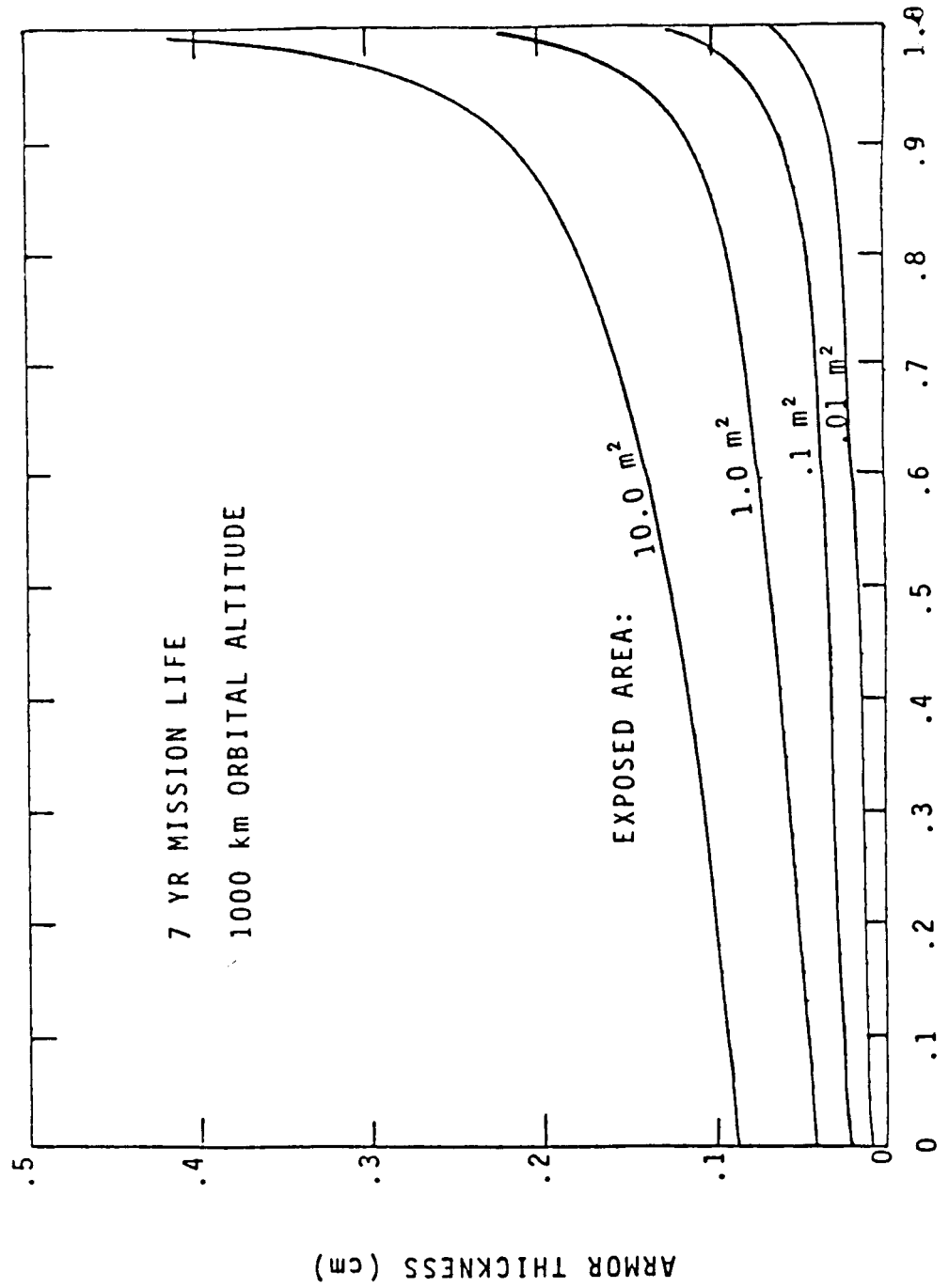


FIG. 4.3.4

# METEOROID PROTECTION ARMOR REQUIREMENTS - NIOBIUM

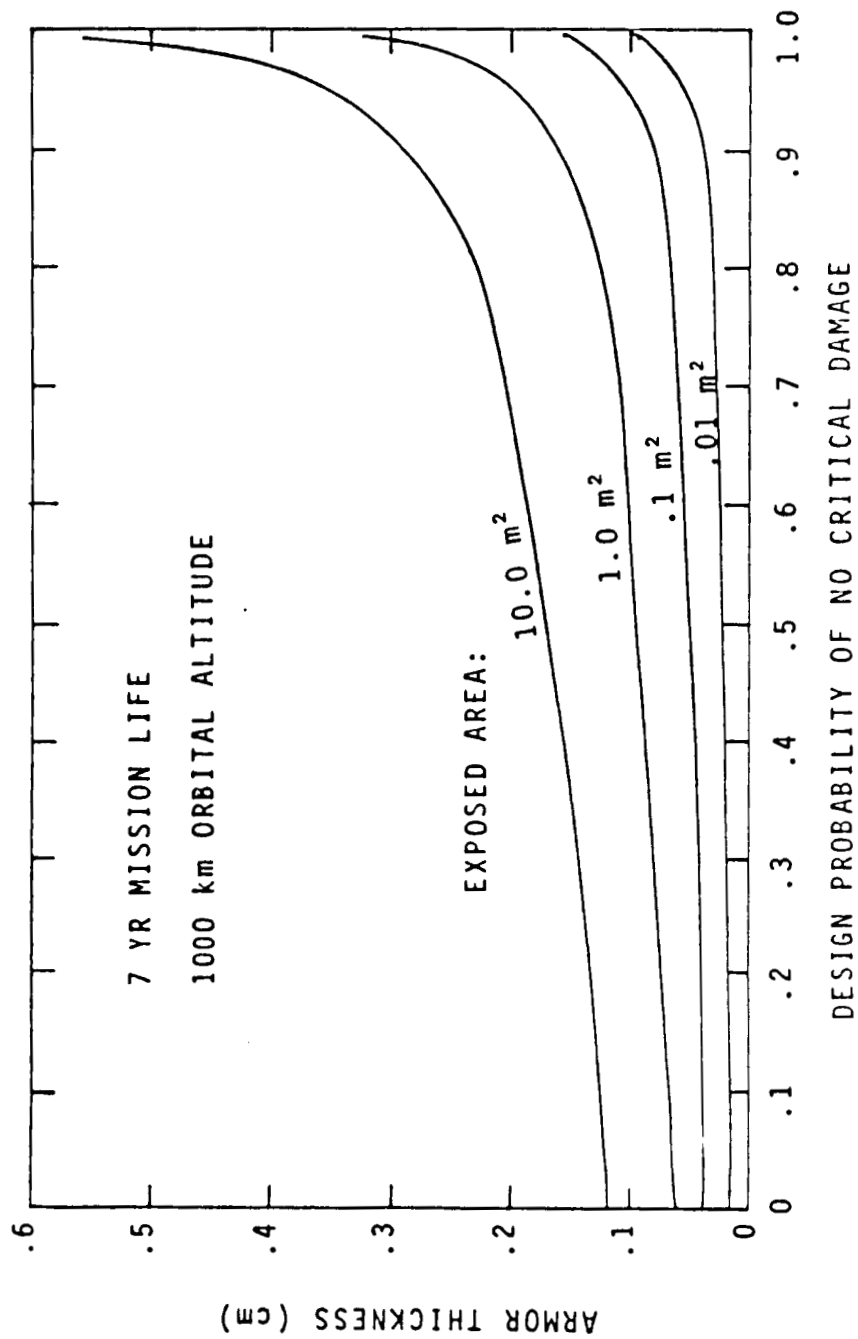


FIG 4.3.5

METEOROID PROTECTION ARMOR REQUIREMENTS - TYPE 316 STAINLESS STEEL

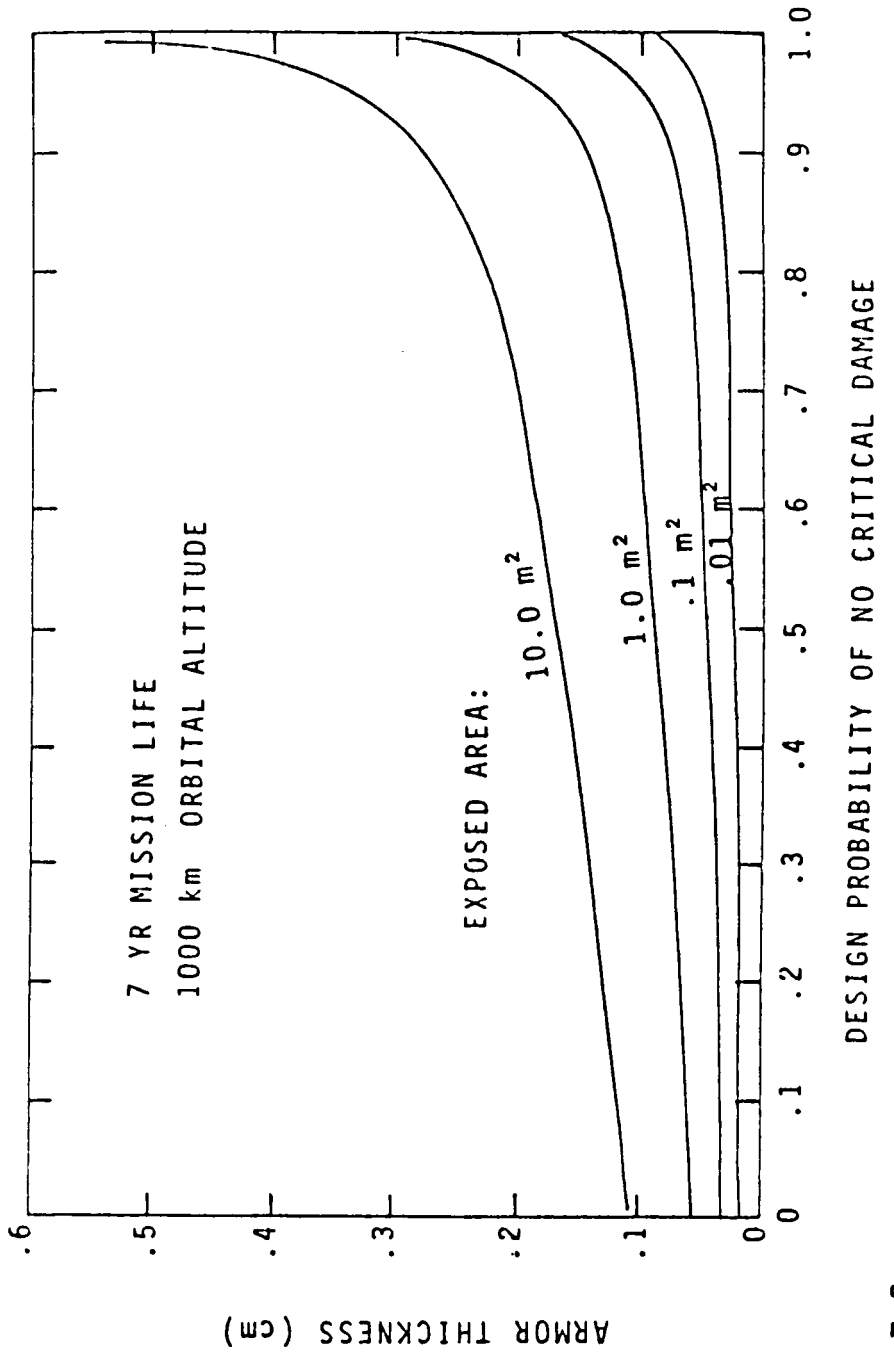
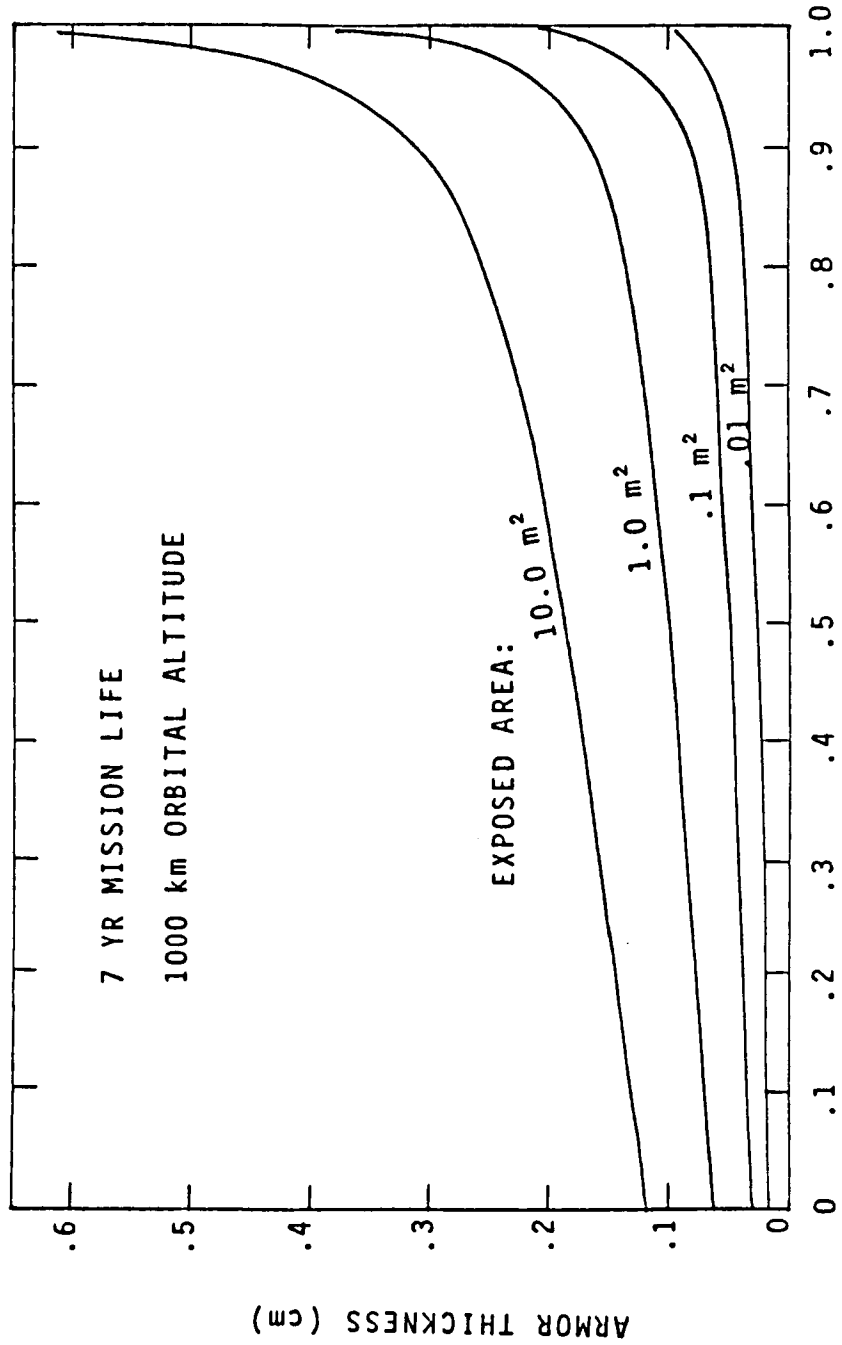


FIG 4.3.6

METEOROID PROTECTION ARMOR REQUIREMENTS - TITANIUM

7 YR MISSION LIFE  
1000 km ORBITAL ALTITUDE



DESIGN PROBABILITY OF NO CRITICAL DAMAGE

FIG 4.3.7

# METEOROID PROTECTION ARMOR REQUIREMENTS ALUMINUM (2024-T6)

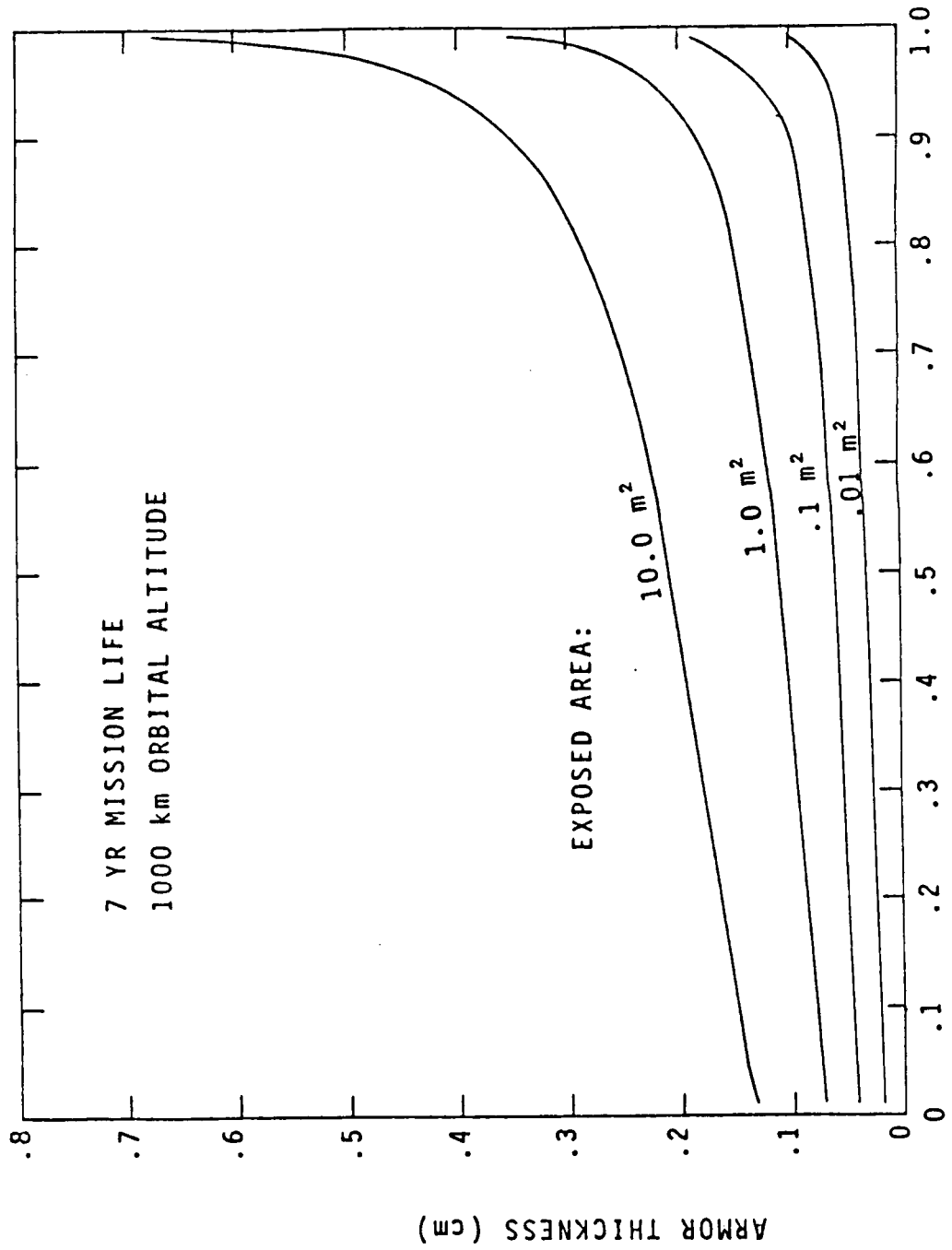


FIG 4.3.8

METEOROID PROTECTION ARMOR REQUIREMENTS - COPPER

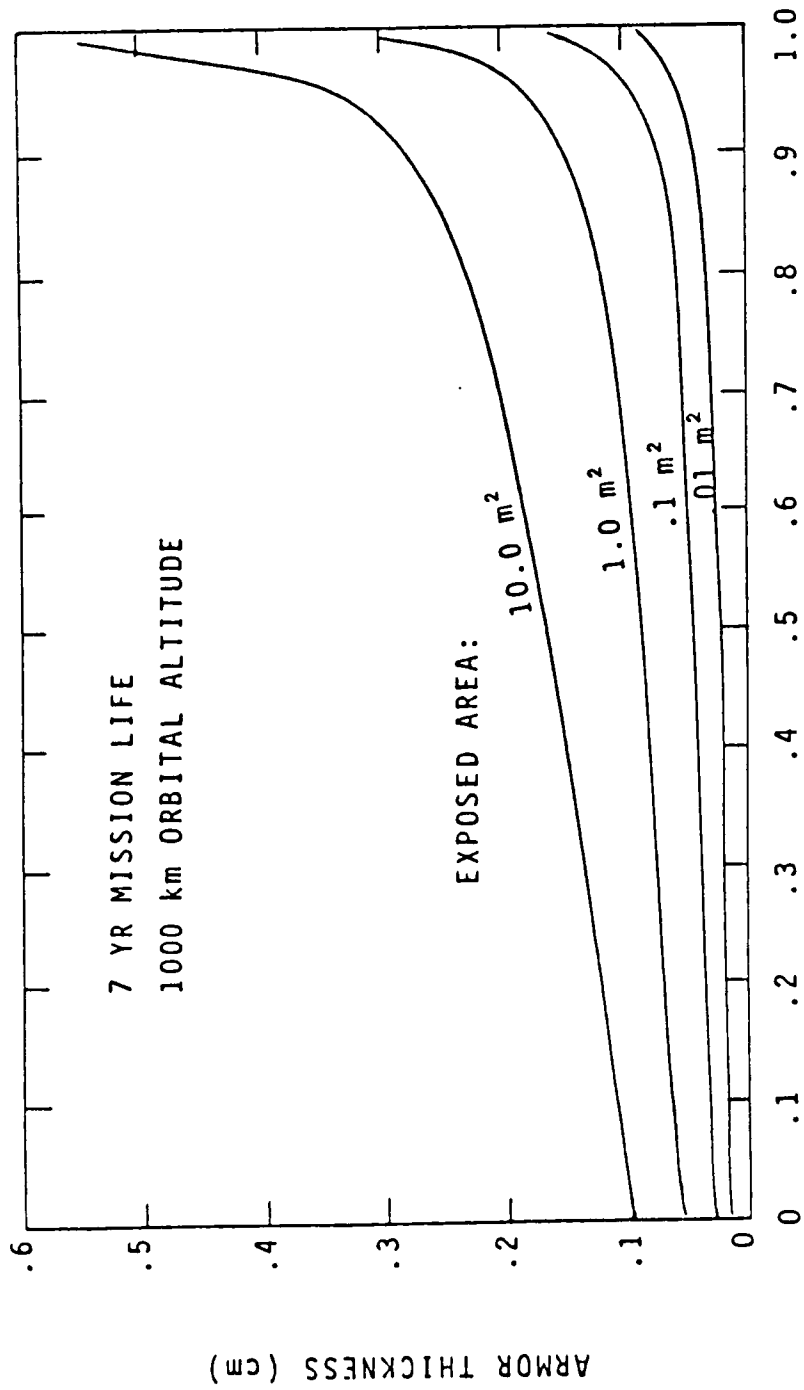


FIG 4.3.9

The armor concept introduced here depends on the kinetic energy of the meteoroid being dissipated by strain energy through the deformation of the material wall. Another method is to allow the kinetic energy of the meteoroid to be absorbed by the heat of fusion and/or heat of vaporization of a sacrificial material. On a mass basis, lithium and beryllium have attractive heats of vaporization at 4640 cal/gm and 8211 cal/gm respectively. By placing a sufficient thickness of beryllium around the heat pipe, sufficient heat capacity, through vaporization, can be incorporated into the design to dissipate the energy of incoming meteoroids/debris. Because of the good thermal conductivity of beryllium, there is only a 4°C temperature drop across beryllium when radiating at 1100 K.

By placing a sheath of molybdenum around the heat pipe and filling a specified annular gap with lithium, liquid lithium can also be used to protect the heat pipe. Although the lithium protects the heat pipe pressure boundary, the functionality of the heat pipe is lost at the location of impact. The hole created in the outer sheath allows the remaining liquid lithium to evaporate over time. By making compartments, or honeycombs, the radiating area lost can be minimized. The thickness of the outer sheath determines the mass and number of meteoroids which penetrate into the lithium. There is a tradeoff between this outer sheath thickness and the number of lithium-filled compartments needed. This tradeoff optimization has not been performed and deserves further study.

A far less hazardous material, calcium, may also be used for this purpose. Although its heat of vaporization, 918 cal/gm, is less than that of lithium and beryllium, it is significantly less toxic, easier to fabricate, and less expensive.

Using the heat of vaporization concept, the following procedure is used to calculate the thickness required to protect a subject radiator [2]:

1. Determine particle flux

$$N = \frac{1}{At \ln P_o} \quad \text{for } P_o \geq .8$$

where

N = particle flux, particles/m<sup>2</sup>-yr

A = exposed area, m<sup>2</sup>

t = time, yr

P<sub>o</sub> = probability of no critical damage

2. Using Fig. 4.3.10, determine the particle mass which corresponds to the calculated particle flux.
3. Using the equation below, determine the thickness of material necessary to dissipate the particle kinetic energy [4]:

$$d = \left( \frac{E}{\rho H_v} \right)^{1/3}$$

where

d = material thickness, cm

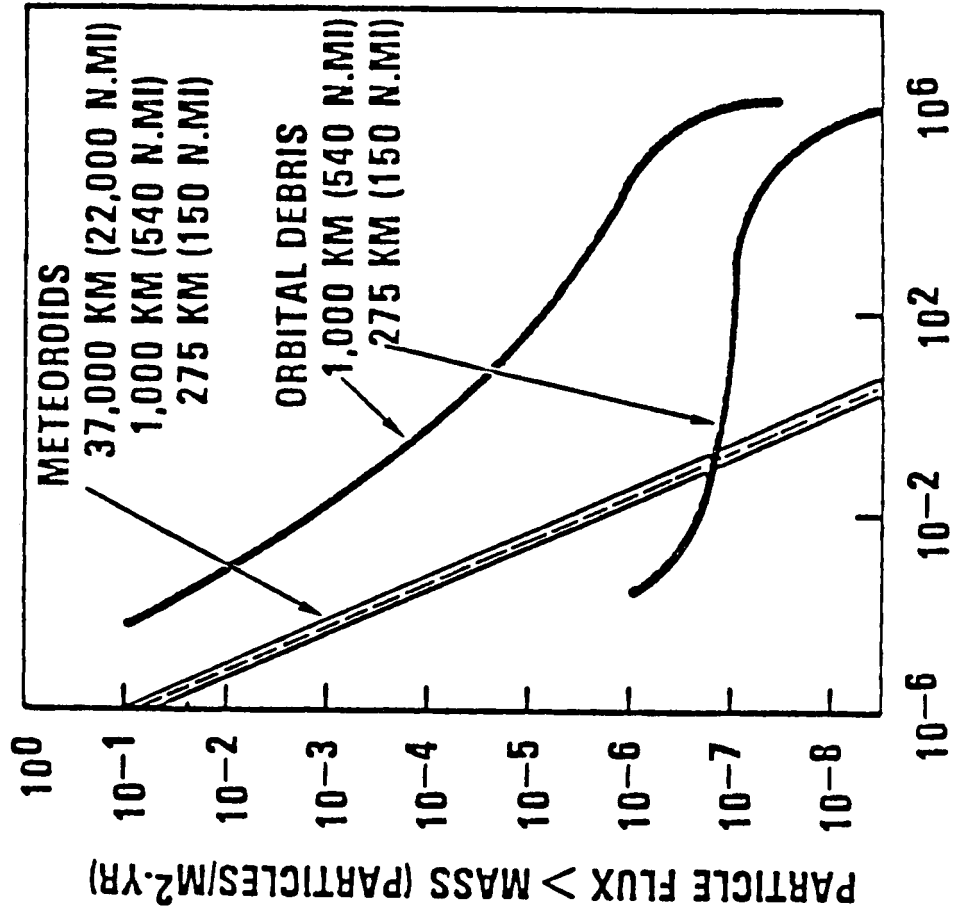
E = kinetic energy of particle, cal  
(20 km/s used as velocity)

ρ = density of material, gm/cc

H<sub>v</sub> = heat of vaporization of material, cal/gm

Comparative weight studies of these two concepts of meteoroid protection are performed in the portion of 4.3.2 dealing with heat pipe radiators.

# INTEGRAL FLUX OF METEORIDS AND ORBITAL DEBRIS PROJECTIONS FOR 1995\* (U)



\* NASA SP-8013

Fig. 4.3.10

### 4.3.2 Heat Rejection Systems

Several candidate heat rejection systems were studied. A technical description and evaluation of each system is presented below. Particular attention was paid to the ability of systems to be packaged into the shuttle envelope.

Rotating Disk. The rotating disk concept is shown schematically in Fig. 4.3.11. The working fluid is sprayed onto the inside of a thin metal disk, near the center. Centrifugal force, caused by the disk rotation, causes the condensate or liquid fluid to be driven outward toward a collector channel on the disc circumference where a stationary scoop retrieves the fluid. The disk radiates heat gained from the working fluid heat capacity or latent heat as the fluid travels outward. Punctures in the disk from meteoroid penetration do not impair the functionality of this concept when used with liquid only. Surface tension of the liquid working fluid is sufficient to prevent the fluid from flowing through the penetration. Using DOW 705 as the working fluid @  $\bar{T} = 357\text{K}$ , the vapor pressure is low enough that only minimal quantities of the working fluid are able to vaporize through the meteoroid punctures. The concept would not be useful as a condenser or gas working fluid cooler.

Reported specific weights of 1-2 kg/m<sup>2</sup> [5] are highly attractive from a weight standpoint. Packagability within the shuttle was not addressed. Fig. 4.3.12 is one concept where a disk of 17 m diameter could be stowed in the shuttle and then deployed in space. This design produces a radiator area of ~430 m<sup>2</sup> at the average referenced [1] temperature of 357 K. At this temperature, one disk would radiate ~250 kWt, while at an average radiating temperature of 750 K, the same disk would radiate ~ 6.5 MWt.

The concept is appealing and the claimed system weights yield attractive specific weight (kg/m<sup>2</sup>) figures. The concept is hindered by the small number of disks (and resulting low radiating area) which can be stowed into the shuttle. As a result, the rotating disk concept won't be considered as a candidate heat rejection system.

# ROTATING DISK RADIATOR (900 K BRAYTON CYCLE, DC 705 RADIATOR FLUID)

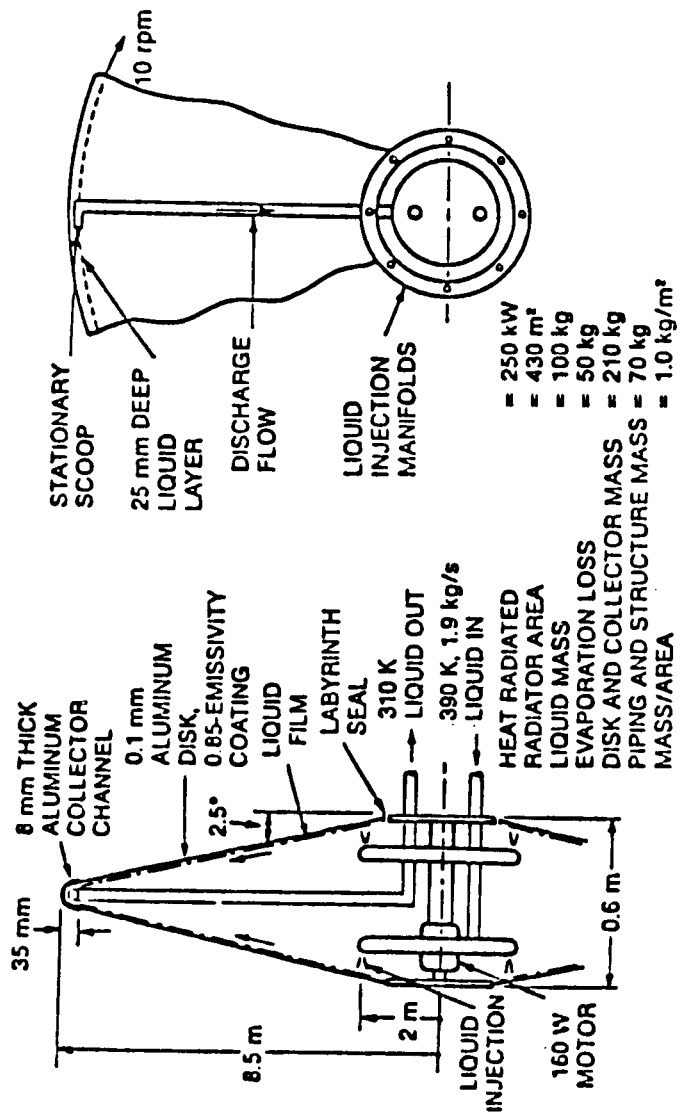


FIG 4.3.11

# ROTATING DISK RADIATOR

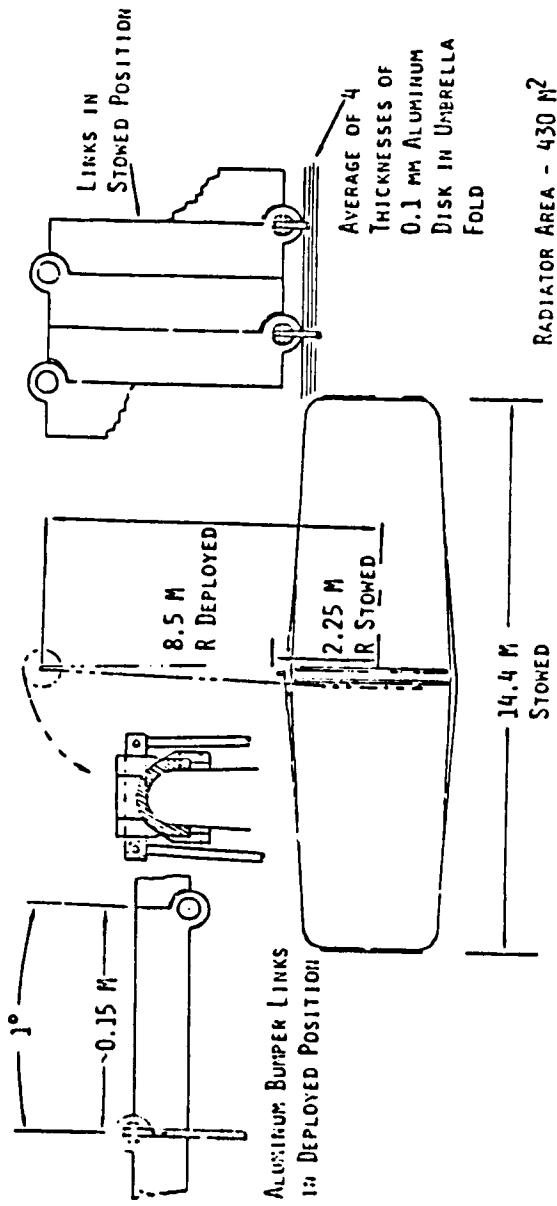


FIG 4.3.12

Liquid Droplets. Literature on liquid droplet radiators [6 through 17] would indicate that the technology may offer substantial weight and shuttle packaging savings over conventional radiators. In the liquid droplet system, minute liquid droplets ( $25 \mu\text{m} \geq d \geq 200 \mu\text{m}$ ) of high specific heat are directed, in a sheet, spray through space vacuum toward a collector to be cooled by direct radiation without evaporation and recaptured after traveling a specified distance. The system is illustrated, schematically, in fig. 4.3.13. Heat is radiated as the drop travels from the generator to the collector. The droplet offers a high surface area to weight ratio, reportedly leading to a light-weight radiator. Several configurations, using the liquid droplet concept, have been studied and are shown in Fig. 4.3.14. There seem to be many technology issues to resolve in the liquid droplet system. The major issues are described below.

Any working fluid utilized in the liquid droplet system will have functional constraints on the temperature range over which it can operate. The working fluid must not freeze or evaporate in its travel from generator to collector. The added complexity of designing a collector which would catch a mixture of solid and liquid droplets and then subsequently remelt the solid droplet for pumping overwhelms the potential benefit. The non-freezing requirement limits the allowable droplet transit time from generator to collector. Since the droplet is directly exposed to a space environment, its upper operating temperature is limited by evaporation losses due to vapor pressure. Fig. 4.3.15 [16] illustrates the range of operating temperatures for the most promising droplet fluids. Tin and lithium seem to hold the most promise for heat rejection temperature ranges of interest.

Individual droplets radiate most effectively when they are widely separated and the resultant view factor is large. This leads to undesirably large radiator areas. When droplets are grouped to form a sheet, the effective emissivity of the sheet exceeds that of the intrinsic emissivity of an individual droplet. Depending on the droplet sheet design, the sheet emissivity can be a factor of three greater than that of the intrinsic emissivity for low-intrinsic-emissivity surfaces [8]. To gain this advantage requires sheets containing 30 layers or more of droplets. From a

# DROPLET RADIATOR SCHEMATIC

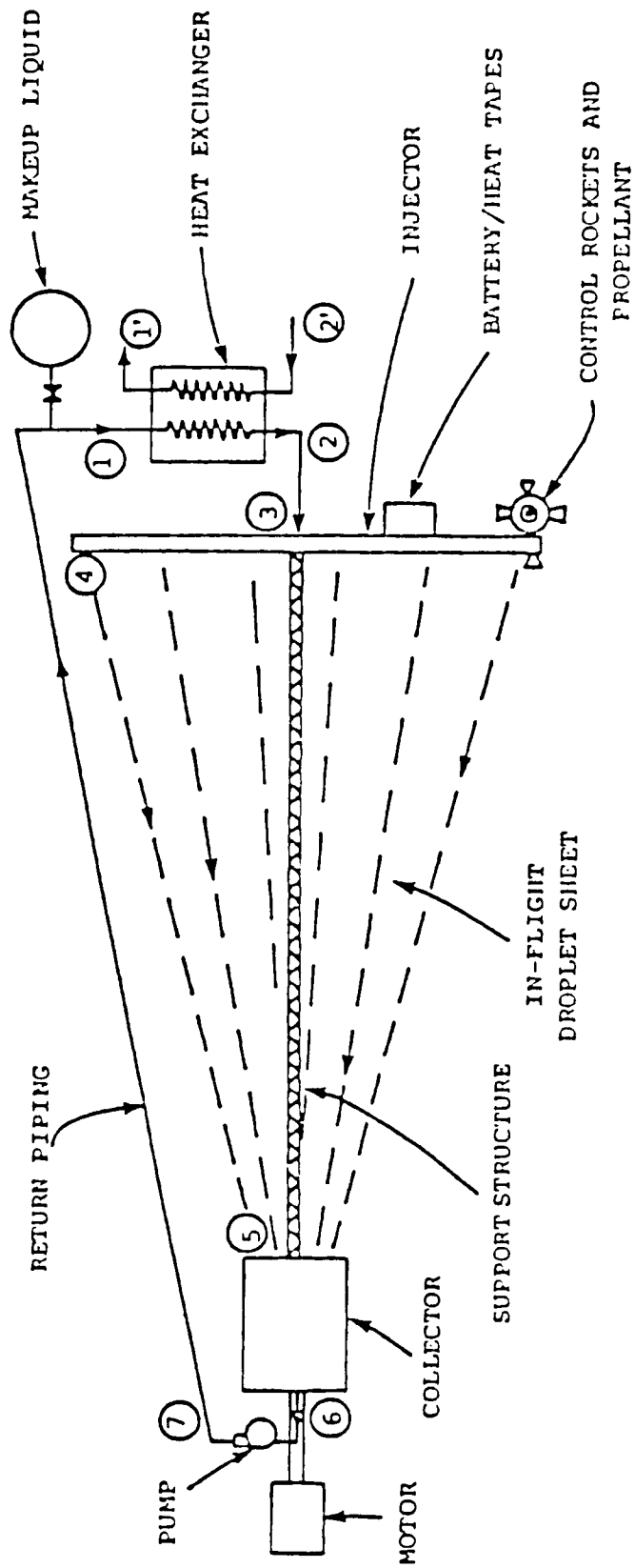
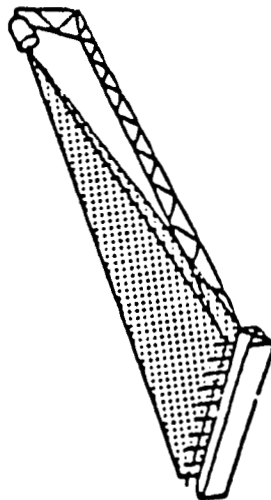


Fig. 4.3.13

# ALTERNATE CONFIGURATIONS FOR THE LIQUID DROPLET RADIATOR

TRIANGULAR

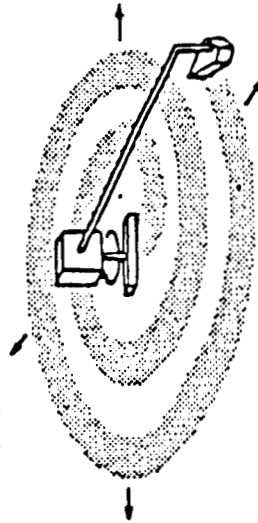
(a)



Stationary  
Extended Injector  
Small Collector

SPIRAL

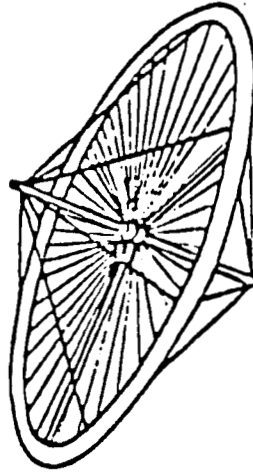
(b)



Rotating  
Small Injector  
Small Collector

EXTENDED DISC

(c)



Rotating  
Transparent Shroud  
Small Injector  
Extended Collector

Fig. 4.3.14

# OPERATING TEMPERATURE RANGES OF CANDIDATE LDR FLUIDS

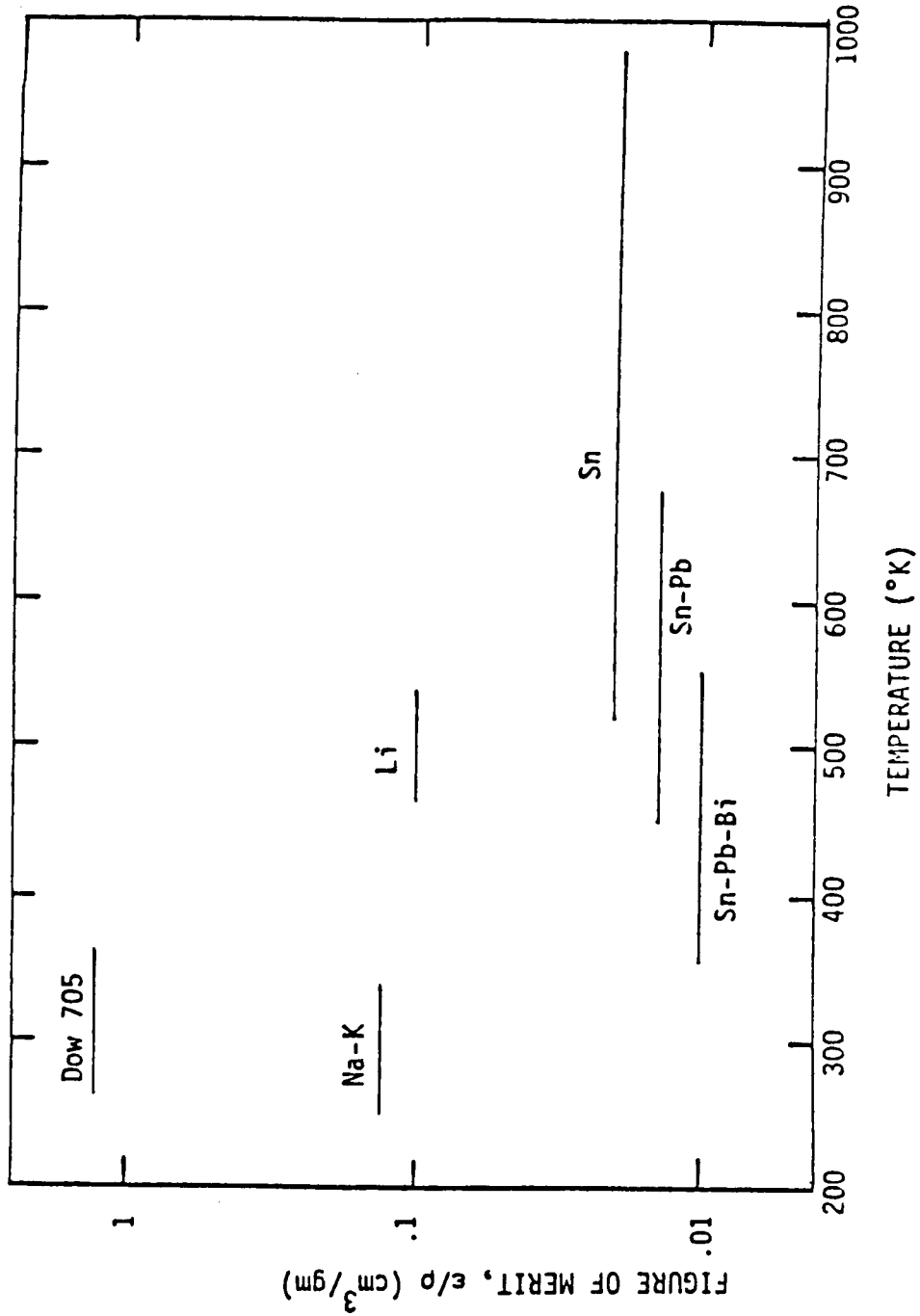


Fig. 4.3.15

sheet mass standpoint, a point of diminishing emissivity enhancement return is reached long before 30 layers of droplets. It is fairly accurate to say that the sheet emissivity can be increased by a factor of two over intrinsic emissivity without incurring excessive weight penalties ( $\leq 10$  droplet layers).

There does not appear to be much data concerning the intrinsic emissivity of the two working fluids, lithium and tin, in their temperature operating ranges, 460 K - 540 K and 525 K - 990 K, respectively. The emissivity of tin at 25°C is quoted at .043 [18]. An approximation for the emissivity can be made by the equation [19]:

$$\epsilon(T) \approx 0.0348 \sqrt{r T}$$

Where  $r$  = electrical resistivity at 273 K,  $\Omega_{cm}$   
 $T$  = temperature, K

Using values of electrical resistivity of  $12.0 \times 10^{-6} \Omega_{cm}$  and  $11.0 \times 10^{-6} \Omega_{cm}$  for lithium and tin at 273 K respectively, yields the following values as a function of temperature:

TABLE 4.3.1

WORKING FLUID INTRINSIC EMISSIVITY

	FLUID TEMPERATURE (K)								
	460	500	525	540	600	700	800	900	990
Lithium	.055	.060	.063	.065	N/A	N/A	N/A	N/A	N/A
Tin	N/A	N/A	.061	.062	.069	.081	.092	.104	.114

The referenced authors [19] believe that these calculated values tend to error on the high side as temperature is increased above room temperature. We note that these values are substantially lower than intrinsic values commonly used, but unreferenced, in droplet radiator literature. Assuming

sheet emissivities are twice that of the working fluid intrinsic emissivity, the following table shows the radiating area necessary to radiate 40 MWt at various average sheet temperatures for lithium and tin.

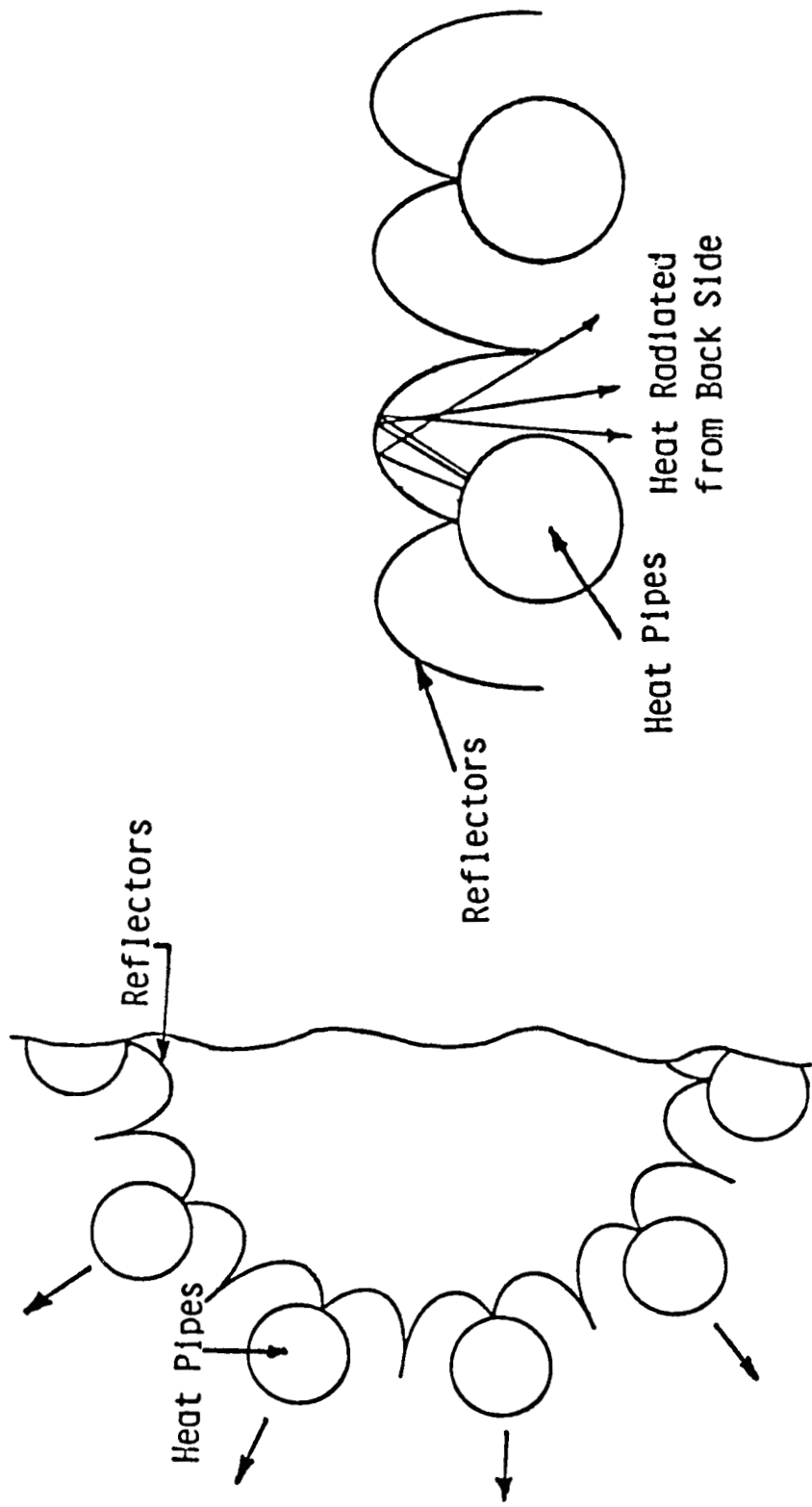
TABLE 4.3.2

AREA NECESSARY TO RADIATE 40 MWt						
AVERAGE LIQUID DROPLET SHEET TEMPERATURE (K)						
	460	500	540	600	700	800
Lithium (m <sup>2</sup> )	158,000	101,000	67,000	N/A	N/A	N/A
Tin (m <sup>2</sup> )	N/A	N/A	70,500	40,800	18,500	9,460

In determining the quantity of radiator area deliverable in a single shuttle, the radiator systems encountered tend to become limited by the volume available in the shuttle rather than the shuttle weight capability. Assuming weight is not the driving constraint, two conceptual designs [9,17] have been found in the literature that deal with the constraint of shuttle launch integration. The deployment sequence proposed by Grumman [17] is shown in Fig. 4.3.16. The deployed area depicted in this figure is roughly 7700 m<sup>2</sup>, assuming the droplet sheet can radiate from both sides.

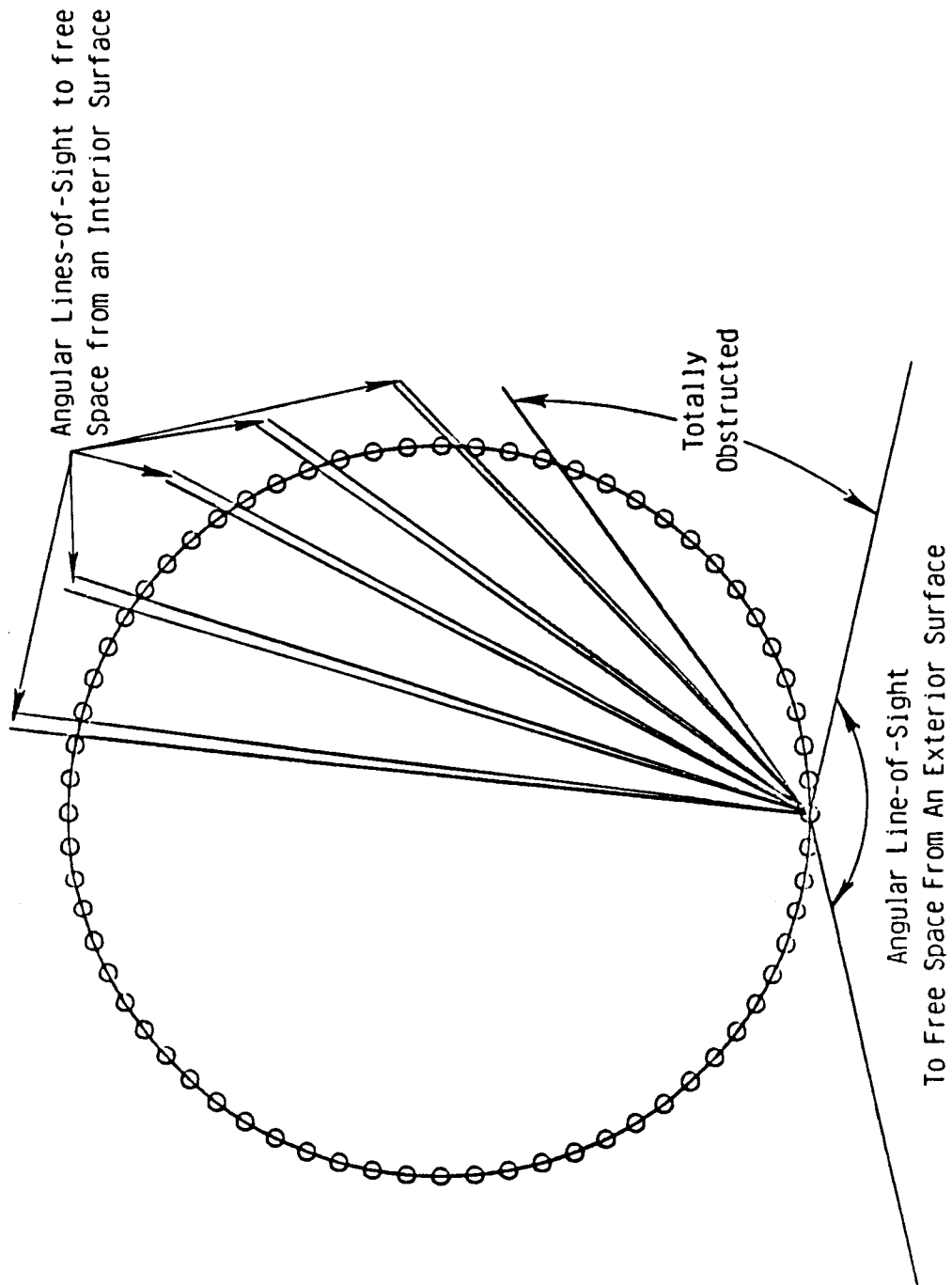
Regardless of the deployment scheme or radiator sheet design, there are some unaddressed basic issues. In order to achieve the large radiator areas necessary, the assembled collector, generator, and return piping lengths will exceed the shuttle bay length. Because these components contain lithium in the 460 K to 540 K range or tin in the 525 K to 990 K range, joints will require welding. Space welding of liquid metal piping is not a demonstrated technology now, but may very well be performed in the future. Regardless of the welding feasibility question, the droplet radiator requires aiming accuracies of  $\pm 1$  mrad. There is certain unavoidable structural deformation to members joined by welding. Although using jigs and preheating helps, tolerances required for liquid droplet radiator

# REFLECTOR HEAT PIPE CONCEPT

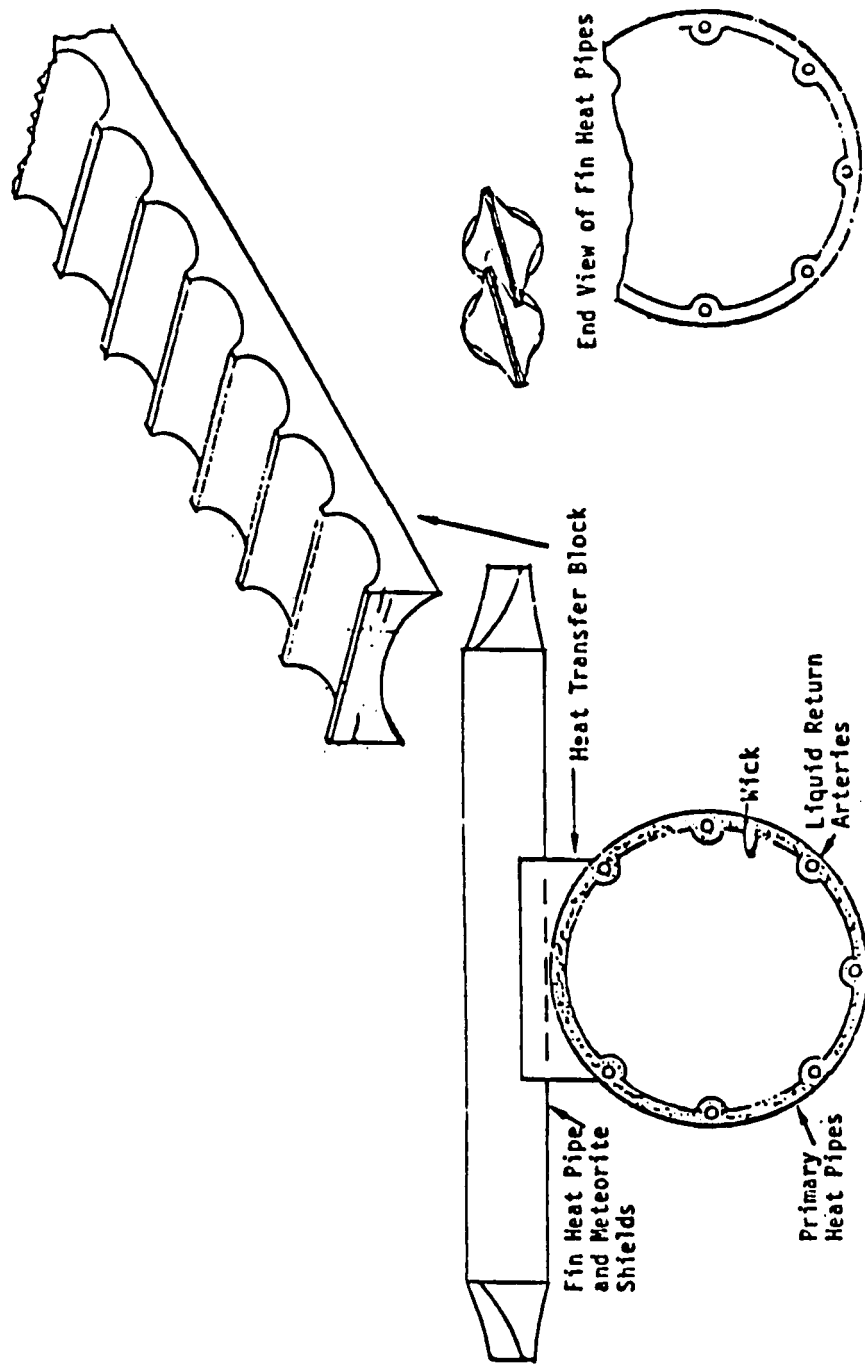


CIRCULAR ARRAY OF HEAT PIPES

GEOMETRY FOR ESTIMATING SKIP TUBE EFFECTIVE VIEW FACTORS  
FOR RADIANT ENERGY TRANSFER TO SPACE



# CROSS-FIN HEAT PIPES ON LONG PRIMARY HEAT PIPE



produces the lowest weight for a given radiator size. In the case of the telescope radiator packaging, the shields could be fabricated thin and flexible to wrap around the individual heat pipes in the stowed position. They would then spring outward in the deployed position and take up a specified preformed shape.

From a weight standpoint, design #3 yields the lowest weight per m<sup>2</sup> of radiating area. From a volume standpoint, design #1 or #5 would produce the maximum radiating area within a given envelope.

SPI has modeled and computer programmed the governing thermal-hydraulic equations of the telescoping, series-connected heat pipes, including the effects of pressure/temperature drops due to wall conduction, wick conduction, vapor inertial energy investment/recovery, and viscous vapor drag. Using this program, SPI has investigated the degradation in the temperature for each heat pipe segment due to the thermal/hydraulic effects stated. The telescoping heat pipe concept is capable of rejecting 90 MWt of heat and fits into one shuttle. Such a capability is essential in order to demonstrate the feasibility of large multimegawatt space power systems. By changing working fluids, the concept also lends itself readily to compact, space deployable payload radiators.

The telescoping radiator heat pipe code has been made a sub-routine of the Rankine and thermionic systems analysis codes described in Section 4.5

A few final comments can be made about survivability considerations of the above telescoping cylindrical radiator alternatives. As is true in the triform configuration, potassium and sodium working fluids and refractory metal heat pipe envelopes have the ability to withstand substantial temperature excursions without forcing system shutdown or damage. Cylindrical arrays of heat pipes provide a long vehicle that can easily be rotated during threat situations to reduce the effective local incoming heat flux by a factor of  $\pi$ . The telescoping cylindrical heat pipe array using skip tubes and Be or Cu armor provides the most compact and survivable overall radiator design. However, the concept using potassium heat pipes is appropriate only to incore thermionic and potassium Rankine conversion

systems. For high temperature Stirling (FPSE) systems mercury must be used as the working fluid. This latter approach was not done for this study, due to excessive radiator size and weight and the potential for spacecraft contamination upon mercury leakage. Instead, the triform radiator was used for the Stirling and Brayton systems.

#### 4.4 SPACE POWER REACTORS AND FUEL

##### 4.4.1 Introduction

The reactor subsystem typically constitutes only 10-20% of the total system mass for space nuclear power systems in the 5-10 MWe continuous power output class. The associated shielding, for unmanned applications, adds another 2-6%. Consequently, while there is always an emphasis on keeping the component masses as low as possible without compromising performance, the incentive to reduce the reactor size and mass for these large systems is tempered by the fact that the reductions may result in only a small reduction in the overall system mass and consequently may not be cost/benefit effective.

The major requirements of the reactor are to provide high fuel burnup and long endurance at temperatures high enough to reduce the heat rejection subsystem size and mass. The temperature, materials and control requirements of past space nuclear power plant design studies and technology developments have addressed much lower power outputs, (a few kilowatts to a few hundred kilowatts). Multimegawatt systems introduce some significant additional reactor requirements which are summarized in Table 4.4.1.

The major differences between the high and low power systems will be the higher reactor temperatures at the longer endurances required. The long endurance (without fuel change) requirement translates to high burnup of nuclear fuel, large fission gas generation, accumulation and the requirement for venting. It also may lead to fuel element swelling or failure.

High power, long endurance, and high burnup of the entire fuel inventory at high temperature increases the control reactivity requirement. The higher power, long endurance systems have larger reactor cores and consequently less reflector control available. Thus, the reactors will be more complex because of requirements for internal control rods or similar devices. Such a complication can jeopardize system reliability.

MCNPS REACTORS (U)

- MUST OPERATE HOTTER FOR A LONGER TIME
- MUST PRODUCE 250-450 MWT-YRS OF ENERGY (W/ NO FUEL CHANGE)
- REQUIRES 6-8% METAL ATOM BURN UP IN CERAMIC FUEL (200-300 LITERS UO<sub>2</sub>)
- THEORY AND INTERPRETATION OF PAST EXPERIMENTS RECOMMENDS PROBABLE SUCCESS OF CAREFUL PROGRAM
- GAS RELEASE IS HIGH AND MUST BE VENTED
- SWELLING OF UO<sub>2</sub> SHOULD SATURATE AT 10%  $\Delta V/V$  (3% DIAMETER)
- HIGH CREEP STRENGTH CLADDING AT 1650-1950 K IS REQUIRED

unclassified

TABLE 4.4.1

The reactors considered in this study are assumed to be fueled with ceramic  $UO_2$  or UN fuel highly enriched in  $U^{235}$ , or  $ThO_2$  mixed with fully enriched  $UO_2$ . These are the only nuclear fuels considered potentially capable of meeting the performance requirements, including considerations of launch safety (which probably precludes the use of  $U^{233}$  or Pu).

The MCNSPS 5-year full power fuel lifetime requirement is some 5 times longer than the fuel lifetime of a typical commercial reactor. Moreover, the higher temperature requirement of MCNSPS fuel may require the atom % burnup limits to be lower than commercial fuel. To achieve this, lower power densities must be used in MCNSPS designs. As a result, thermal-hydraulic and high power density considerations do not control the design as much as do temperature and endurance.

Due to the endurance requirements, the reactors considered for MCNSPS are all relatively large, and criticality (which establishes the minimum size) is not an issue. The reactors will be sized primarily by how much fuel the reactor must contain in order to provide the necessary integrated energy output.

The fissioning of 1.25gm of  $U^{235}$  will produce about 1 megawatt-day of energy in the form of heat. For typical  $UO_2$ :

1 metal atom % burnup corresponds to  $2.1 \times 10^{20}$  fission/cc of  $UO_2$

or  $\approx 0.21$  kWt-yrs/cc- $UO_2$

or  $\approx 0.21$  MWt-yrs/liter  $UO_2$

For typical UN:

1 metal atom % burnup corresponds to  $2.7 \times 10^{20}$  fissions/cc of UN

or  $\approx 0.27$  kWt-yrs/cc-UN

or  $\approx 0.27$  MWt-yrs/liter-UN

Fig. 4.4.1 provides a graphic representation of the total possible energy release versus the volume of  $UO_2$  in a core, as a function of the average fuel burnup. If the total system conversion efficiency is  $\eta_s$ , then the reactor fuel volume can be determined by :

$$VF = \frac{P_e E X}{0.21 \eta_s (BU)} = \text{liters } UO_2$$

where  $P_e$  - Required electrical power, MWe  
 $E$  - Equivalent years full power endurance  
 $X$  - Fuel peak power/average power ratio  
 $\eta_s$  - System conversion efficiency  
 $(BU)$  - Maximum allowable metal atom % burnup of  $UO_2$

The same equation is used for UN fuel, replacing the 0.21 factor in the denominator with 0.27 MWh-yrs/liter.

The remaining reactor materials volumes are determined by thermal, stress, and hydraulic requirements. When the thermal-hydraulic requirements are satisfied, the total core volume is determined. It is assumed in this study that fuel enrichment or concentration will be varied in the radial and axial directions to provide nearly flat power distribution, limited to an overall 1.2 peak/average ratio. Reflectors are provided to reduce the fuel distribution requirement, to reduce shielding requirements and to provide for leakage reactivity control. For purposes of analysis, all reflectors are assumed to be BeO backed by  $^{10}B_4C$  poison in both the axial and radial direction.

Molten lithium alkali metal is the reactor coolant for all reactors except for the gas cooled reactor. Lithium pumping power for the same heat removal in the same equipment is 1/12 that of sodium and 1/45 that of NaK. It has the lowest vapor pressure at elevated temperatures and the lithium 7 isotope has a very low activation cross section, a very short decay 1/2 life (0.85 sec), and a very good scattering cross section at mean fission energies (.2 to .6 MeV). Lithium containment and startup problems simply must be solved for MCNSPS feasibility.

REACTOR THERMAL ENERGY RELEASE VS.  
CORE FUEL VOLUME AS FUNCTION OF BURNUP

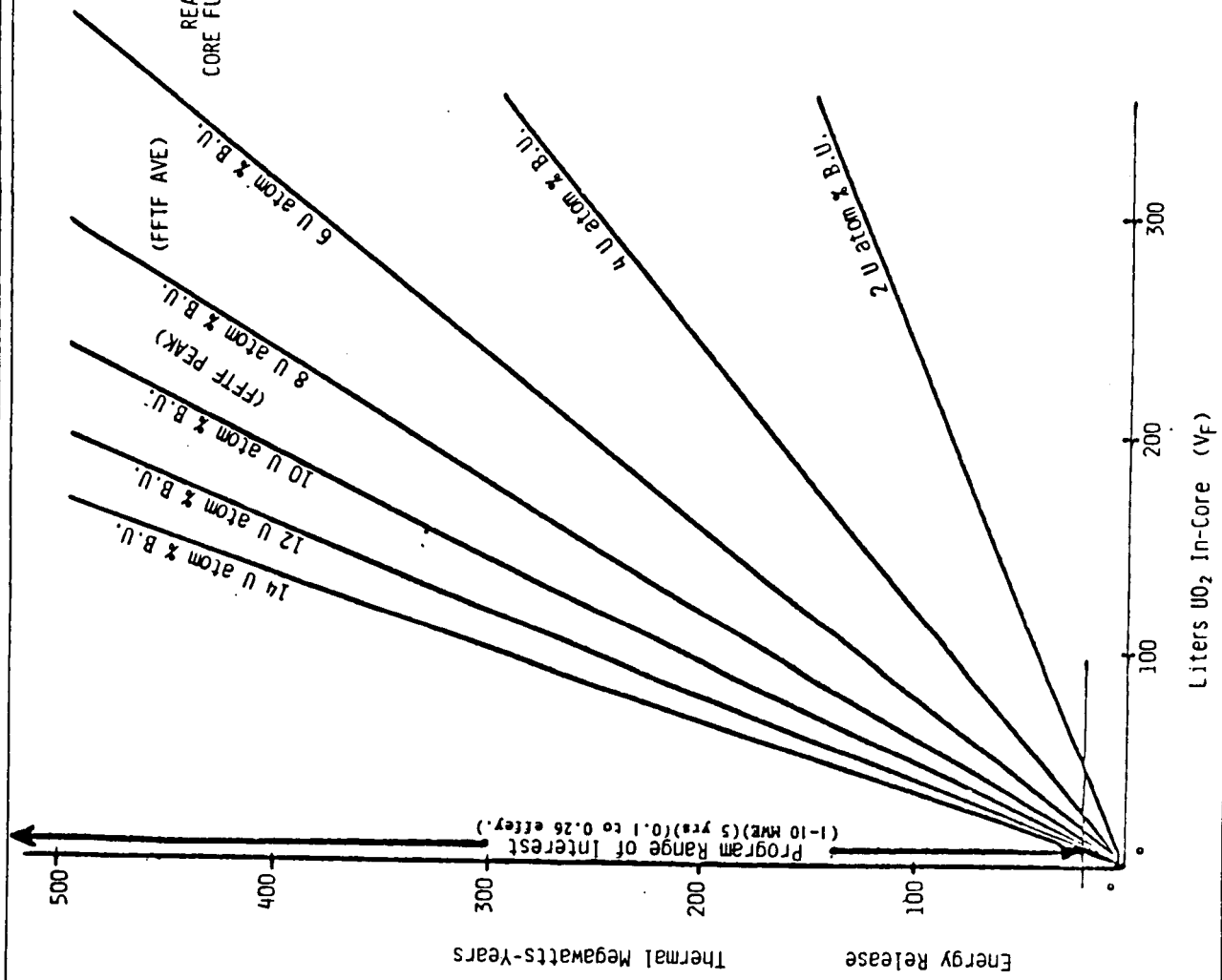


Fig. 4.4.1

An advanced liquid lithium coolant technology was pioneered in the Aircraft Nuclear Propulsion program conducted at Pratt Whitney in the 1950's and early 1960's. This technology was picked up by NASA Lewis and General Electric Co. in the short lived SNAP-50 program of the mid 1960's.

Lithium can be contained in refractory metals such as tungsten, tantalum, molybdenum, niobium, and rhenium, when extremely low O, N, H, and C limits are maintained in the lithium. The refractory metals are usually alloyed with a small amount of Zr, Hf or Ti to getter oxygen and hydrogen. Tantalum and niobium tend to be more sensitive to oxygen and hydrogen than are tungsten or molybdenum. However, these latter two materials tend to be very difficult to fabricate. Rhenium alloys of tungsten and molybdenum tend to be more workable and might be favored in many applications.

Aluminum, copper, nickel, cobalt, iron, chrome, etc. in essentially decreasing order are soluble in lithium at elevated temperatures and therefore must be avoided.

In this study gas reactors require 1800 K outlet coolant (turbine inlet) temperatures in order to begin to compete, as will be discussed in the Brayton Gas turbine system discussion in Section 4.5.3 of Volume III. Resultant fuel surface temperatures are 1950 to 2000 K. Experience at Oak Ridge National Laboratories [23] has shown that high temperature refractory metal loops containing inert gases are subject to mass transfer under large temperature gradients. It was suggested in that study that O<sub>2</sub> and N<sub>2</sub> concentrations below .005 ppb would be required. Such low levels are beyond detection and control limits.

Fuel surface and coolant outlet temperatures were assumed as follows:

The in-core thermionic and gas cooled reactors have 1900-1950 K and 2000 K fuel surface temperatures, respectively. The thermionic systems require lithium coolant temperatures of 1100 K. The gas cooled reactors require high pressure He/Xe temperatures of 1800 K. The lithium cooled reactors to power the potassium Rankine turbine cycle and the Stirling engine cycle

require coolant outlet temperatures from 1550 to 1650 K. Fuel surface temperatures for these reactors are of order 50-100°C higher.

#### 4.4.2 Fuel Cladding and Coolant Selection - Safety Implications

Gas Venting. At these elevated fuel surface temperatures and at the high 6% to 8% burnup, the majority of fission gases will be released from the fuels. The issue of gas release is more thoroughly discussed in Section 4.4.3 of this Volume. Approximately 0.27 gas atoms ( $\approx 85\%$  Xe,  $15\%$  Kr) are eventually formed per fission of  $U^{235}$  or  $(0.27 \text{ gas atoms/fiss})(2.1 \times 10^{20} \text{ fiss/cc})(6\% \text{ BU}) = 3.4 \times 10^{20} \text{ gas atoms/cc}$ .

If the fission gases are collected inside the reactor in extensions of the fuel cladding (as is done in commercial reactors), and if the fuel pin gas collection volume is assumed equal to the fuel volume, then internal gas pressures would be of the order of 1000 psi by the end of life. Even early in life the generated pressures would quickly cause creep, distortion and failure of the cladding at MCNSPS temperatures. For UN, the release of only 30% of its gas at 1600 K surface temperatures, would produce pressures in excess of 300 psi and a cladding stress of 2000 psi. A cladding leak into the lithium coolant of a LMCR would release a very dangerous bubble into the low pressure coolant system that could lead to further fuel element failures and reactor vessel failure. Fission gas venting or chilled storage for these reactors will be required.

Venting the fission gases overboard or into a cool activated charcoal cannister is also required for thermionic reactors and gas cooled reactors in order to prevent cladding distortion when using  $UO_2$  fuel. Gas cooled reactors might tolerate Xe and Kr leakage into the He-Xe coolant without adverse consequences if a cold trap can be placed to condense out  $Cs_2O$ ,  $Rb_2O$ ,  $SrO$ ,  $BaO$ , etc. These products would probably attack a refractory metal system. Carbide fueled (UC-ZrC) gas cooled reactors would release Cs, Rb, Sr, Ba, Te, etc. metals into the gas stream. These elements might be more tolerated by refractory metals than their oxides would be.

Lithium coolant attacks  $\text{UO}_2$  to release  $\text{Li}_2\text{O}$  and free uranium into the coolant. These two contaminants can be destructive to the system. Consequently, uranium nitride may be a required fuel for single clad elements cooled by lithium.

As noted above, the fuel elements must be vented overboard or to chilled activated charcoal cans. A single coolant leak into a warm charcoal can could conceivably lead to carbon diffusion back into the lithium. Carbon in lithium would generally be destructive to containment metals. Thus, the charcoal trap should be held below the lithium freezing point at all times. The system could then be well protected from the contamination effects by a lithium freeze plug in each fuel element vent line. The vent line would extend all the way to the chilled charcoal (avoiding the possibility that one leak could plug a vent manifold for many fuel elements). Overboard venting will probably be permissible, but the vent lines must also be individual and freeze plugged between venting periods to prevent lithium leaks due to failed fuel elements.

The thermionic systems might best use  $\text{UO}_2$  based fuel even with lithium coolant. The fuel is contained within a double cladding: the tungsten emitter encapsulation and the niobium fuel sheath. Hence, a leak in a niobium sheath would require simultaneous leakage through the tungsten emitter before the possibility of interacting with  $\text{UO}_2$  could take place. When such a leak should occur, lithium would leak into the electrode gap, into the fission gas vent line and to the chilled vent where the Lithium will freeze plug. Periodically an electric heater on the plug will soften the plug and release accumulated fission gas pressure.

Long-Lived Isotopes. The lithium cooled reactor model used for both the Stirling engine and the potassium Rankine systems is fueled with UN. The fuel could be  $\text{UO}_2$ , if suitably high integrity cladding proves to be available. The fuel cladding is presumed to be a tantalum alloy (i.e., Astar 811-C), tungsten-rhenium or a tungsten-Hf alloy. These refractory alloys (see Figs. 4.4.2. and 4.4.3 [24]) are preferred, because they promise to have suitable compatibility with lithium and suitably high creep strength

# TANTALUM CREEP STRENGTH

STRESS TO PRODUCE 1% STRAIN IN 5 YEARS

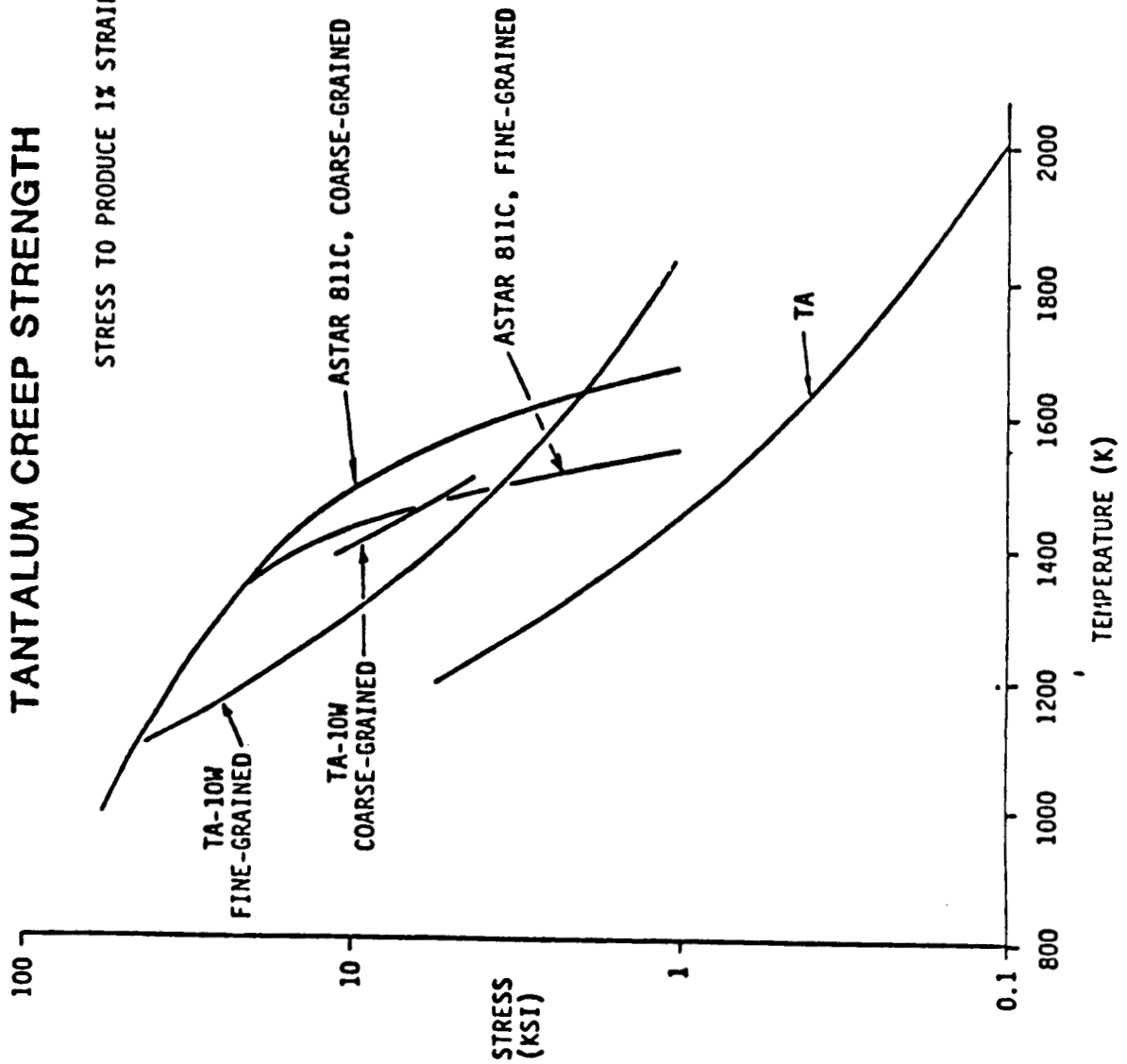


FIG. 4.4.2

W. KLOPP

# TUNGSTEN CREEP STRENGTH

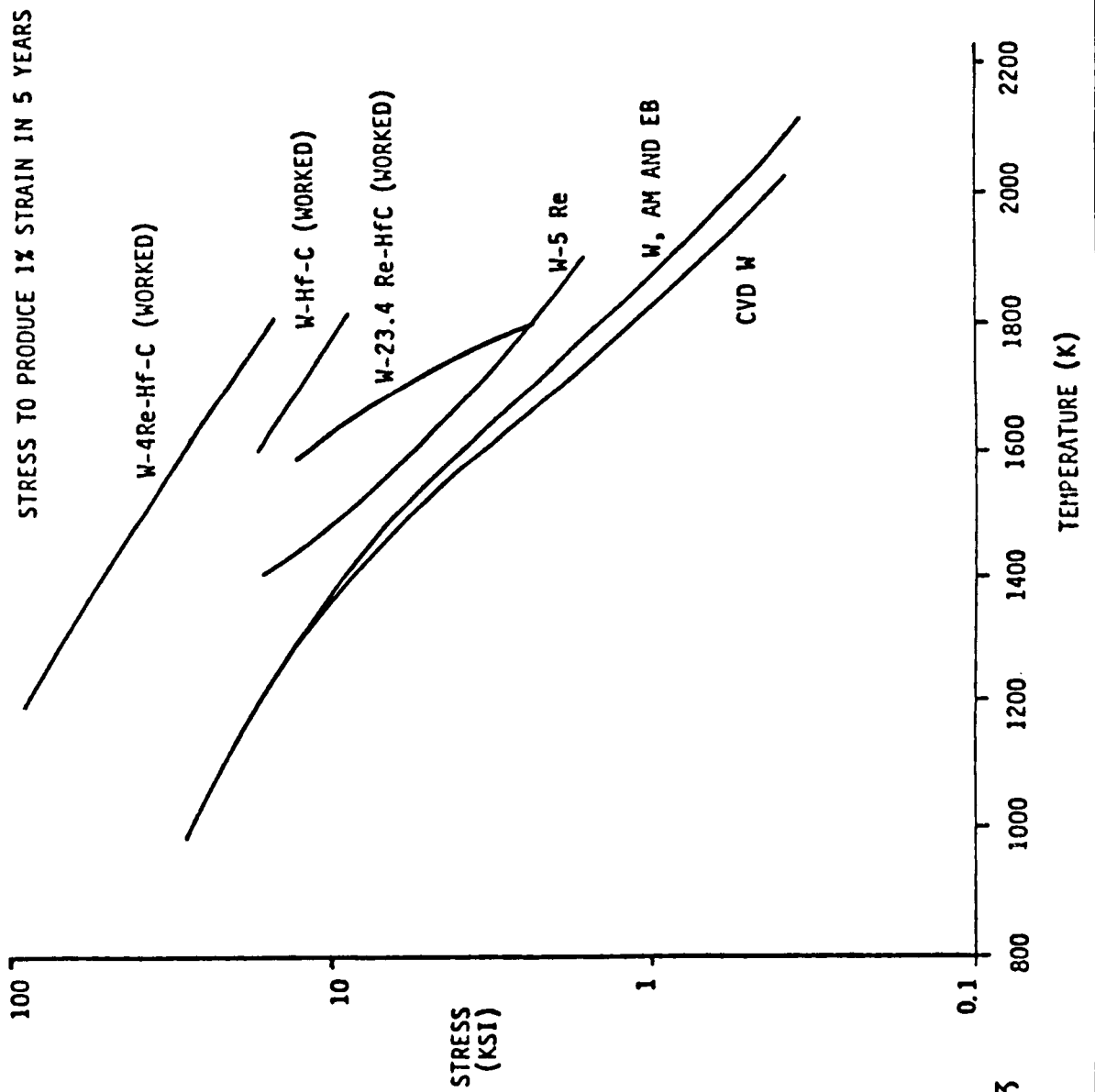


Fig. 4.4.3  
W. Klopp

to contain high burnup fuel. Tantalum, tungsten and rhenium have short-lived daughters when irradiated, whereas niobium and molybdenum form 20,000 year and 200,000 year daughters, respectively. Consequently, after the 300 year  $^{90}\text{Sr}$  and  $^{137}\text{Cs}$  decay, the long-lived daughters ( $^{94}\text{Nb}$  and  $^{98}\text{Tc}$ ) dominate the reentry hazard of large fully enriched systems as shown in Figs. 4.4.4 and 4.4.5 from Origen II calculations

Water Immersion. The neutron absorption cross section of Ta, W, Re, Th,  $\text{U}^{238}$ ,  $^{10}\text{B}$ , etc. are sufficiently low in the fission neutron energy range of .1 MeV to 1 MeV, that these materials may be used in a fast reactor core. These cross sections are shown in figure 4.4.6. Thorium and  $^{238}\text{U}$  absorption cross sections are low enough to serve as fuel diluents. All of these absorption cross sections increase as the neutron energy is decreased by moderation, and at a rate greater than that of the fission cross section. Thus, a combination of these materials in the correct quantities can prevent water flooding criticality in large fast spectrum reactor cores. Extensive calculations of representative lithium cooled reactors have been performed to verify inherent subcriticality upon water flooding. In every case, a large margin of subcriticality is calculated, consistent with expected behavior based on cross section energy dependence considerations.

Reactivity Control. In order to meet the 250 MWt years of energy output requirement, reference to Fig. 4.4.1 shows that the core will require 230 liters of  $\text{UO}_2$  or 185 liters of UN (the fraction 0.21/0.27 that of  $\text{UO}_2$ ) at a peak metal atom burnup of 6% (corresponding to an average of 5% at the assumed 1.2 peak/average power ratio). At a safe and reasonable peak power density output of 10 kW/ft (.328 kW/cm) of fuel rod, Fig. 4.4.7, some 50,000 kW/0.328 kW/cm = 152,000 cm of fuel rod are required for good heat transfer. The resultant fuel rod diameter for these conditions is 1.4 cm. When suitable cladding and thermal-hydraulics considerations are applied, the core diameter is 62 cm and the core length is 124 cm with a core L/D of 2.

This large core would contain excessive reactivity, if it were fueled with fully enriched  $\text{U}^{235}$ . Consequently the  $\text{U}^{235}$  fuel must be diluted. That is, fully enriched fuel will be unnecessary. The various reactors studied

# ACTIVATION AND FISSION PRODUCTS

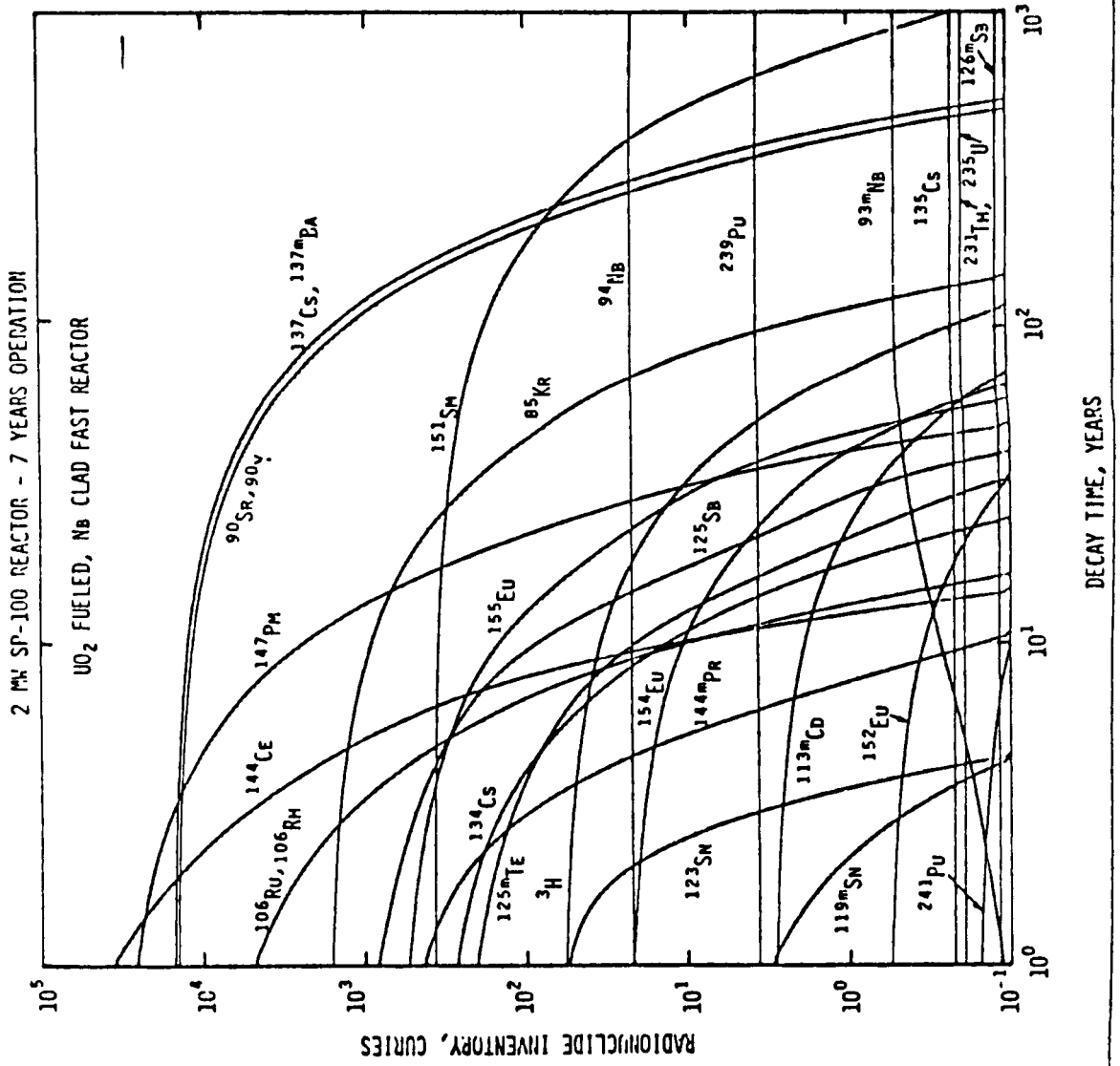


FIG. 4.4.4

# ACTIVATION AND FISSION PRODUCTS

50 MW REACTOR - 4 YEARS OPERATION

$U^{235}$  FUELED, MOLYBDENUM-CLAD FAST REACTOR

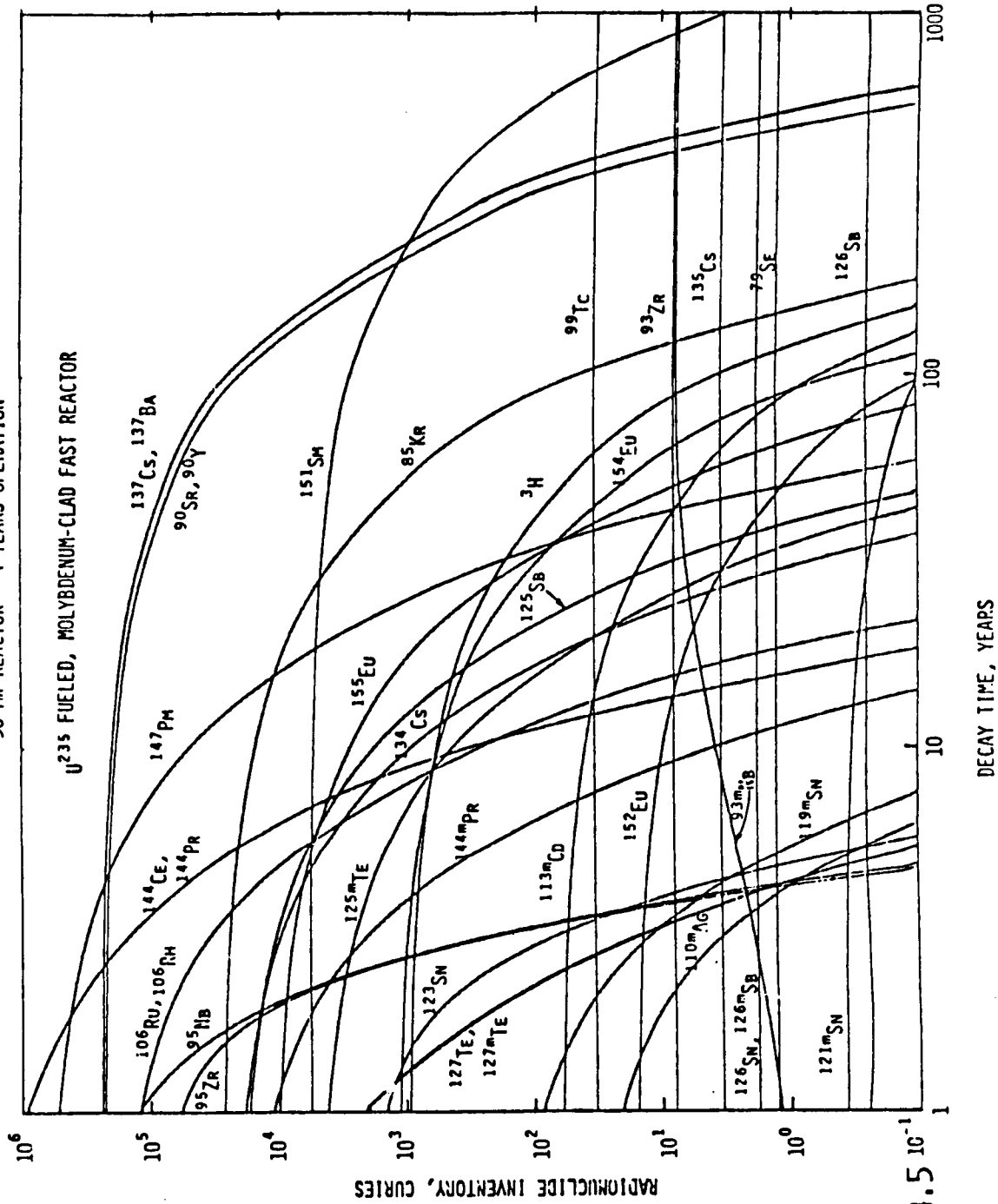


FIG. 4.4.5  $10^{-1}$

ORIGINAL PAGE IS OF POOR QUALITY

ABSORPTION AND FISSION CROSSSECTIONS VS. NUETRON ENERGY

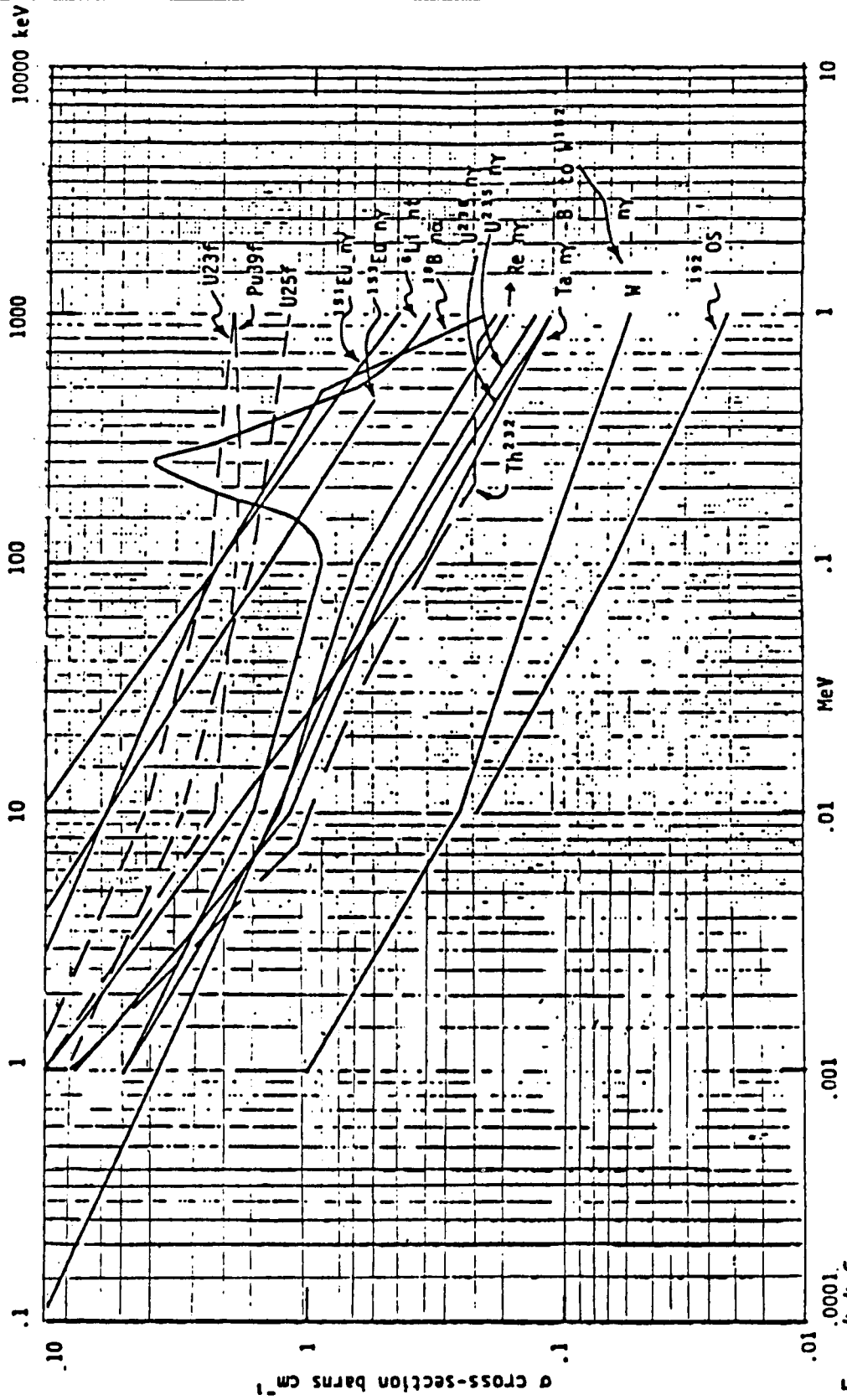


FIG. 4.4.6

# UO<sub>2</sub> LINEAR POWER DENSITY VS. CLADDING TEMPERATURE

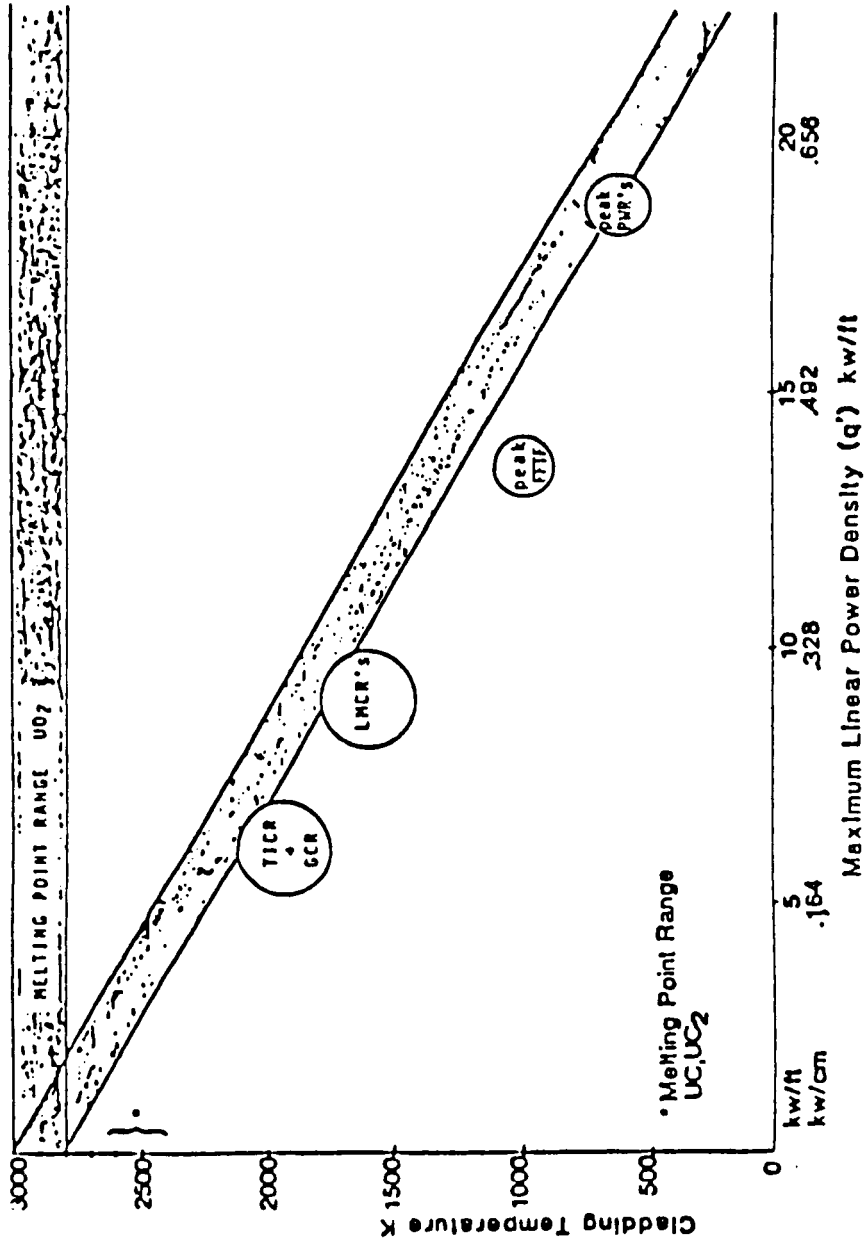


Fig. 4.4.7 Maximum linear power density in UO<sub>2</sub> fuel pins vs. cladding temperature.

required only 40 to 60% enrichment of  $U^{235}$  for criticality. Lower enrichment in a  $UO_2$  or UN (U-238) matrix leads to  $Pu^{239}$  generation, which has the beneficial consequence of reducing the reactivity requirement necessary to compensate  $U^{235}$  burnup. Conversion ratios of  $U^{235}$  to  $Pu^{239}$  were calculated to be about 0.15 to 0.2 Pu atoms/fission of  $U^{235}$  [25]. Approximately 27 kg of  $Pu^{239}$  are generated and about 1 to 1-1/2% in burnup reactivity loss is avoided. However,  $Pu^{239}$  is a toxic alpha emitter with a 24,000 year half-life, so that reentry and/or atmospheric burnup of these reactors would be environmentally unacceptable.

Pu generation can be virtually eliminated by using fully enriched uranium diluted with a suitable inert material (i.e., ZrC dilution of UC, or a cermet  $UO_2$ -Mo, etc. The reactivity associated with the breeding gain (~1% reactivity) may be saved by diluting  $UO_2$  with  $ThO_2$  or UN with ThN. These fertile materials will generate  $U^{233}$  rather than  $Pu^{239}$ . Thorium oxide has a 250°C higher melting temperature than  $UO_2$  and should be able to resist thermal ratcheting at temperatures of at least 1900 K. These types of mixed thorium-uranium ceramics should be studied more carefully for possible use to meet multimegawatt long-endurance applications.

The control of the LUNR (liquid-cooled, UN fueled, reactor) is complicated at the 10 MWe level because the reflector control margin is reduced in such large, high density fast reactors. Table 4.4.3 presents representative control reactivity requirements estimated for a typical 50 MWt LUNR and Table 4.4.4 the potential available control.

If active control requires 8.5 to 11.5% reactivity then rotating poison backed drums may not suffice. A combination of poison backed drum rotation and actual reflector removal, as in SNAP-10A or "Rorsat" may be adequate.

A central  $^{10}B_4C$  poison plug, as in SPAR-100 and some SP-100 designs, would provide about 2-2.5% towards launch shutdown but could represent a launch abort hazard if 2% reactivity were to move the wrong way upon impact.

The typical core layout, Fig. 4.4.8, indicates that approximately 16 reflector drums and two large coolant header positions will be available on

ESTIMATED REACTIVITY REQUIREMENTS

50 MWt LUNR

	<u>Reactivity</u>
6 ATOM% Burnup Reactivity Swing	-7% - 9%
Doppler, Fuel and Other Core Materials	.3
<sup>7</sup> Li Density Change	0.1
Radial Expansion	0.3
Axial Expansion	0.4
Reactivity Reserved for Shaping Power	0.3-0.5
Bowing Effects	<u>0.2-0.5</u>
ESTIMATED ACTIVE CONTROL REQUIREMENT	
	8.5-11.5%
<u>Non-Active Margins</u>	
Launch Abort Safety Margin, Shutdown and Stuck Drum Reserve	<u>3-4%</u>

POTENTIAL AVAILABLE REACTOR CONTROL

Available Control:

1.	Total reflector (leakage control)	15-20%*
2.	Total control drums worth (in-out) (includes $^{10}\text{B}_4\text{C}$ backing)	7-9.5%*
3.	$\text{U}^{233}$ conversion from Th	1 to 1-1/2%
4.	Central large poison ( $^{10}\text{B}_4\text{C}$ ) rod	2-2.5%
5.	Distributed poison control rods	2-5%
6.	$^6\text{Li}$ addition to coolant to reduce the .7% structural temperature defect.	-0.5%
7.	$^6\text{Li}$ coolant dilution by $^7\text{Li}$ during lifetime	0-3%
	PROBABLE TOTAL POSSIBLE	-10-18

\* Depends on core size

# LITHIUM COOLED - URANIUM NITRIDE CORE LAYOUT

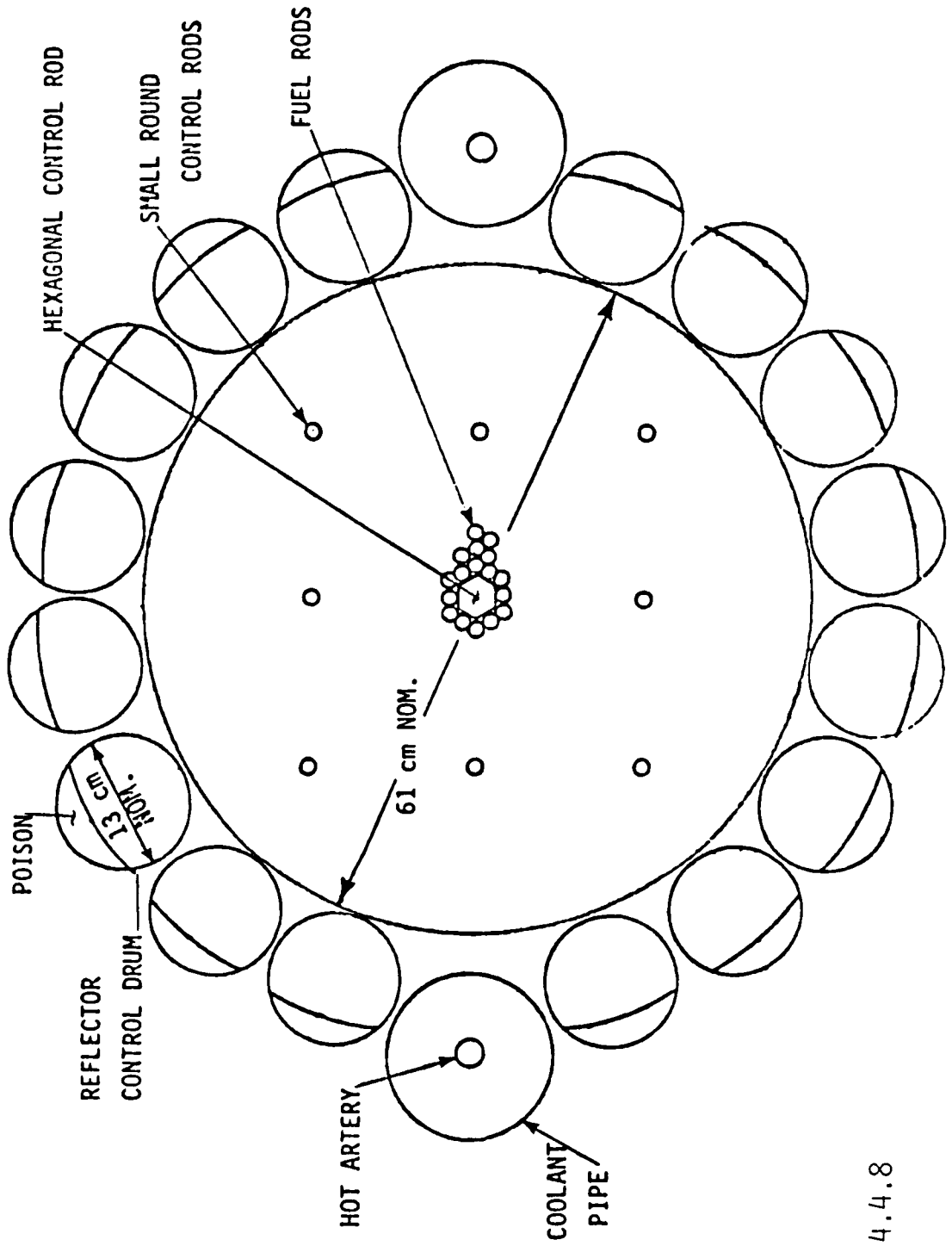


Fig. 4.4.8

the core circumference. At 8% total drum worth, each drum will be worth 0.5%. Thus, with a delayed neutron fraction of 0.0068 the reactivity is \$.74 per drum. One dollar is required for a prompt critical reactor. The prompt neutron generation time is 0.06  $\mu$ s in the drum poison out position. The total prompt negative temperature coefficient of reactivity is  $-1.4 \times 10^{-6} \Delta k/k \cdot ^\circ C$  of fuel temperature rise. The total reactor negative temperature coefficient can be designed into the system to be nearly what is needed. In summary, the control design of the 10 MWe (50 MWt) LUNR will be difficult, but should be feasible.

The control requirements for the 10 MWe incore thermionic system have not yet been calculated. However, the larger core will have less reflector control available and the segmented fuel will provide a little less prompt negative coefficient. There will be a greater reliance upon incore poison rods, spectral shift, Li-7 dilution of Li-6 in coolant, etc.

4.4.3 Fuel Behavior. Regardless of the power conversion system choice, there is a driving force to extend fuel surface temperature and burnup ranges. In order to meet the weight and envelope requirements of a single shuttle, fuel surface temperatures in excess of 2000 K and burnups of 6% to 7% will be required for all of the candidate systems.

Three types of fissionable nuclear fuel were considered:  $UO_2$ ; UN and UC. UC fuel generally exhibits significantly more swelling than either  $UO_2$  or UN under similar conditions. Because of the lower thermal conductivity of  $UO_2$  relative to UN, higher thermal gradients exist in  $UO_2$  and these contribute to fuel microcracking and resultant gas release. This higher percentage gas release reduces the swelling rate in  $UO_2$ , attributable to the buildup of fission gases. A detailed description of the behavior of each of the three fuels is beyond the scope of this report.

Since the behavior of  $UO_2$  is the best understood at this time, we present a summary of its characteristics when subjected to the anticipated space nuclear reactor environment of required fuel surface temperature, power density, and burnup. Moreover, this presentation is given in the context of

its application to the thermionic reactor, for which the cladding is assumed to be high strength tungsten.

For comparison, projected fission gas release and swelling for the other two fuels are compared against those of  $UO_2$ , and the creep strengths of other refractory cladding material candidates are compared against tungsten. Although the presentation is in the context of the thermionic application, qualitatively the results are applicable to the LUNR or gas cooled reactor, since the dominant environmental factors of fuel surface temperature, power density, and burnup are comparable, independent of the reactor type.

Cladding distortion due to  $UO_2$  fissioning is attributable to any combination of three causes: bladder effect, ratcheting, and fuel swelling.

Bladder Effect. This effect arises from a buildup of fission gas pressure within the fuel central void. When  $UO_2$  fuel of less than theoretical density is subjected to temperatures greater than 1500 K in the presence of thermal gradient, the fuel redistributes by vaporization and condensation down the gradient to form a dense (typically 98%) outer shell and a large internal void (see Fig 4.4.9). Upon neutron bombardment, certain gaseous fission products are created and released from the  $UO_2$  fuel over the system lifetime. Because of the radial temperature gradient, these gases migrate to the central void and, over time, lead to a pressure buildup. This pressure is structurally resisted by the strength of the outer  $UO_2$  fuel shell and the W cladding. Because of the low creep strength of both  $UO_2$  and W at operating temperatures, central void pressure could force the fuel and cladding outward over time. If unchecked, this bladder effect deformation will lead to emitter/collector shorting of the thermionic converter or, in a fuel pin type may create cladding hot spots and failures. The refractory metals are generally limited to about 2-3% elongation by creep before failure at operating temperatures [24].

The pressure buildup in a fueled pin having a 5% fuel void is plotted vs. burnup in Fig. 4.4.10, at various percentages of fission gas diffusion through the fuel skull. It is readily apparent that in order to attain high burnups (6% to 7% FIMA), the bladder pressure must be vented from the

# BLADDER EFFECT

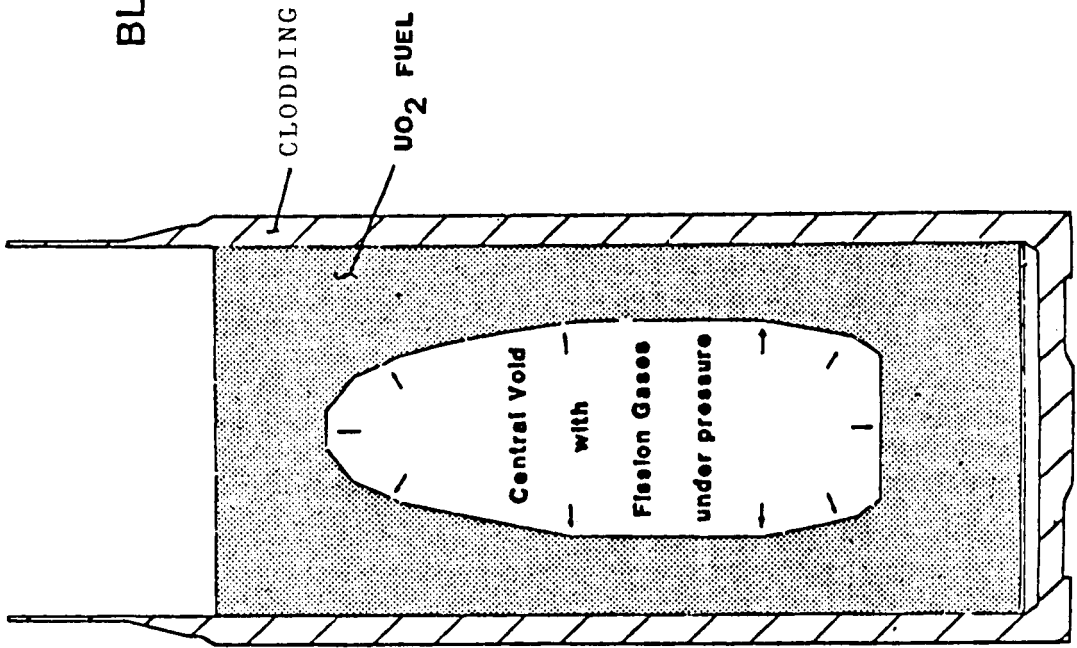
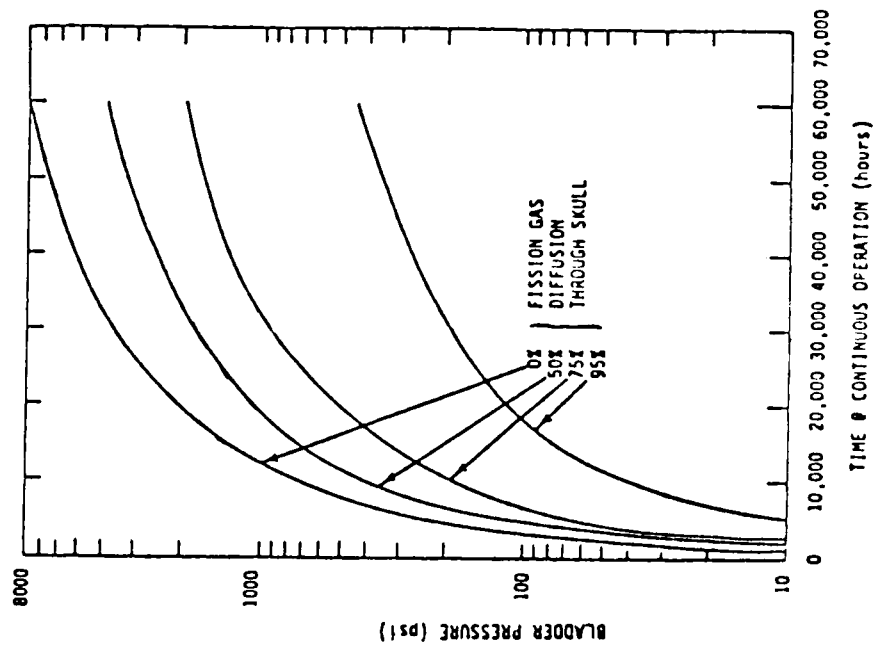


FIG. 4.4.9

# BLADDER PRESSURE vs. TIME at CONTINUOUS OPERATION 5% FUEL VOID



C-2

FIG. 4.4.10

central void. A critical aspect of multimegawatt feasibility development will center around guaranteeing adequate fuel venting. The fission gas snorkel vent, as proposed in Fig. 4.4.11, might provide this function.

The use of a snorkel is intended to guarantee venting of fission gas without relying on gas diffusion through the  $UO_2$  fuel and cap or on the formation and maintenance of cracks in the fuel. A snorkel design must satisfy the following criteria: it must vent fission gas at a sufficient rate to prevent a large pressure build-up in the central void; it must not become plugged with condensing  $UO_2$  during the operating lifetime of the reactor; and the snorkel must remain structurally intact at the very high temperatures of the fuel central void.

The thick portion of the snorkel contains a very small diameter orifice. It sits entirely in the central void, and may be hotter than the fuel center temperature due to gamma heating of the rhenium material. The small diameter of the orifice allows venting of fission gas while keeping the loss of  $UO_2$  vapor through the snorkel small. Because the entire orifice is at high temperature it cannot plug with  $UO_2$ . The inner diameter is made large to reduce the chance of plugging in colder regions. The plate at the top doubles as a fuel retainer plate. Rhenium was chosen as the snorkel material for its high strength, low thermal conductivity and vapor pressure, relatively good oxidation resistance in a  $UO_2$  environment, and ability to be formed using CVD.

Thermal Ratcheting. This effect may occur at the high surface temperatures required by MCNSPS fuels, if the fuel is subjected to temperature cycling, as would occur by changing the reactor power from time to time. Initially, the  $UO_2$  fuel pellet is designed to result in a slight interference fit with the cladding, such that the cladding is not subjected to excessive stress at operating conditions while maintaining good thermal contact.

If the power level and consequently the temperature of the fuel is decreased, the fuel will tend to pull away from the emitter surface because of its greater expansion coefficient, creating an annular gap of approximately 0.2 mil on radius/100 K for 1cm diameter. Evaporation of the

# PROPOSED FUEL SNORKEL VENT

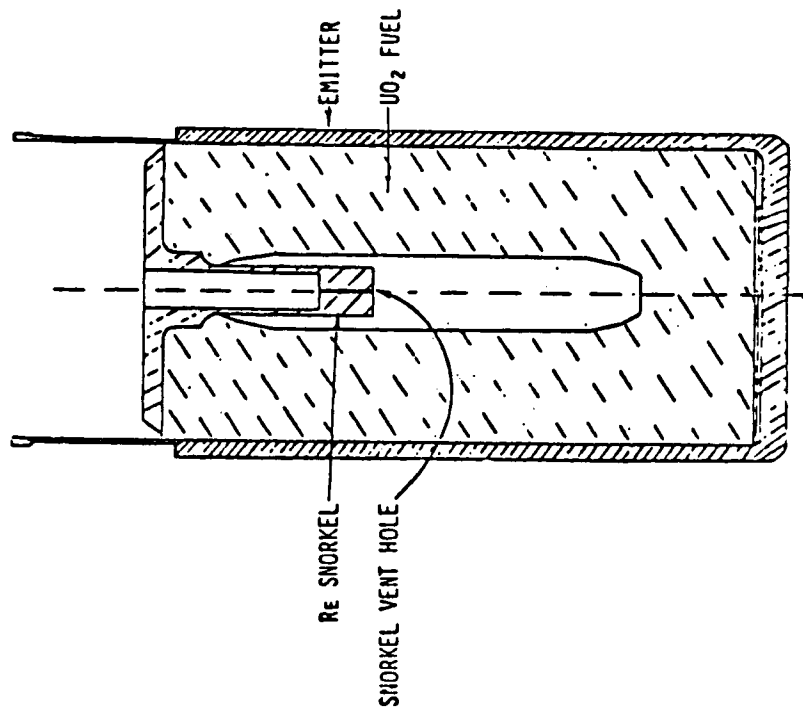


FIG. 4.4.11

relatively hot fuel and condensation on the cooler cladding occurs and the gap is eventually closed, as illustrated in Fig. 4.4.12. When the fuel element is subsequently returned to a higher temperature, the cladding is stressed because of the fuel's higher thermal expansion coefficient. If the stress is sufficient, plastic deformation of the cladding shell results. Fifty to one hundred such temperature cycles could result in accumulated plastic deformation sufficient to cause cladding rupture, hot spots on the cladding surface, or emitter shorting in the case of a thermionic fuel element.

An obvious way to prevent thermal ratcheting is to restrict the number and/or duration of thermal cycles. If the magnitude of the cycles are held small enough, the differential fuel/cladding strain will be absorbed by stored elastic strain.

If repetitious startup/shutdown operation is required, then relatively rapid temperature ramps could be used to heat or cool the fuel before significant fuel vaporization has time to occur.

If operation for significant periods of time at widely different power levels is required, electric power dumps may be used so that the reactor power output remains constant while the power utilized is varied. In the case of a thermionic unit, changes in power demand can be achieved by changing the emitter current density through cesium reservoir temperature control, while maintaining constant emitter (cladding) temperature.

Still another possibility is to coat the  $UO_2$  fuel with a material having a lower vapor pressure than  $UO_2$ , precluding or retarding the fuel evaporation and condensation process. The use of  $ThO_2$  coated fuel pellets might prove attractive in MCNSPS reactors, because these reactors require fuel dilution anyway, i.e. need not be fully enriched. Thoria vapor pressures are about 2 orders of magnitude less than  $UO_2$  at equivalent operating temperatures.

Fuel Swelling. This aspect of fuel element distortion is due to fission-induced swelling of the  $UO_2$  fuel, which can exert a stress on the cladding as indicated in Fig. 4.4.13. Both solid and gaseous fission products are

# THERMAL RATCHET EFFECT

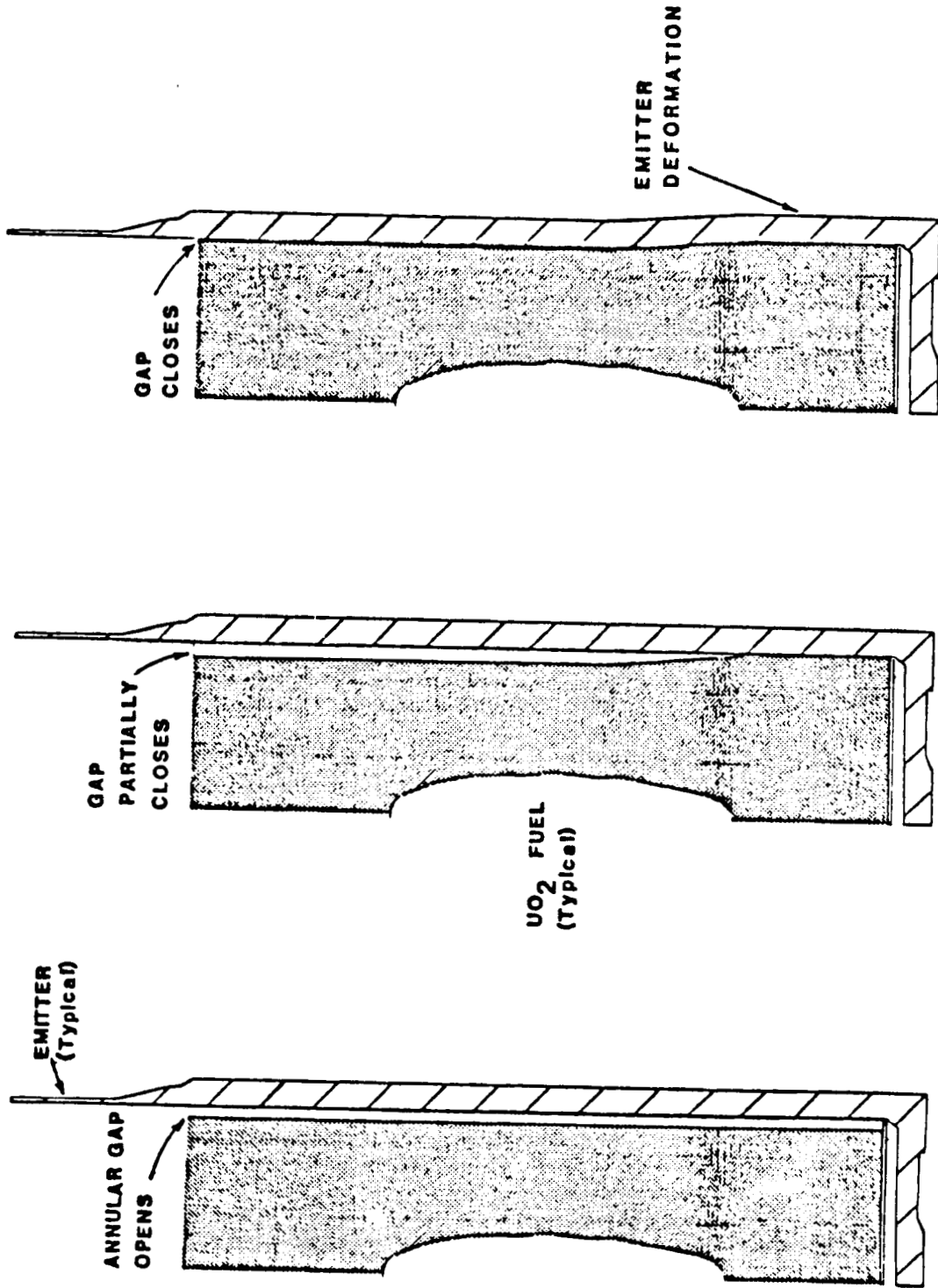


FIG. 4.4.12

FUEL SWELLING

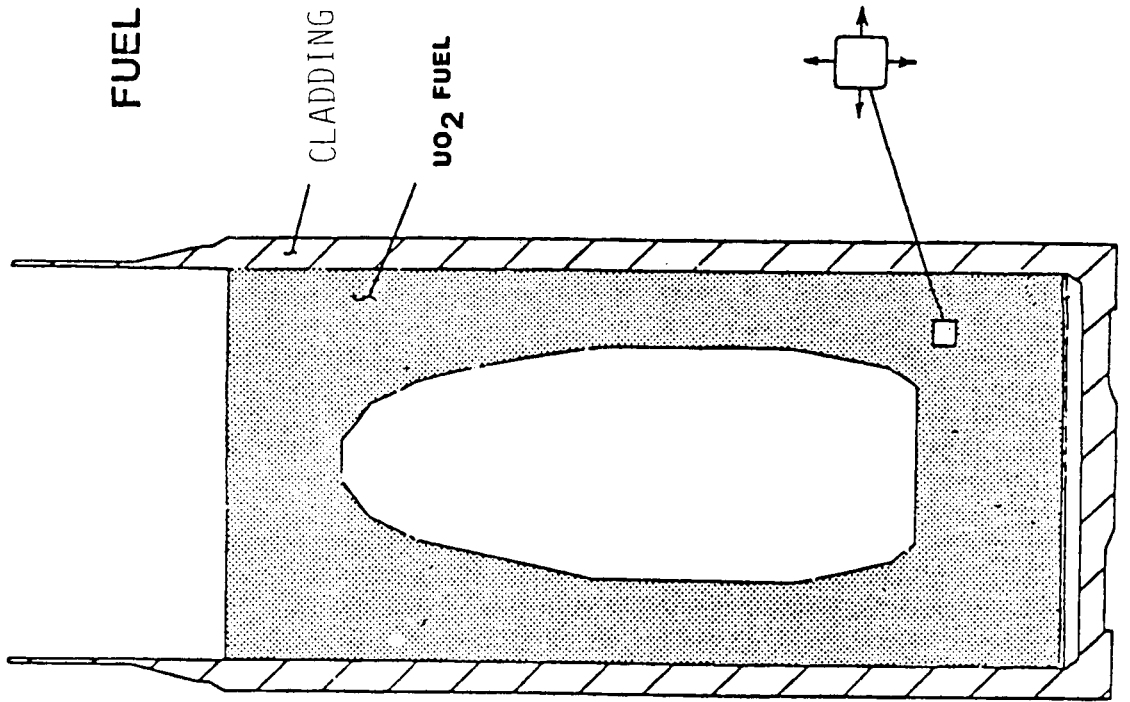


FIG. 4.4.13

accumulated in the fuel due to uranium fissioning. These fission products decrease the fuel density, and the subsequent volume increase may press the cladding outward.

Fuel swelling can be considered as arising from two distinct parts:

- 1) swelling due to gaseous fission products, e.g., xenon and krypton, and;
- 2) swelling due to solid fission products, e.g., everything else (selenium to gadolinium).

The swelling due to solid fission products differs for  $UO_2$  and  $PuO_2$ . For  $UO_2$  fuel, it is generally agreed that solid swelling occurs at the rate of 0.5 volume % /% atom burnup.

The potentially more serious problem may be due to gaseous fission products. It is in this area where there is a large amount of what appears to be conflicting data and models. One of the major contributions to the confusion in this area is the lack of a universal meaning of swelling. Many investigators report external volume changes which may not be due uniquely to fuel swelling; they may in fact result from a variety of mechanisms, e.g., they could be in part the result of thermal ratcheting or gas pressure induced creep, etc. Thus, the conditions under which the experiments were performed must be carefully considered when interpreting external volume change measurements.

Another area of confusion is the large number of influencing parameters which either go unreported or are reported in a non-consistent manner. Most fuel swelling information is reported in the form of  $\Delta V/V$  (fuel density change) vs. burnup at various temperatures. Sometimes the reported temperature is the average fuel temperature and sometimes it is the surface temperature. For the same surface temperature, the average fuel temperature is different for a thermal vs. a fast reactor. Correspondingly, given a surface temperature, the average fuel temperature will also vary with power level. All else being equal, data of late indicates that fission rate can have a significant effect on  $\Delta V/V$ .

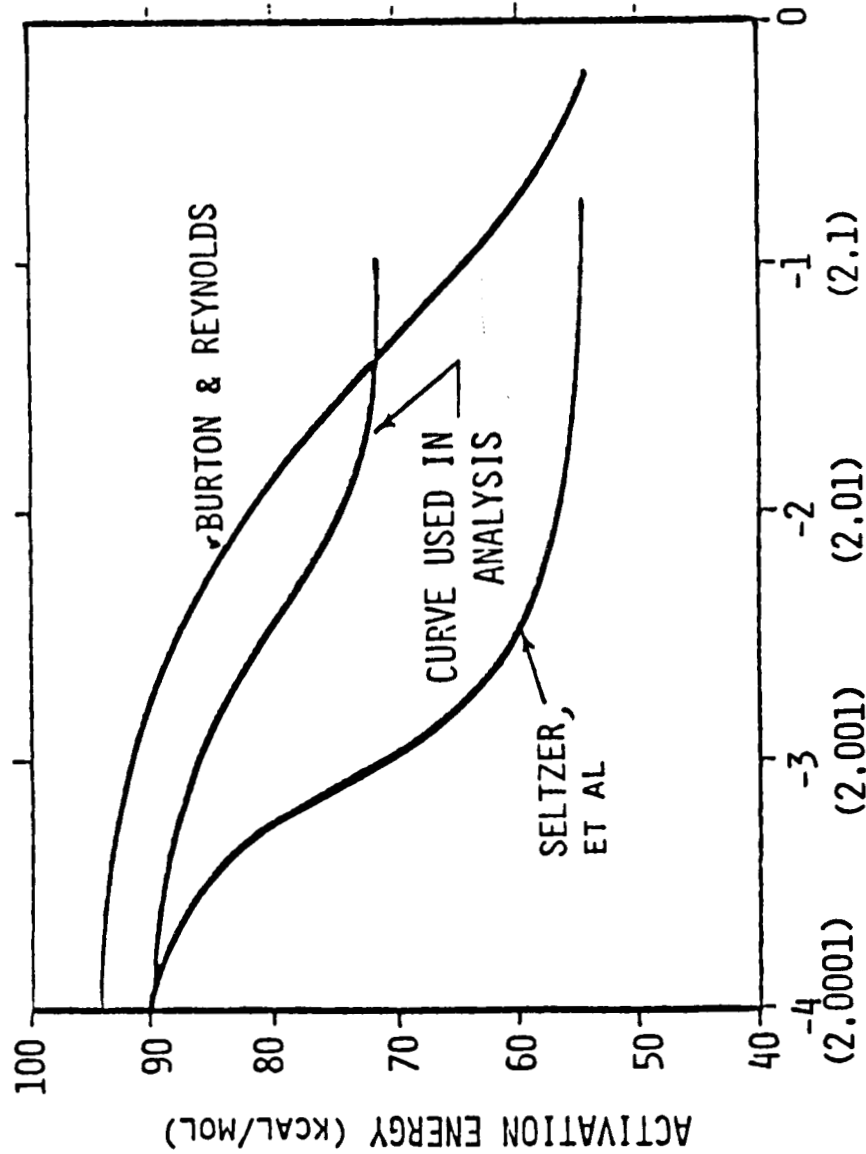
For  $UO_2$ ,  $\Delta V/V$  is dependent on so many parameters that it is not possible to report a single value of swelling for the multimegawatt application. What is known is that fuel swelling does have the potential to cause significant cladding deformation. The magnitude is dependent upon and can be controlled by such system factors as fuel and cladding temperatures, fuel composition, burnup and fission rate. Given these parameters, cladding deformation can be controlled by engineering the relative creep strengths of the fuel and cladding.

Fuel creep strength is highly sensitive to stoichiometry. As shown in Figs. 4.4.14 and 4.4.15, slightly hyperstoichiometric fuel in the range of  $O/M = 2.005$  dramatically drops both the diffusion and dislocation creep activation energies [26,27,28,29]. Since the values of these energies are used as exponentials in the  $UO_2$  creep laws, fuel creep strength can be reduced an order of magnitude through slight and metallurgically acceptable variance from stoichiometric conditions. The fuel may also be doped with impurities which cause the same effect.

CVD-tungsten has been successfully used as  $UO_2$  cladding at surface temperatures of  $\sim 1850$  K. As shown in Fig 4.4.16, several potential cladding materials exist which have demonstrated enhanced creep strengths relative to CVD-tungsten [24]. Because increased cladding creep strength would reduce emitter distortion, it becomes an important criteria. The feasibility of these materials to perform as cladding is also dependent on criteria such as  $UO_2$  compatibility, neutronics, bilayer diffusion, fission-induced swelling, etc., all of which need to be investigated for the particular system of interest.

SPI conducted an extensive survey to determine the most applicable high temperature fuel behavior analysis codes available [30]. The results of that study indicated that the program "Gas Release and Swelling - Steady State and Transient" (GRASS-SST) was the most advanced analytical tool available to predict high temperature gas release and fuel swelling under space reactor conditions. This program has been condensed to FAST GRASS for computational economy. FAST GRASS used together with LIFE-4, a one dimensional code developed for estimating fuel swelling and fission gas

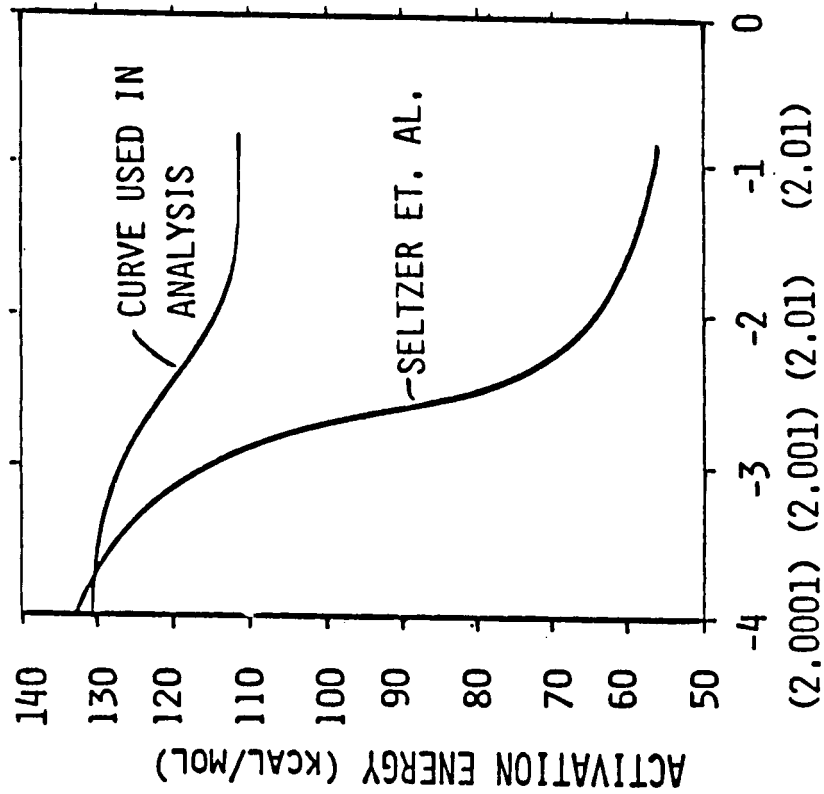
UO<sub>2</sub> CREEP  
 DIFFUSION CREEP ACTIVATION ENERGY  
 DEDUCED FROM CREEP TESTING



STOICHIOMETRY:  $\log_{10} X$ , FOR UO<sub>2+X</sub>

FIG. 4.4.14

UO<sub>2</sub> CREEP  
 DISLOCATION CREEP ACTIVATION ENERGY  
 DEDUCED FROM CREEP TESTING



STOICHIOMETRY: LOG<sub>10</sub> X FOR UO<sub>2+X</sub>

FIG. 4.4.15

# CREEP STRENGTHS OF REFRACTORY ALLOYS

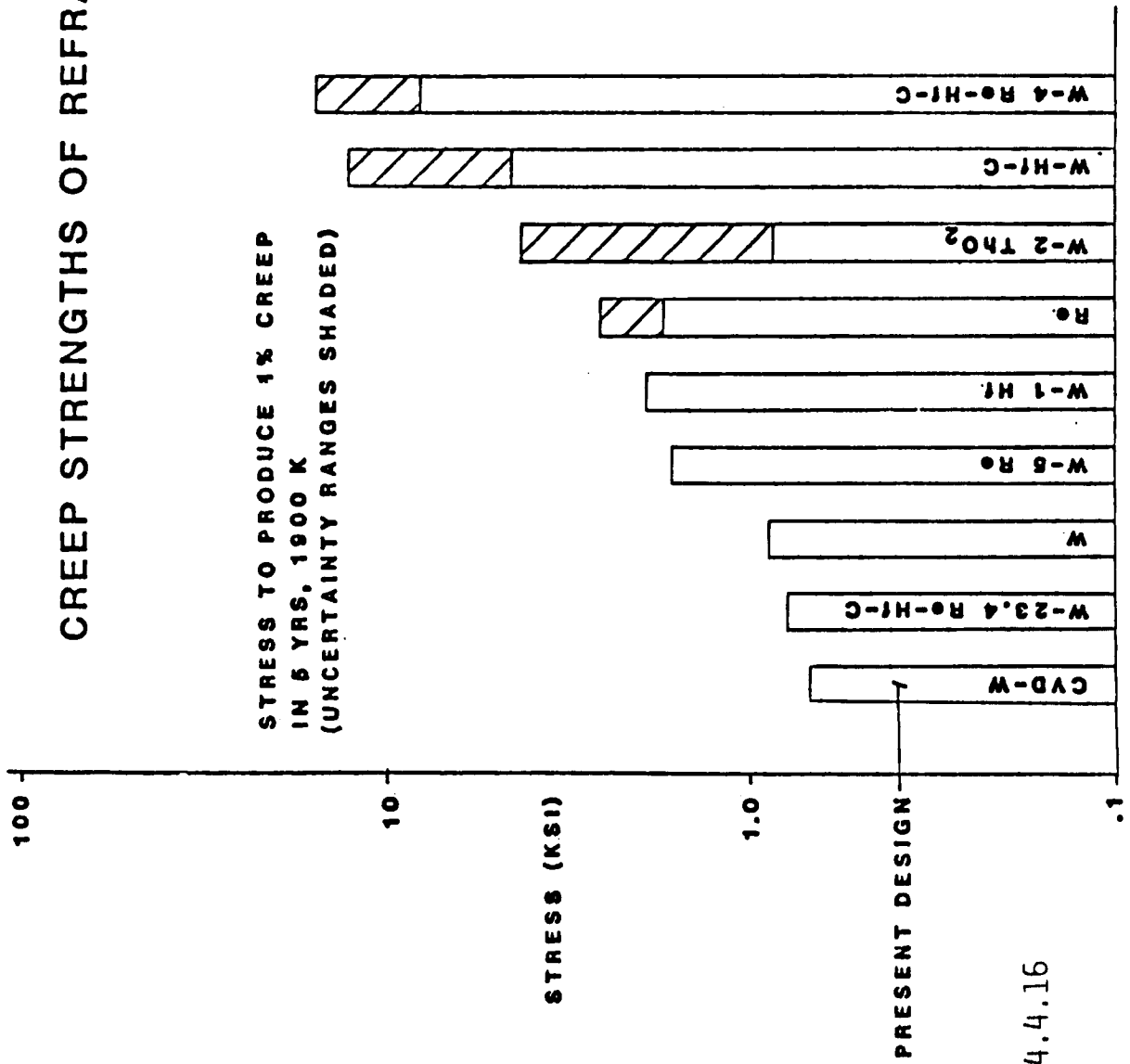


FIG. 4.4.16

release for commercial low surface temperature commercial fuels best predict one dimensional swelling of the high surface temperature fuels in the radial direction.

Outputs of the one dimensional analyses have been used by SPI to provide input to an ANSYS two dimensional fuel element model that examines the high temperature fuel element distortion mechanisms, including fuel swelling, the bladder effect, and thermal ratcheting in thermionic and other cellular fuel arrangements. Fig. 4.4.17 shows the gas release predicted by FAST GRASS for  $UO_2$  [31]. Note that at greater than 1600 K fuel surface temperatures and greater than the 0.06 fractional burnup appropriate to this study, greater than 96% of the fission gas will be released from the fuel.

Hanford Engineering Development Laboratories (HEDL) has compiled the known fission gas release data for applicable ceramic fuel irradiations. Their composite results are shown in Fig. 4.4.18. Note that the gas release is plotted versus mean fuel temperature rather than surface temperature. Their data refer to surface temperatures usually below 1000 K. Still the trend predicted by FAST GRASS is apparent and differences between  $UO_2$ , UC and UN are visible. General conclusions from these studies are: Uranium oxide vents quite completely above 1600 to 1700 K surface temperatures; relative to UN and UC,  $UO_2$  has the least swelling (Figs 4.4.19 and 4.4.20); uranium carbide experiences breakaway swelling and venting at higher temperatures; uranium nitride is very promising, but has not yet been taken to high 6-8% burnup at high surface temperatures. There may be some reason to expect UN could experience breakaway swelling and gas release at higher surface temperatures.

It is notable that FAST GRASS predicts that high temperature unconfined swelling of  $UO_2$  will be limited to less than 10% by volume (i.e., 3% radially, or 0.006 mils radially on a 1 cm (.400 inch) diameter fuel pin). Theoretically,  $UO_2$  fuel swelling should saturate at 2 to 3% burnup, if the fuel is hot enough and the gases are allowed to vent. The Turnbull-Tucker [32, 33] data indicate that swelling may continue at very high fission rates of  $5 \times 10^{13}$  to  $5 \times 10^{14}$  fission/cc-sec (the fission rates of the Zimmerman and the Chubb experiments), whereas saturation would occur at the MCNSPS

**FAST-GRASS CALCULATED  
UO<sub>2</sub> FISSION GAS RELEASE VS. BURNUP FOR MEDIUM POWER**

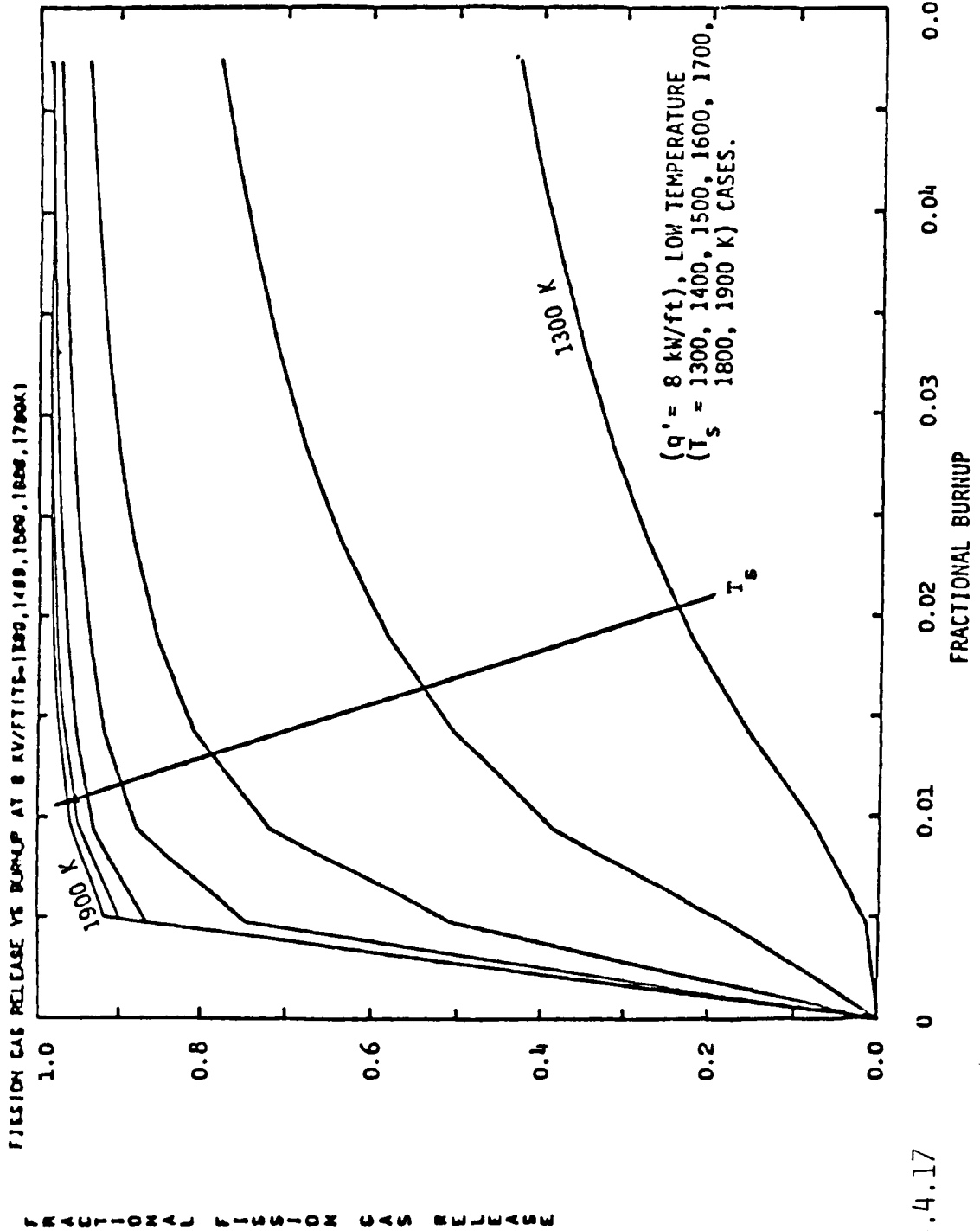


Fig. 4.4.17

FISSION GAS RELEASE AT 4 ATOM PERCENT BURNUP

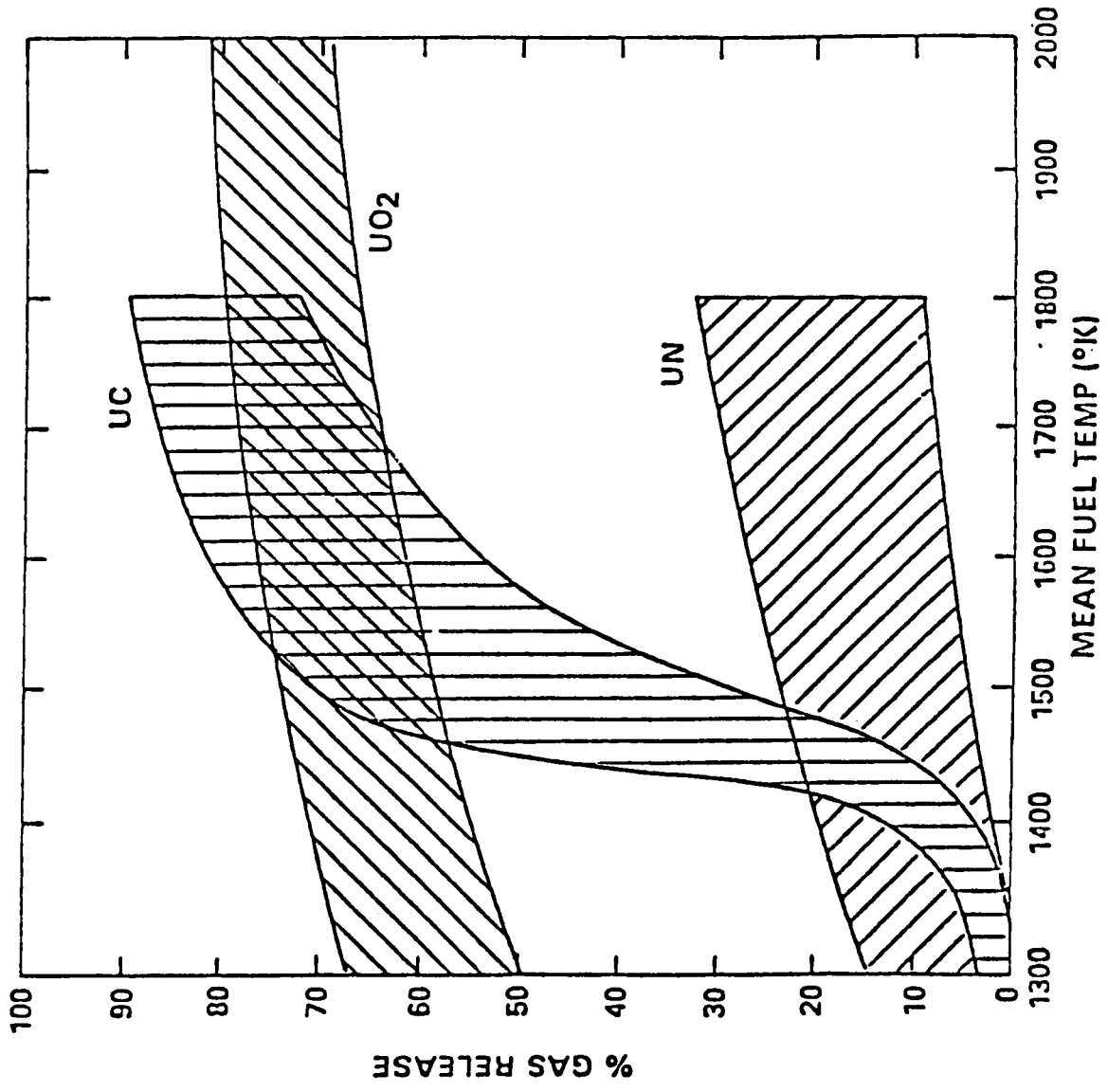


Fig. 4.4.18

FAST-GRASS CALCULATED UO<sub>2</sub> RETAINED GAS SWELLING VS. BURNUP FOR MEDIUM POWER

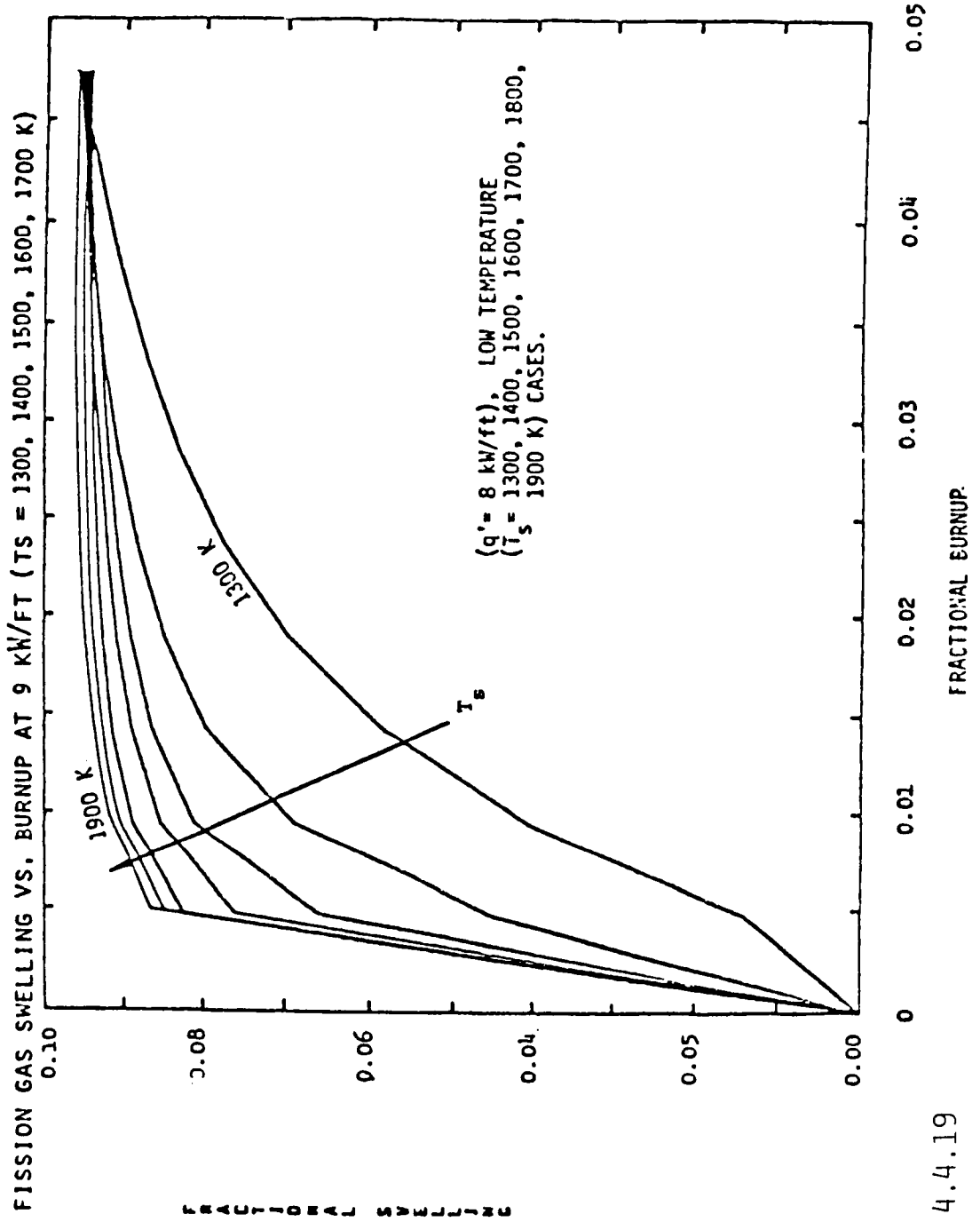


Fig. 4.4.19

# FUEL SWELLING AT 1 ATOM PERCENT BURNUP

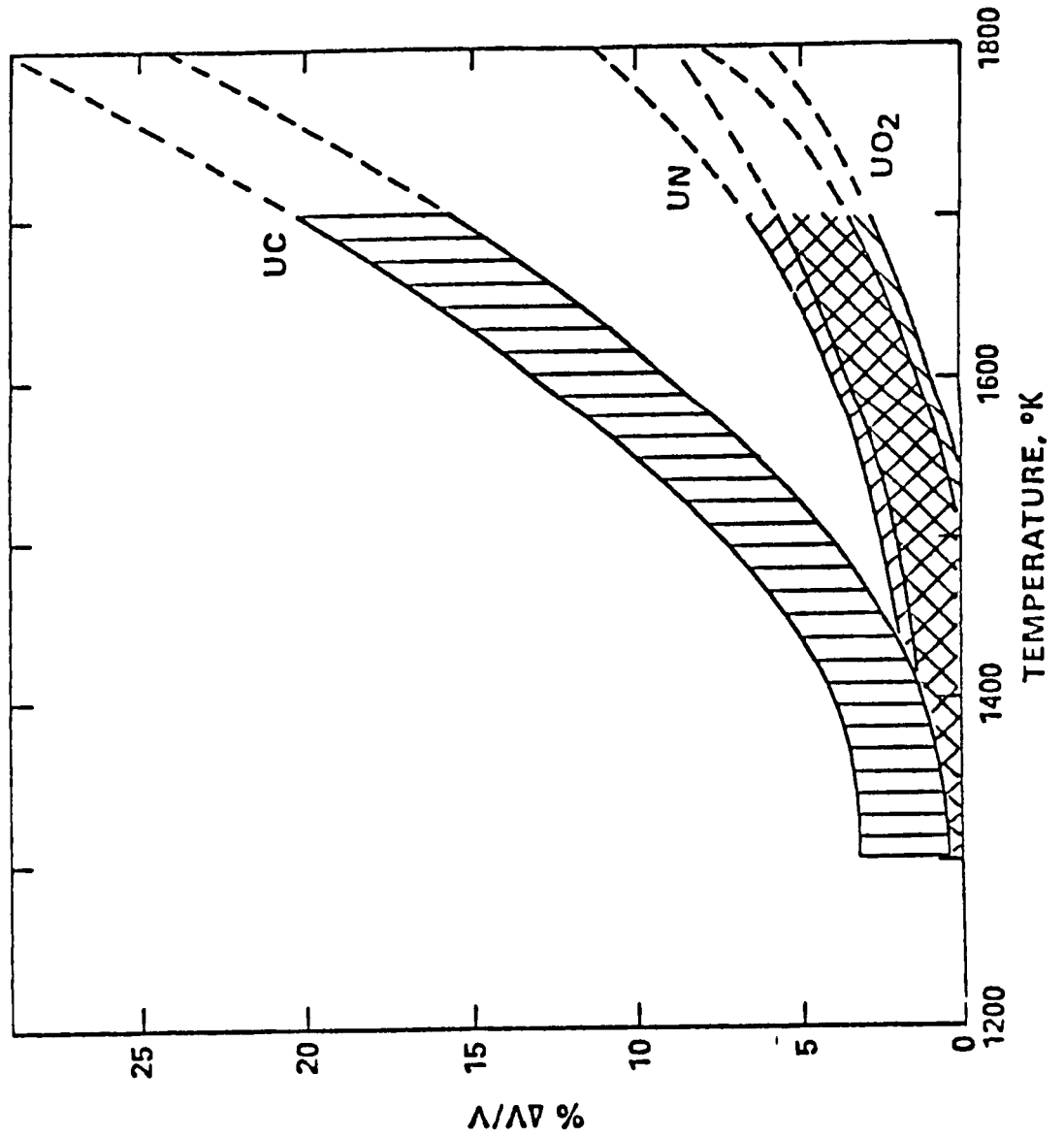


Fig. 4.4.20

fission rates of about  $6 \times 10^{12}$  fissions/cc-sec. In other words, swelling can continue when the rate of gas generation exceeds the rate of gas diffusion and release, and when the temperatures are high enough for the fuel to creep in visco-elastic deformation. The low fission rate of long life MCNSPS reactors and their high temperature of operation should lead to very high fuel burnup capability.

In summary, the mechanisms of cladding deformation are known and understood to varying degrees. There is no basic reason why system design cannot advance to higher burnups and temperatures than used previously. There is a need for technology development in the fields of fuel swelling and gas release behavior, snorkel design and stronger cladding materials. This technology is needed to define the solution to the problem and specify the limits of burnup and temperature.

Note that a promising fuel form UC-ZrC and "TRISO Beads" have not been discussed here. The omission is due to the fact that these fuels are relatively low in uranium content and therefore lead to rather large fast reactors. However, the results of this study indicate the reactors may be fairly large in the 5 MWe to 10 MWe power range in any event and these fuels may warrant a further investigation. Based on this limited study, these fuels may be best suited to large "100 MWe" outputs for very short endurance (i.e.,) "Burst" power applications.

#### 4.4.4 Reactor Core Arrangements Considered

Mini Heat Pipe Reactor. A small mini heat pipe cooled core was considered for potassium Rankine and Stirling engine applications. The core would be similar to the Los Alamos SPAR-100 reactor being advanced in 1982 and shown in Fig. 4.4.21. In order to achieve MCNSPS power densities and total power output the reactor must utilize many more small diameter short length heat pipes. The general core arrangement is shown schematically on Fig. 4.4.22. Tungsten or moly-rhenium heat pipes with lithium working fluid would be required. Fuel-coolant compatibility may require use of UN fuel. The calandria-contained fuel must be arranged in such a fashion that individual pieces may thermally expand independently. Fuel swelling must be tolerated

SPAR - 100 REACTOR

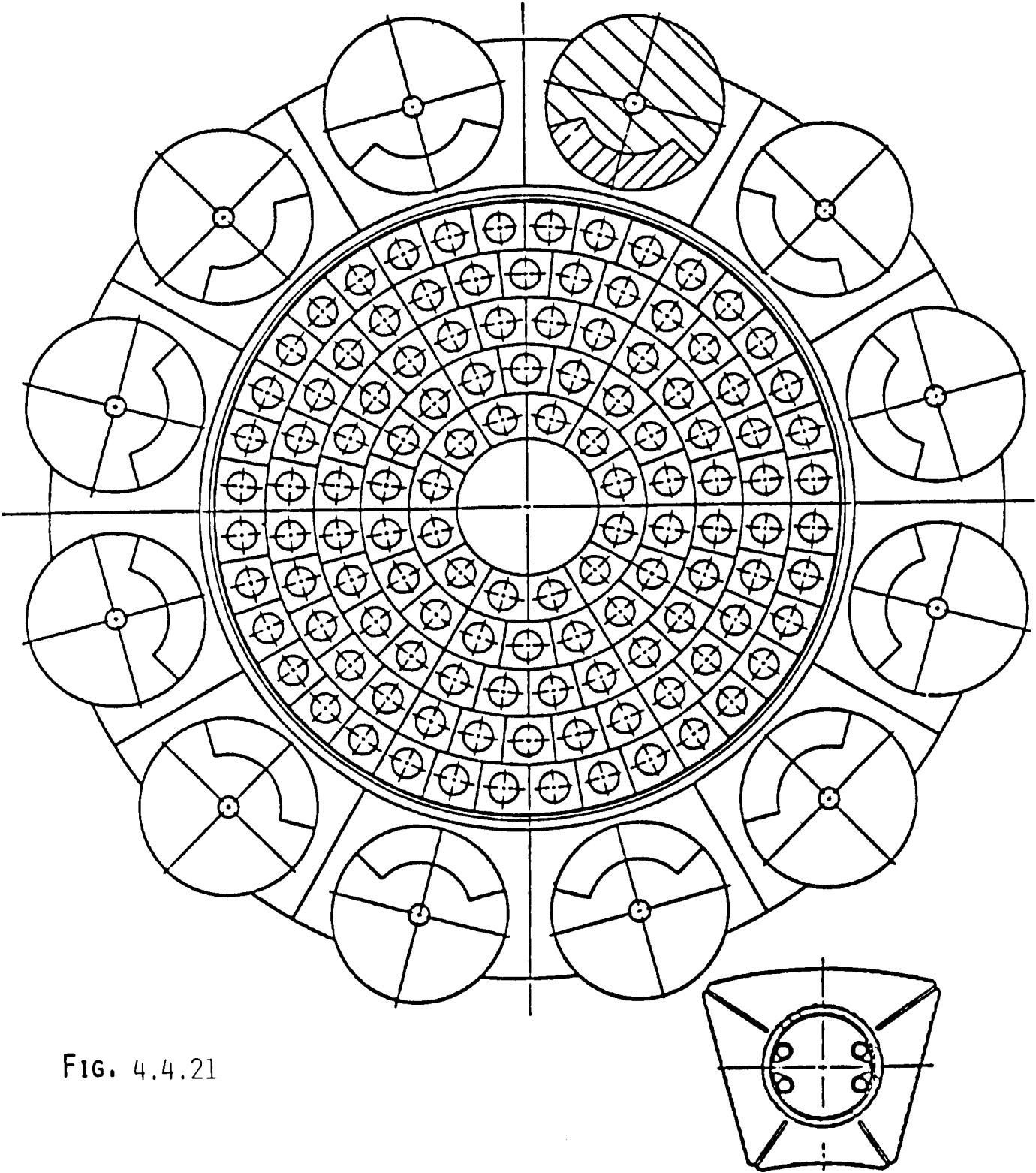


FIG. 4.4.21

MINI HEAT PIPE REACTOR  
EXTERNAL LI HEAT EXCHANGER

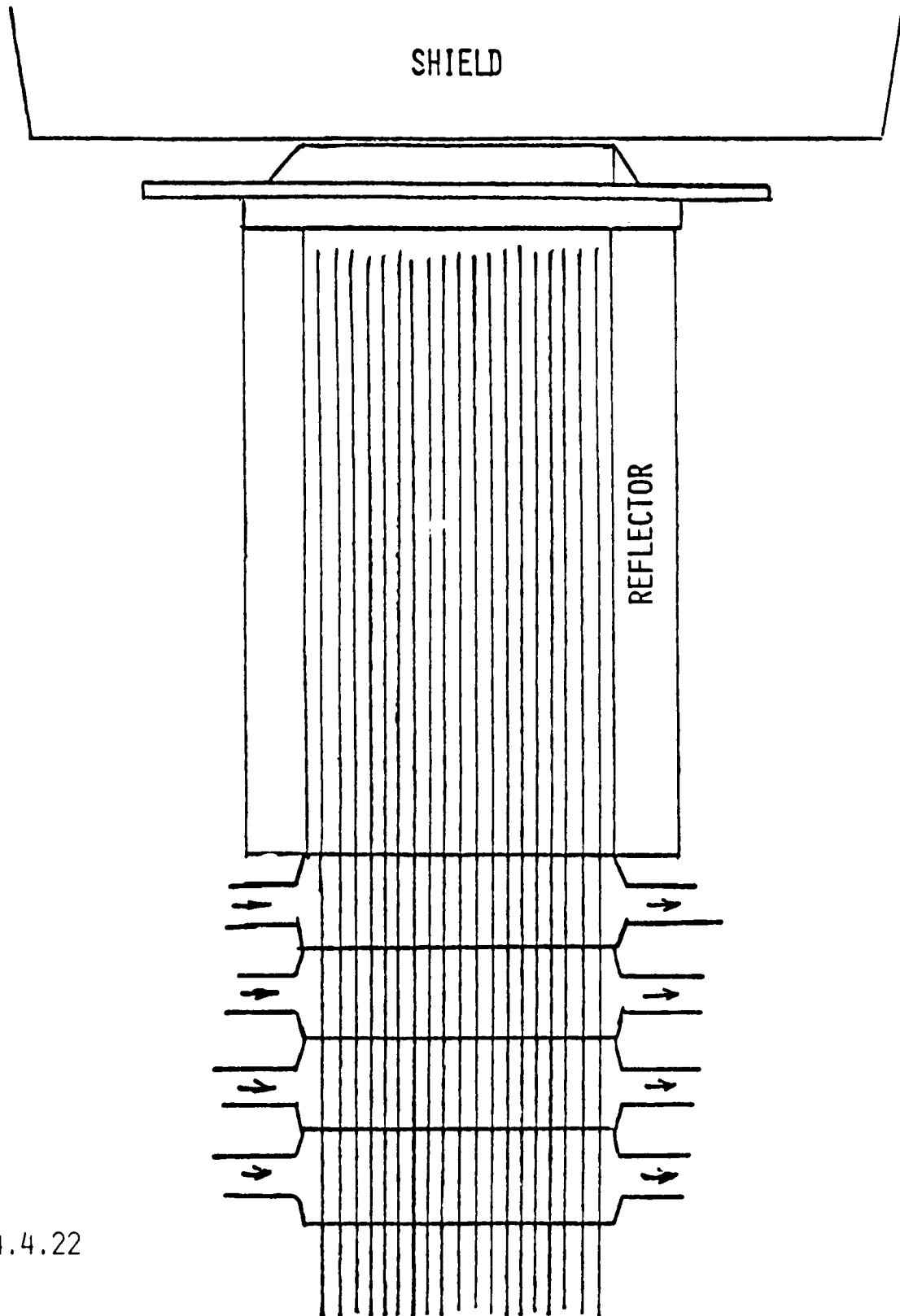


FIG. 4.4.22

without allowing across-core cumulative dimensional changes. Excellent fuel fission gas venting must be provided during the entire reactor lifetime while maintaining sufficient over pressure to prevent UN decomposition by means of nitrogen loss. A great deal of analytical and experimental work will be required to determine the feasibility of such a core. If the core is feasible, then the heat pipes could be cooled by a series of parallel lithium coolant loops or potassium vapor boilers. The geometry and zero gravity would most likely preclude potassium boiling. The parallel lithium loops could directly heat a line of Stirling engines or potassium boilers. Such an arrangement might result in very high reliability, if single mini heat pipe leaks can be tolerated. This arrangement would allow failures of power conversion subsystem loops with minimal effect upon the reactor. If individual core heat pipe failures can be tolerated in the reactor, then such failures would have little effect upon the power conversion systems. This approach might be attractive for manned systems, because there would be very little coolant activation and very little gamma shine brought in front of the shield.

Boiling Potassium Reactor. The relatively low power (150 kWe) ORNL-MPRE reactor design utilized fuel pins in a boiling potassium reactor in the configuration shown in Fig. 4.4.23. The pressure containment vessel in this reactor must be heavy walled. Thus, reflector control is severely impaired unless the pressure vessel is external to the reflector. This would substantially increase the vessel mass and requires that the reflector controls operate hot and internal to the vessel. The Soviet Topaz control drum thimble arrangement, Fig. 4.4.24, would likely lead to excessive control drum temperatures at the high MCNSPS power levels.

It is suggested that a boiling potassium reactor might be built without a radial heavy pressure vessel in order to allow effective use of external control drums. This might be configured along the lines of the Hanford production reactor header and through-tube concept in which pressurized tubes are suspended between two pressurized heads, as shown in Fig. 4.4.25, in an arrangement similar to the SPAR heat pipe reactor, Fig. 4.4.21. The boiling tubes would be equipped with twisted ribbon internal flow baffles to throw liquid to the hot walls centrifugally as vapor forms in the central

# CROSS SECTION THROUGH THE MPRE REACTOR ASSEMBLY

ORNL-LR-DWG 63-8043

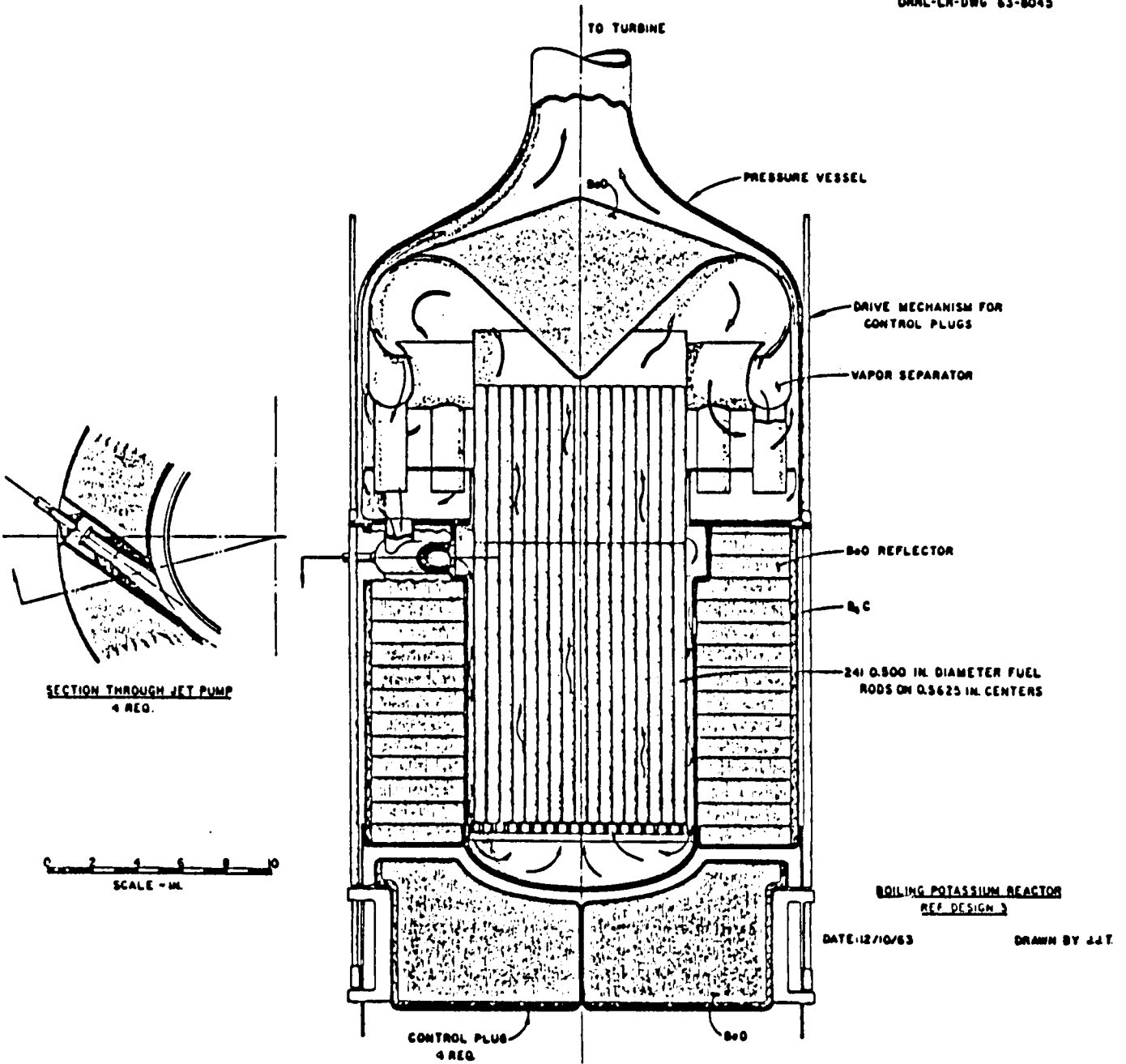


FIG. 4.4.23

# CROSS SECTION OF THE TOPAZ THERMIONIC REACTOR

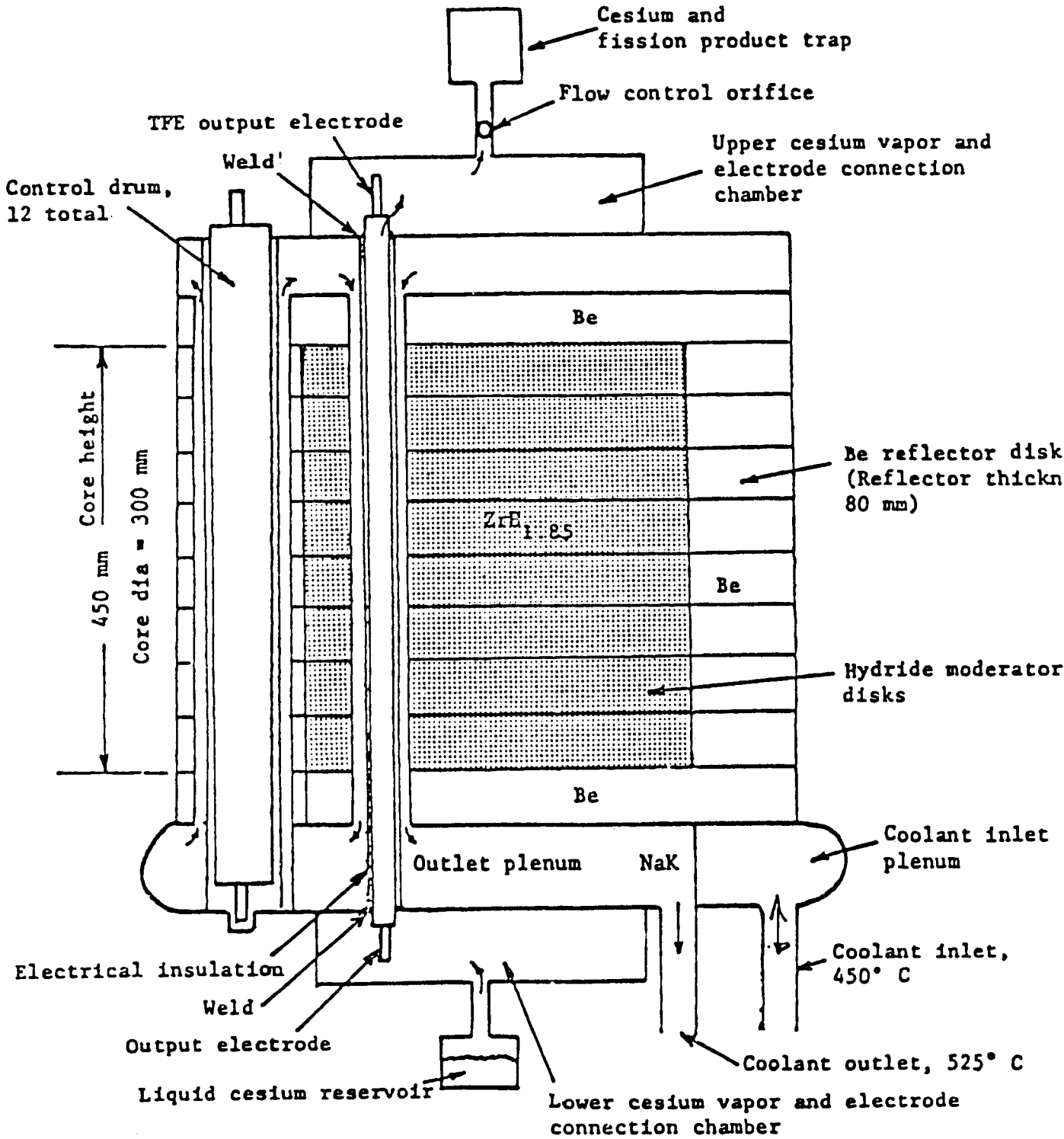


Fig. 4.4.24

# URANIUM NITRIDE BOILING POTASSIUM REACTOR CONCEPT

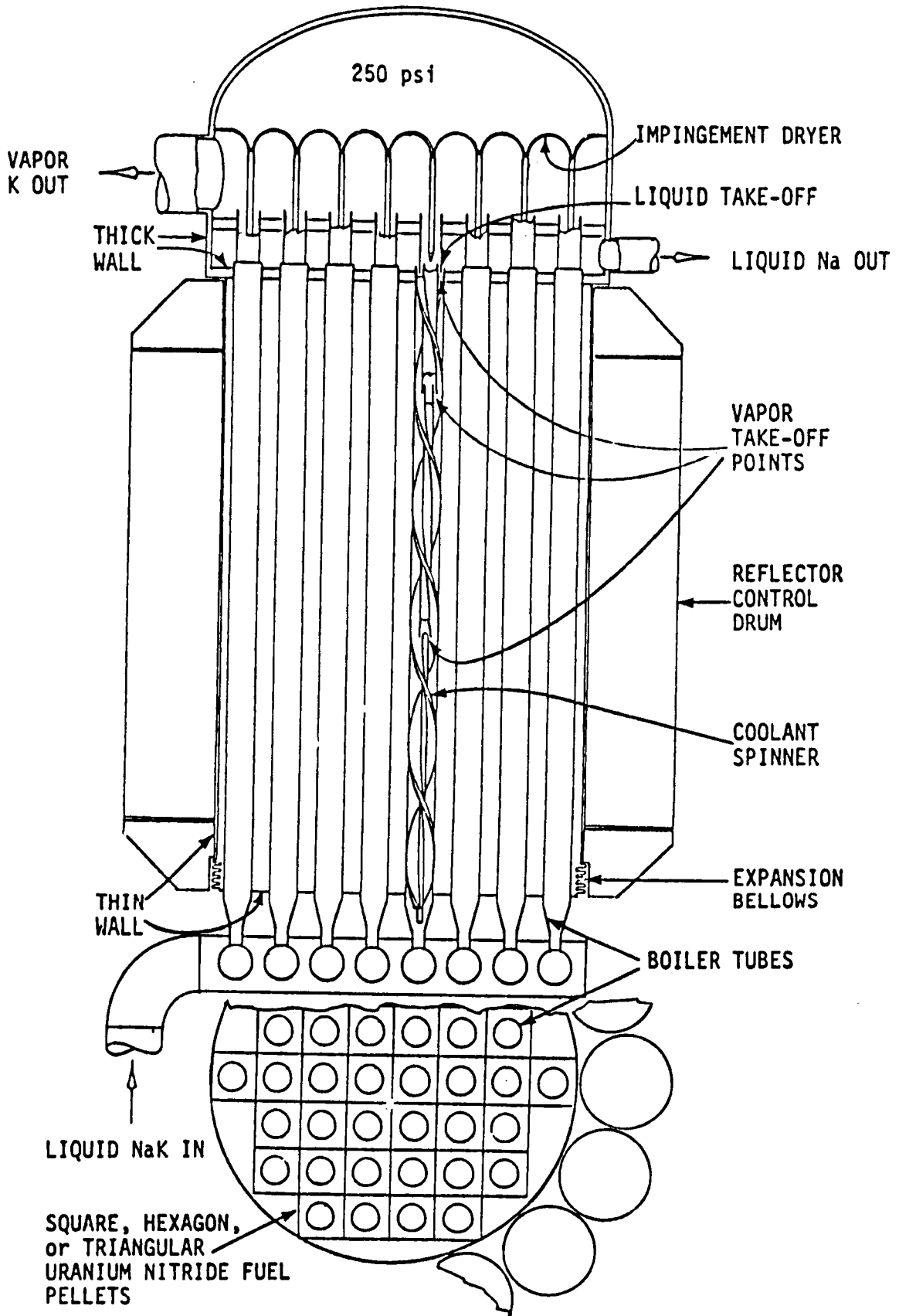


Fig. 4.4.25

core of each tube. Inlet orifices to each tube will guarantee stable and uniform flow across the reactor core. The heat transfer from the fuel could be very similar to the LASL-SPAR-100 heat pipe design. In fact, due to the use of boiling potassium or sodium, rather than lithium,  $UO_2$  fuel rather than UN could be used. On the other hand the high thermal conductivity of UN relative to  $UO_2$  could simplify the design and eliminate the need for the moly fins of SPAR-100 heat pipe design. The venting of fission gases and the prevention of non-cumulative fuel swelling are critical aspects of the design. This design concept should be considered in more detail, if the potassium or sodium Rankine cycles are explored in future studies.

Fuel Pin Reactor. Virtually all power reactors built to date have axially aligned fuel pins with axial coolant flow. The small diameter ( $\approx 1$  cm) pins are usually grouped into hexagonal or square arrays containing from 19, 37 etc. to over 100 fuel rods. Even boiling reactors have been built with this concept. In this preliminary study the fuel pin reactor has been emphasized for the liquid metal systems, because it is better understood.

As will be seen, the reactor is not the dominant system weight component in liquid metal systems nor does the reactor mass vary greatly between liquid metal cooled fast reactor concepts. For example, a liquid lithium cooled pin type reactor, with pump and potassium boiler, will represent nearly the same mass as a boiling-potassium reactor, recirculation pump and separator. For purposes of this basic feasibility and technology selection study these two reactors can be used interchangeably to evaluate potassium Rankine cycles.

The lithium cooled pin reactor is well suited to large Stirling engine systems and for high powered Rankine systems. The nominal liquid metal cooled reactor studied for a 10 MWe system was 50 MWt to cover the range of dynamic power conversion system efficiencies. The lithium cooled pin type reactor with BeO reflector was modeled in the SPI system analysis computer program and was utilized for Stirling and Rankine system studies and in the preliminary Brayton gas turbine system studies.

Gas-Cooled Reactor Design - Concept Choice. Three types of gas-cooled reactor designs were investigated: fixed bed; modular element bed; and fuel pin. Relative comparisons of the size of the three reactor core types were made using the following common parameters:

Reactor Output:	65.6 MWt
Reactor Outlet Temperature:	1800 K
Reactor Inlet Temperature:	1250 K
Pressure	600 psi
Fuel Burnup:	6%
Fuel Life:	5 years

The selection of a working gas in the direct Brayton cycle is a compromise between heat transfer and turbo-machinery performances. He-Xe gas mixtures seem to offer significant advantages over single-gas selections.

Fixed Bed. The fixed bed concept [34] is shown in Fig. 4.4.26. The reactor fuel is a fixed bed of TRISO beads. The TRISO bead is a spherical ball of fuel encapsulated by a protective, ceramic-type coating. The fuel bed of TRISO beads allows a very high fuel surface area/volume ratio to be achieved, thereby allowing high heat fluxes with a low fuel-to-gas temperature drop. In the fixed bed concept, gas travels across the fuel bed, radially inward, picking up heat from the TRISO beads.

Although TRISO beads are capable of attaining higher uranium burnups than 6%, reactivity control with reflector drums and reasonable startup rods limits burnup to about 6 to 8%. Only about 18.7% of the TRISO bead is fuel. In the fuel bed itself, the TRISO beads can be packed no denser than 61% of the fuel bed volume. Multiplying these factors yields a fuel fraction in the core of about 11.4% by volume. As a result, even the fully enriched TRISO bead gas cooled fast core is excessively large.

In the fixed bed configuration, the thickness of the bed is dictated by the pressure drop through the bed which translates to an allowable pumping power. This consideration limits the bed thickness to about 4.6 cm. With the bed thickness fixed, and maintaining an L/D ratio of 2.5, the core would measure 6 m long by 2.4 m OD. This results in a large, thin-walled cylinder with a void in the center. Most of the enclosed volume of the core is

# GAS-COOLED REACTOR-FIXED BED

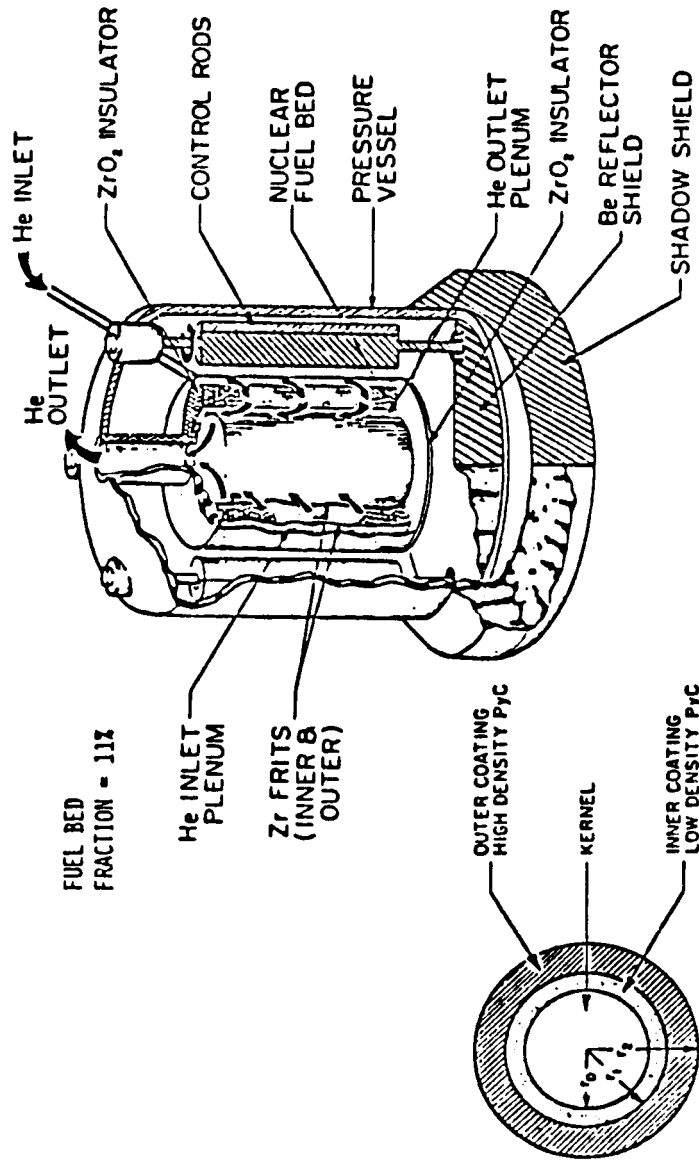


FIG. 4.4.26

actually the hollow center cavity. Clearly, the bed must be folded to eliminate the void.

Modular Bed A modular bed reactor, as shown in Fig. 4.4.27, folds the beds by incorporating many smaller cylindrical beds of TRISO beads. The individual cylindrical beds are grouped together to form a core. The result is a much better utilization of volume. If the core height is limited to 2 m for system compatibility, the modular bed core would be comprised of 288 cylindrical beds forming a core 2 m tall by 2.4 m in diameter. If the height is extended to achieve a better L/D ratio for reflector control, the core becomes too long for system integration within the shuttle envelope.

Fuel Pin A conventional fuel pin reactor configuration was also studied. Several combinations of fins and center to center (c-c) spacing between fuel pins were analyzed and are presented in Figs. 4.4.28 and 4.4.29. At the required design point, sufficient heat transfer could best be accomplished without the use of fins. The resulting core dimensions were 2 m tall by 0.87 m in diameter.

Recommended Configuration Relative dimensions of the three types of cores studied are presented in Fig. 4.4.30. The pin-type reactor is the obvious choice having a core volume about an order of magnitude smaller than either the fixed or modular bed. The fixed-bed core is too bulky, because only about 11% of the core volume is occupied by fissionable material. Either the fixed or modular bed type of core might be acceptable for applications which require very high heat fluxes (i.e., high power for a short time), but for the MCNSPS requirements, these approaches cannot be considered competitive.

The reactor cores listed on Fig. 4.4.30 were sized at 615 psia. The gas cooled cores are relatively large, but they have slightly higher energy neutron spectra than do lithium cooled cores. The high pressure containment vessel must be placed outside of the control drums, as shown in Fig. 4.4.31 in order to have any control drum effectiveness.

# GAS-COOLED REACTOR-MODULAR BED

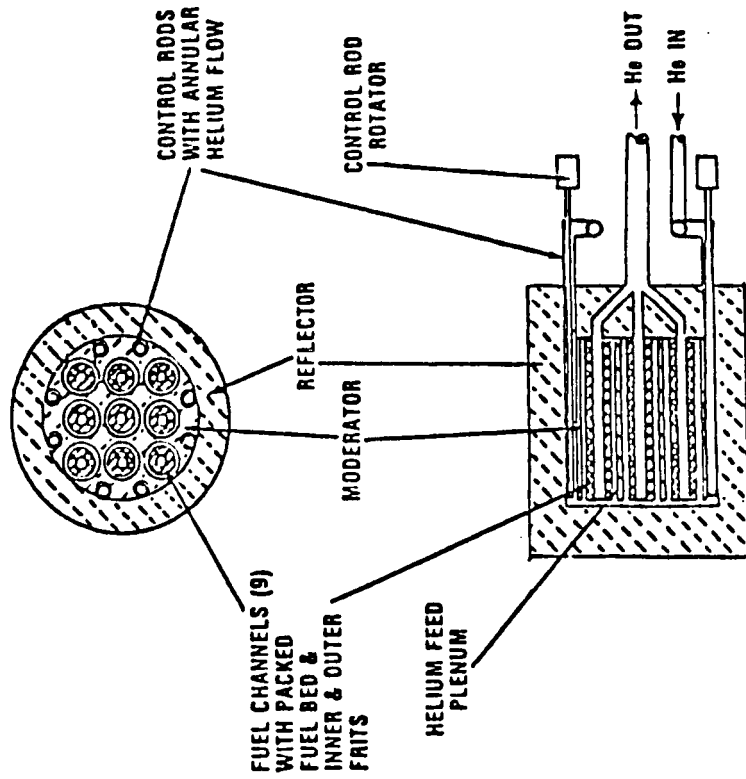
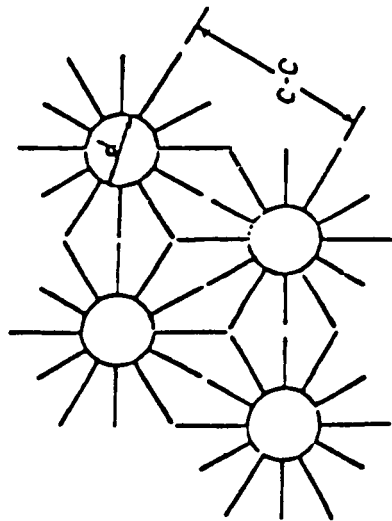


FIG. 4.4.27

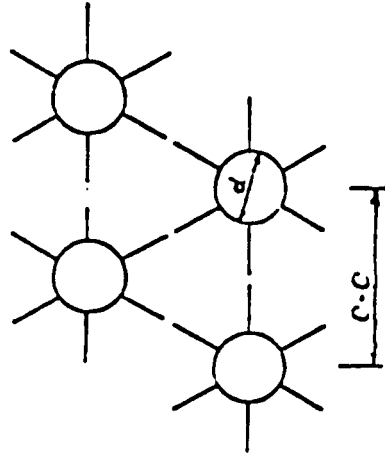
# GAS-COOLED REACTOR-PIN TYPE

REACTOR CAPACITY: 65.6 MWt



## 12 FINS/FUEL PIN

$D = .230''$   
 $C-C = .761''$   
 $CORE L/D = 6'/5.08' = 1.18$   
 $\Delta P = 10.9 \text{ psi}$   
 $PUMP POWER = 2.4 \text{ MWe @ } \eta_c = .86$   
 $T_{surf} - T_{fluid} = 42 \text{ K}$   
 $CORE DIAMETER = 5.08'$



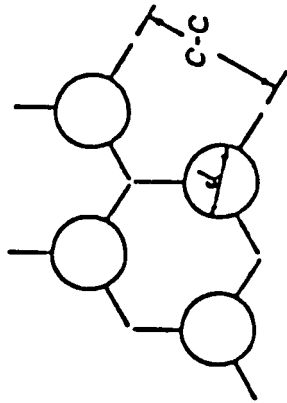
## 6 FINS/FUEL PIN

$D = .230''$   
 $C-C = .510''$   
 $CORE L/D = 6'/3.41' = 1.76$   
 $\Delta P = 10.5 \text{ psi}$   
 $PUMP POWER = 2.3 \text{ MWe @ } \eta_c = .86$   
 $T_{surf} - T_{fluid} = 120 \text{ K}$   
 $CORE DIAMETER = 3.41'$

FIG. 4.4.28

# GAS-COOLED REACTOR-PIN TYPE

REACTOR CAPACITY: 65.6 MWt



## 3 FINS/FUEL PIN

$D = .230''$

$C-C = .461''$

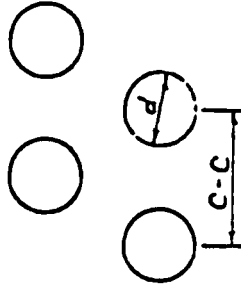
$CORE L/D = 6' / 3.07' = 1.95$

$\Delta P = 10.4 \text{ psi}$

$PUMP \text{ POWER} = 2.3 \text{ MWe} @ \eta_c = .86$

$T_{surf} - T_{fluid} = 214 \text{ K}$

$CORE \text{ DIAMETER} = 3.07'$



## NO FINS

$D = .230''$

$C-C = .431''$

$CORE L/D = 6' / 2.88' = 2.1$

$\Delta P = 8.2 \text{ psi}$

$PUMP \text{ POWER} = 1.8 \text{ MWe} @ \eta_c = .86$

$T_{surf} - T_{fluid} = 201 \text{ K}$

$CORE \text{ DIAMETER} = 2.88'$

### GAS-COOLED REACTOR-CORE SIZES

	FBR	MBR	PIN
REACTOR SIZE (Mwt)	65.6	65.6	65.6
FUEL VOLUME (ft <sup>3</sup> )	80.9	80.9	9.2
CORE DIMENSIONS	20'x8'φ	6'x7.8'φ	6'x2.88'φ
BED THICKNESS	1.8"	288 @ 1.8"	--
# PINS, DIA.	--	--	7073 @ .23"φ

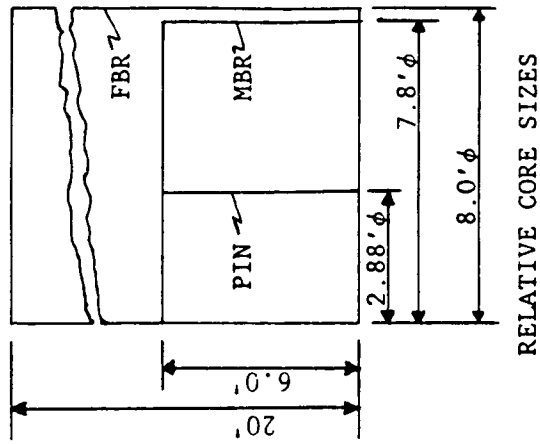


Fig. 4.4.30

# GAS - COOLED REACTOR

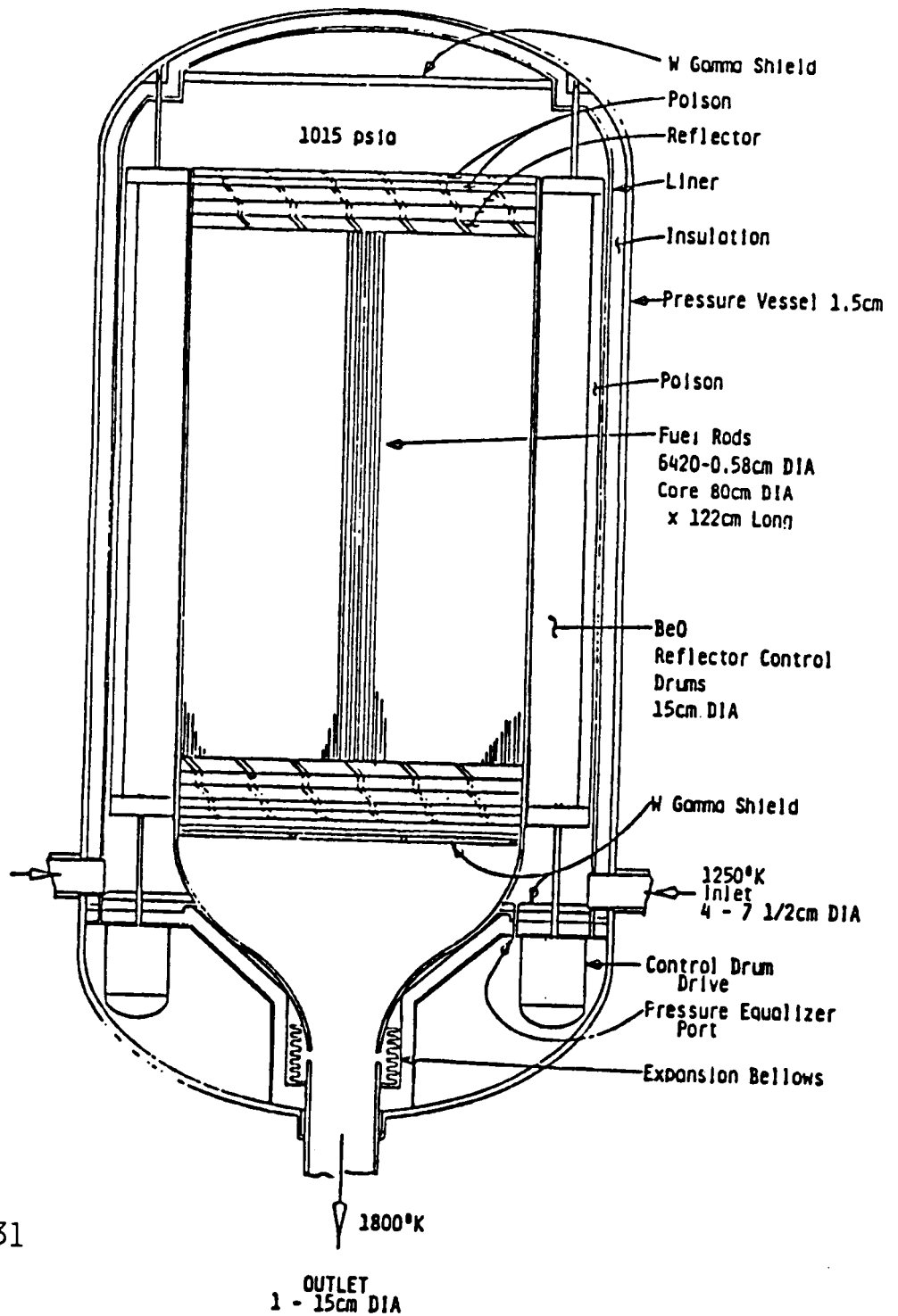


Fig. 4.4.31

The high neutron leakage of gas cooled cores could result in a greater reflector control swing. However, the need for resisting external differential pressure (the core pressure drop) and large temperature differentials could require a fairly rugged wall between the core and reflector.

After conducting system optimization studies, the preferred gas cooled reactor was of the fuel pin design at 38 to 40 MWt. The optimum reactor inlet conditions were 1000 psia and 1250 K. An 80% effectiveness recuperator. The required reactor outlet temperature is 1800 K. The reactor containment construction must be double walled with insulation sandwiched between the vessel walls. The insulation must drop the temperature from 1250 K gas inlet to about 1000 K at the pressure vessel wall. The heat flux at the reflector surface would be 5 W/cm<sup>2</sup>.

It is vital that the thermal insulation not be porous or ceramic. It must outgas and clean easily. The gaseous O<sub>2</sub> level must be held to .005 ppb. The control motors must be contained within the high pressure envelope, in a high neutron-gamma flux and at temperatures near 1000° K. Since the peak fuel surface temperature will be near 2000 K, the fuel cladding must be a W-4Re-HfC or W-HfC alloy, as was indicated in Fig. 4.4.16. Furthermore, these 0.58 cm diameter fuel pins must each be individually vented. The venting of 6412 rods must be into a manifold before being passed out of the high pressure containment. Cs-CsO<sub>2</sub>, Rb-RbO<sub>2</sub>, Sr-SrO, etc. must be cold trapped before venting Kr and Xe gas overboard or into the working fluid.

## REFERENCES

- [1] R.V. Anderson, et al, "Space Reactor Electric Systems, Subsystem Technology Assessment", Rockwell International, Contract No. DE-AT03-82SF11687, March 1983.
- [2] "Conceptual Design Studies in Support of SP-100 Program", GA Technologies, JPL Contract 956472, 6 December 1983.
- [3] H.C. Haller and Seymour Leiblein, "Analytical Comparison of Rankine Cycle Space Radiators Constructed of Central, Double and Block-Vapor-Chamber Fin-Tube Geometries", NASA-TN-D-4411, February 1968.
- [4] "Space Data", TRW Systems, Redondo Beach, CA, 1965.
- [5] D.G. Elliott, "External Flow Radiators for Reduced Space Powerplant Temperatures", 1st Symposium on Space Nuclear Power Systems, Albuquerque, N.M., January, 1984.
- [6] A.T. Mattick and A. Hertzberg, "Liquid Droplet Radiators for Heat Rejection in Space", AIAA-80-9477R, 1980.
- [7] A.T. Mattick and A. Hertzberg, "The Liquid Droplet Radiator: An Ultralight Heat Rejection System in Efficient Energy Conversion in Space", XXXIInd Congress of the Intl. Astron. Fed., September 1981.
- [8] A.T. Mattick and R.T. Tausig, "New Thermal management and Heat Rejection Systems for Space Application, Annual Report 22 July 1981 - 15 December 1982", AFRPL Contract #FD4611-81-K-0040, January, 1983.
- [9] G. Beals, J. Chin, J. Day, C. Gibson, K. Grevstad, G. Larson, D. Treibes, "Light-Weight Nuclear-Powered OTV Utilizing a Liquid Droplet Radiator", AIAA-83-1346, AIAA/SAE/ASME 19th joint Propulsion Conference, June, 1983.

- [10] A.T. Mattick and A. Hertzberg, "Liquid Droplet Radiator Technology Issues", 1st Symposium on Space Nuclear Power Systems, January, 1984.
- [11] K.K. Knapp, "Lightweight Moving Radiators for Heat Rejection in Space", AIAA-81-1076, AIAA 16th Thermophysics Conference, June, 1981.
- [12] B. Brandell, et al, "Liquid Droplet Heat Rejection Systems Status", 19th IECEC, August, 1984.
- [13] R.F. Brown, R. Kosson, "Liquid Droplet Radiator Sheet Design Considerations", 19th IECEC, August, 1984.
- [14] R.A. Haslett, V. Calia, R. Kosson, "Liquid Droplet Radiator Collector Development", 19th IECEC, August, 1984.
- [15] R.R. Fullwood, J.R. Fragda, J.R. Powell, "Promises and Problems of Liquid Droplet Radiators for Megawatt Applications", 19th IECEC, August, 1984.
- [16] A.T. Mattick, R.T. Taussig, "New Thermal Management and Heat Rejection Systems for Space Applications", AFRPL TR-84-039, June, 1984.
- [17] R. Haslett, R. Brown, "Liquid Droplet Radiator Collector Component Development: Program Status", AFRPL, June, 1984.
- [18] "Handbook of Chemistry and Physics", 55th Edition, CRC Press, Cleveland, Ohio, 1974.
- [19] R. Siegel, J.R. Howell, "Thermal Radiation Heat Transfer", Second Edition, Hemisphere Publishing Corporation, New York, 1981.
- [20] K. Knapp, "Study of Moving Belt Radiators for Heat Rejection in Space", AFRPL Contract #F04611-83-C-0012, November 1983.

- [21] R.C. Weatherston, and W.E. Smith, "A New Type of Thermal Radiator for Space Vehicles", IAS Paper No. 60-78, IAS National Summer Meeting, Los Angeles, California, June 1960.
- [22] J.E. Jones Jr., R.E. McPherson, J.P. Nichols, "Multimegawatt Space Nuclear Power Concept", First Symposium on Space Nuclear Power Systems, Albuquerque, NM, January 11-13, 1984.
- [23] "Refractory Alloy Technology for Space Nuclear Power Applications", CONF-8303130, Proceedings of a symposium held at Oak Ridge, TN, 10-11 August 1983.
- [24] W. Klopp, work done in support of this study.
- [25] "Evaluation of Multimegawatt Space Power Plants for Air Force Missions", ANL-SPC-3, Rev.1, 20 April 1984.
- [26] "LIFE-4 (Rev.0) Programmers' Manual", WARD-DX-94000-12, January 1983.
- [27] D.L. Hagrman, et al, "Matpro-Version II, A Handbook of Materials Properties for Use in the Analysis of Light Water Reactor Fuel Rod Behavior", NUREG/CR-0497, TREE-1280, February 1979.
- [28] B. Burton and G.L. Reynolds, "The Influence of Deviations from Stoichiometric Composition on the Diffusional Creep of Uranium Dioxide", Acta Metallurgica, Vol. 21, December 1973.
- [29] M.S. Seltzer, A.H. Clauer and B.A. Wilcox, "The Influence of Stoichiometry on Compression Creep of Polycrystalline UO<sub>2</sub> ", Journal  
+x  
of Nuclear Materials, 44, 1972.
- [30] J.R. Wetch, L.L. Begg, C.J. Nelin, "Thermionic Conversion Reactor Technology Assessment", DOE Contract No. DE-AC03-83SF11725, February 1984.

- [31] Y.Y. Lieu, J. Rest, "Scoping Analysis of Fission Gas Behavior in  $UO_2$  Fuel Used for an In-Core Thermionic Converter", ANL, work done in support of this study, 6 March 1984.
- [32] J.A. Turnbull, "The Effect of Grain Size on the Swelling and Gas Release Properties of  $UO_2$  During Irradiation", Phil. Mag., Vol. 30, p. 47, July 1974.
- [33] J.A. Turnbull, M.O. Tucker, "Swelling in  $UO_2$  Under Conditions of Gas Release", Phil. Mag., Vol. 47, p. 47, March 1974.
- [34] Brookhaven National Laboratory, "DOE Space Reactor System Development Program, Phase I - Reactor Studies Briefing", Germantown, MD, January 1983.

1. Report No. NASA CR-179614		2. Government Accession No.		3. Recipient's Catalog No.	
4. Title and Subtitle Megawatt Class Nuclear Space Power Systems (MCNSPS) Conceptual Design and Evaluation Report  Volume II—Technologies I: Reactors, Heat Transport, Integration Issues				5. Report Date September 1988	
				6. Performing Organization Code	
7. Author(s) J.R. Wetch, et al.				8. Performing Organization Report No. SPI-25-1	
				10. Work Unit No. 586-01-11	
9. Performing Organization Name and Address Space Power, Inc. 621 River Oaks Parkway San Jose, California 95134				11. Contract or Grant No. NAS3-23867	
				13. Type of Report and Period Covered Contractor Report Final	
12. Sponsoring Agency Name and Address National Aeronautics and Space Administration Lewis Research Center Cleveland, Ohio 44135-3191				14. Sponsoring Agency Code	
15. Supplementary Notes Project Manager, John M. Smith, Power Technology Division, NASA Lewis Research Center. This research was funded by a Memorandum of Agreement among the Department of Defense, the National Aeronautics and Space Administration, and the Department of Energy.					
16. Abstract <p>This study was conducted in 1984 under the direction of the NASA Lewis Research Center, for the Triagency (DARPA, NASA, DOE) SP-100 program office. The objective was to determine which reactor, conversion and radiator technologies would best fulfill future Megawatt Class Nuclear Space Power System Requirements. Specifically, the requirement was 10 megawatts for 5 years of full power operation and 10 years system life on orbit. A variety of liquid metal and gas cooled reactors, static and dynamic conversion systems, and passive and dynamic radiators were considered. Four concepts were selected for more detailed study. Namely:</p> <ol style="list-style-type: none"> <li>1) A gas cooled reactor with closed cycle Brayton turbine-alternator conversion with heat pipe and pumped tube-fin heat rejection.</li> <li>2) A Lithium cooled reactor with a free piston Stirling engine-linear alternator and a pumped tube-fin radiator.</li> <li>3) A Lithium cooled reactor with a Potassium Rankine turbine-alternator and heat pipe radiator.</li> <li>4) A Lithium cooled incore thermionic static conversion reactor with a heat pipe radiator.</li> </ol> <p>The systems recommended for further development to meet a 10 megawatt long life requirement are the Lithium cooled reactor with the K-Rankine conversion and heat pipe radiator, and the Lithium cooled incore thermionic reactor with heat pipe radiator.</p>					
17. Key Words (Suggested by Author(s)) Nuclear space power Space power conversion systems Multimegawatt space power			18. Distribution Statement Unclassified—Unlimited Subject Category 44		
19. Security Classif. (of this report) Unclassified		20. Security Classif. (of this page) Unclassified		21. No of pages 135	22. Price* A07